**U.S. Department of Energy**
**Office of Advanced Automotive Technologies**
**1000 Independence Avenue S.W.**
**Washington, DC 20585-0121**

**FY 2000**

# Progress Report for Propulsion Materials

Energy Efficiency and Renewable Energy
Office of Transportation Technologies
Office of Advanced Automotive Technologies
Energy Conversion Team

**Steven Chalk** **Energy Conversion Team Leader**

**October 2000**

# CONTENTS

# 1. INTRODUCTION

## Automotive Propulsion Materials R&D: Enabling Technologies to Meet Technology Program Goals

**Patrick B. Davis**
**Program Manager**

On behalf of the Department of Energy's (DOE's) Office of Transportation Technologies (OTT), I am pleased to introduce the FY 2000 Annual Progress Report for the Automotive Propulsion Materials Research and Development Program. Together with DOE national laboratories and in partnership with private industry and universities across the United States, the Office of Advanced Automotive Technologies (OAAT) engages in high-risk research and development (R&D) that provides enabling technology for fuel-efficient and environmentally friendly, light-duty vehicles. This introduction summarizes the objectives and progress of the program in FY 2000 and highlights the technical barriers remaining and future directions of the program.

The Automotive Propulsion Materials Research and Development Program supports the Partnership for a New Generation of Vehicles (PNGV), a government-industry partnership striving to develop by 2004 a mid-sized passenger vehicle capable of achieving 80 miles per gallon (mpg) while adhering to future emissions standards and maintaining such attributes as affordability, performance, safety, and comfort. PNGV achieved an important milestone this year, unveiling year-2000 concept cars. These concept cars demonstrated that making an 80-mpg vehicle available to consumers is not merely a distant goal but is achievable in this decade. They also demonstrate that the Automotive Propulsion Materials Research and Development Program is focusing on the right technologies, striving to improve the performance and lower the cost of critical materials components for compression-ignition, direct-injection (CIDI) engines and power electronics (both featured in all three concept vehicles) and critical materials for fuel cell vehicles (showcased in a fuel cell version of the General Motors Precept PNGV concept car). The propulsion materials developed under this program will facilitate higher efficiencies, lower emissions, improved alternative fuel capabilities, and lower specific weight and volume for these advanced vehicles without compromising cost, safety, and recyclability.

**General Motors Precept fuel cell concept car.**

The Automotive Propulsion Materials Program is an integral partner with the Vehicle Power Electronics and Electric Machines, the Combustion and Emissions Control for Advanced CIDI Engines, and the Vehicle Fuel Cell Power Systems R&D programs. Projects within the Automotive Propulsion Materials Program address materials concerns that directly impact the critical technical barriers in each of these programs—barriers such as thermal management, emissions reduction, and reduced manufacturing costs. Only barriers that involve basic, high-risk materials issues are engaged by the program.

## Enabling Technologies

The Automotive Propulsion Materials Program focuses effort on enabling materials technologies—technologies that are critical in removing barriers to the power electronics, fuel cell, and CIDI engine combustion and emissions control research programs.

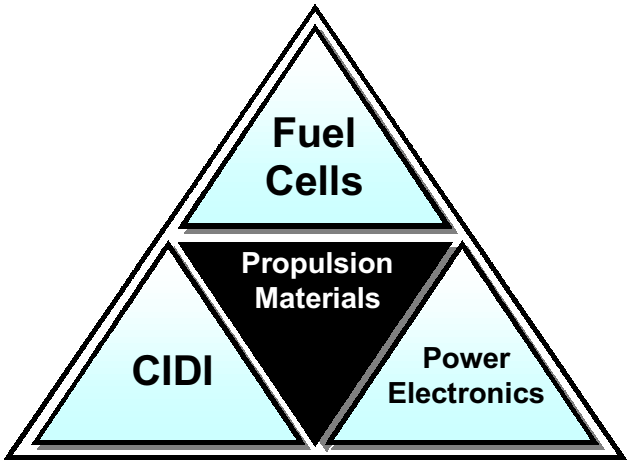


**The Propulsion Materials Program focuses on three applications.**

Thermal management remains a cross-cutting materials issue, affecting both the power electronics and fuel cell programs. For power electronics, the components necessary for the high-fuel-economy, low-emission PNGV vehicles require electronics to be smaller and lighter in weight and to operate at higher temperatures. These requirements are being addressed by developing electronic materials (i.e., capacitor dielectrics) that operate at higher temperature and by improving our ability to dissipate heat generated in these devices. Fuel cell systems also require improved heat dissipation because the lower operating temperature of the fuel cell system (80°C) provides a smaller temperature differential between the fuel cell system and ambient conditions. The Program has been addressing both heat dissipation issues through the development of advanced carbon foam technology.

The Program is supporting the development of a microporous inorganic membrane for polymer electrolyte membrane (PEM) fuel cells. These high-surface-area porous oxide ($TiO_2$ and $Al_2O_3$) membranes should be capable of operating at temperatures of above 100°C to minimize platinum requirements, improve waste heat dissipation, and display minimal water management problems and less CO poisoning.

CIDI engine and aftertreatment development will greatly benefit from the Program through research in advanced wear coatings and the development of improved particulate filters for diesel engines. Cast aluminum and titanium alloys are being used to reduce the weight of internal combustion engine components, and cost-effective surface treatments are being developed to reduce wear of light metal components such as engine blocks, fuel pumps, and compressor housings. Wear of components can lead to increased emissions, lower efficiency, and lower durability.

In addition, current CIDI engine technology faces the difficult balance of engine efficiency versus tailpipe emissions. The Propulsion Materials Program is working to maximize efficiency while reducing emissions through the development of advanced filters to reduce particulate matter from combustion engines.

## Collaboration and Cooperation

As with other programs under PNGV, collaboration and cooperation across organizations is a critical part of the Automotive Propulsion Materials Program. Across the materials projects, scientists at the national laboratories are collaborating with manufacturers to identify and refine the necessary characteristics for meeting performance requirements. Component manufacturers and national laboratory and contractor scientists are also working together to identify the technological barriers to manufacturing optimal materials to meet component requirements.

There is also cooperation among national laboratories to take advantage of the expertise of each facility. Oak Ridge and Argonne National Laboratories, for example, are collaborating in the development of smaller, lighter, more efficient radiators for fuel cell vehicles. Carbon foam materials developed at Oak Ridge and nanofluids developed at Argonne are advanced heat transfer materials with significantly higher

thermal conductivities and improved heat transfer characteristics. Combining carbon foam with nanofluid technology could lead to a breakthrough in advanced thermal management system designs. In another project, Sandia National Laboratory (SNL) is fabricating higher-temperature dc buss capacitors and Oak Ridge National Laboratory is developing testing algorithms to assess and improve the mechanical reliability of such electronic devices.

**Laboratory/Contractor-Industry Collaboration**

| Laboratory | Industrial Partner | | | |
|---|---|---|---|---|
| Argonne National Laboratory | ✔ | Ability Engineering Technology, Inc. | ✔ | Daimler-Chrysler Corporation |
| | ✔ | Atlas Cylinders, Inc. | ✔ | Ford Motor Company |
| | ✔ | Bronson and Bratton, Inc. | ✔ | Lucas-Varity |
| | ✔ | Cryomagentics, Inc. | ✔ | Purdue University |
| | ✔ | CRUMAX | ✔ | UGIMAG, Inc. |
| Oak Ridge National Laboratory | ✔ | AVX | ✔ | Industrial Ceramic Solutions |
| | ✔ | Bronson and Bratton, Inc. | ✔ | Kemet |
| | ✔ | Conoco Corporation | ✔ | Motorola |
| | ✔ | Cryomagnetics, Inc. | ✔ | Murata |
| | ✔ | CRUMAX | ✔ | Poco Graphite |
| | ✔ | Daimler-Chrysler Corporation | ✔ | Plug Power, LLC |
| | ✔ | Dow Chemical Company | ✔ | UGIMAG, Inc. |
| | ✔ | Ford Motor Company | ✔ | University of Tennessee |
| | ✔ | Florida International University | ✔ | University of Wisconsin |
| | ✔ | General Motors | ✔ | SatCon |
| Sandia National Laboratory | ✔ | AVX | ✔ | Murata |
| | ✔ | Daimler-Chrysler Corporation | ✔ | Pennsylvania State University |
| | ✔ | Ford Motor Company | ✔ | TAM |
| | ✔ | General Motors | ✔ | Tokay |
| | ✔ | Degussa | ✔ | TPC Ligne Puissance |
| | ✔ | Ferro | ✔ | TPL, Inc. |
| | ✔ | Kemet | ✔ | TRS Ceramics |
| | ✔ | Materials Research Associates | | |

In addition to national laboratory and large industry participation, the FY 2000 Automotive Propulsion Materials Program included important R&D conducted by a small business. Industrial Ceramic Solutions, LLC, located in Oak Ridge, Tennessee, is developing a ceramic filter to reduce particulate emissions from diesel engines. As in the collaborative efforts of national laboratories with industry, researchers at Industrial Ceramic Solutions are working closely with representatives from DaimlerChrysler, Ford, and General Motors to develop a filter that will help meet PNGV emissions targets.

## Accomplishments

FY 2000 featured notable accomplishments in all three materials program areas. While the remainder of the report provides summaries on all of the Automotive Propulsion Materials projects, this section provides a highlight of some of the major accomplishments during FY 2000. Materials development in support of power electronics, for example, featured breakthroughs in the use of polymer dielectric film technology to fabricate smaller and higher-temperature dc buss capacitors. Fuel-cell-related materials activities demonstrated a technique for preparing transmission electron microscope (TEM) specimens that can be used to optimize the catalyst microstructure and distribution in membrane electrode assemblies for low cost and high performance. Finally, material research in the support of combustion engine and aftertreatment technologies led to the demonstration of microwave-regenerated exhaust particulate filters in engine test cells.

## Power Electronics

Smaller, lighter-weight electrical components that operate at higher temperatures than in present-day automobiles are needed to make new-generation electric hybrid vehicles commercially competitive. Since substantial volume and performance improvements for dc buss capacitors can be obtained through materials science development, this technology has been targeted by the PNGV. A specific challenge for SNL researchers is to develop polymer film capacitors for electric hybrid vehicles that are half the size of and will permit 30$^{o}$C higher operating temperatures than the aluminum electrolytic capacitors presently used.

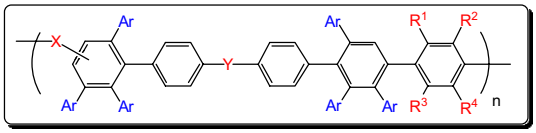


**Base structure of polyconjugated aromatic dielectric film.**

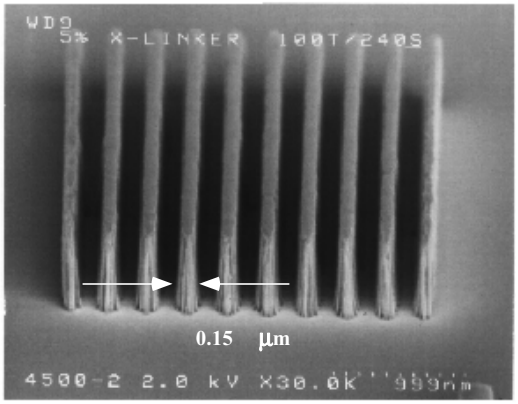


**Extreme UV lithographic polymer film dielectric.**

SNL researchers have contacted automobile engineers, dielectric powder and polymer film suppliers, and capacitor manufacturers to determine state-of-the-art capabilities and to define market-enabling technical goals. Specifically, a joint project plan has been developed among SNL researchers, General Motors and AVX/TPC engineers, and DOE program managers to design and synthesize a polymer film dielectric material worthy of large-scale commercialization. It has been agreed that synthesis of a polymer film with dielectric constant (K) > 6 and loss (DF) < 0.01 is sufficient for commercialization. Our first scale-up effort will result in the fabrication of 160 200-µF capacitors. Our approach for polyfilm improvement is to leverage knowledge gained from our development of commercialized high-resolution extreme UV lithographic polymer films for top surface imaging to develop highly-temperature-stable polymer film dielectrics. We have invoked a molecular engineering approach to create higher polarizabilities in our polyconjugated aromatic base structure to obtain higher dielectric constants.

Our first generation of polyconjugated aromatic films have 33% greater dielectric constant (K = 4) than the commercial standard (K = 3) and are voltage- and temperature-stable at up to 125°C. We have recently developed chemical synthesis procedures that resulted in polyfilms of K = 6 and dissipation factors of 0.013 at 25°C and suffered no loss in dielectric constant at 1 MV/cm fields. However, high temperature loss was unacceptable for these films. Recent molecular modifications by SNL researchers have resulted in voltage-stable polymer dielectric films with K = 5.4 and DF < 0.008 at 110°C. The SNL-developed technology is being considered for scale-up in October 2000.

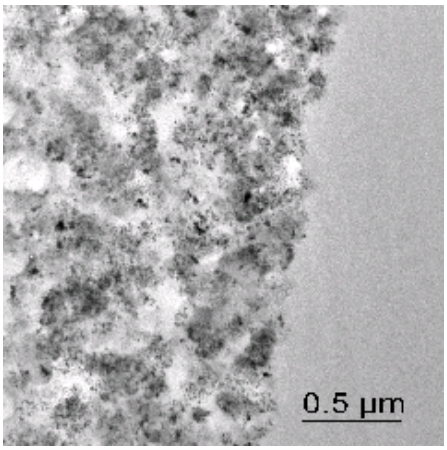


**TEM micrograph of an unused MEA.** Small dark areas are platinum particles within the catalyst layer.

**Fuel Cells R&D**

The successful development of fuel cell technology in vehicles requires breakthroughs in cost, durability, size, and performance. During FY 2000, researchers at Oak Ridge National Laboratory developed a specimen preparation technique that produces thin cross-sections of PEM fuel cell membrane electrode assemblies (MEAs) suitable for microstructural and microchemical characterization in a TEM. Cross-sections have been produced that preserve the geometry and distribution of the MEA components and are thin over wide areas, allowing for the simultaneous study of the microstructure and chemical composition representative of the cathode, membrane, and anode of an MEA as it existed during use in a fuel cell. Initial observations of precious metal catalyst content and distribution indicate that the microstructure of the catalyst layer is far from optimized in a commercially available PEM MEA.

One of the key hurdles in making PEMs commercially viable is to reduce the cost by minimizing the amount of precious metal catalyst necessary to provide high-power-density operation at low temperature. The specimen preparation techniques developed in FY 2000 will be utilized in future work to optimize the catalyst microstructure and distribution in MEAs for low cost and high performance. By carefully

maintaining the spatial relationships in the real system, it becomes possible to correlate fuel cell performance and performance changes with the microstructure and microchemistry of the MEA as observed by TEM.

## Advanced Combustion Engine and Emissions R&D

A major PNGV goal is to develop a vehicle with outstanding fuel economy that meets stringent emissions standards. Balancing high fuel economy with low emissions is a challenge that is being addressed through the materials activities in support of the Combustion and Emission Control for Advanced CIDI Engines R&D program. Specifically, work conducted at Industrial Ceramic Solutions, LLC, has led to the development and demonstration of an advanced exhaust filter system capable of capturing more than 90% of carbon particulates from diesel engine exhaust.

**Silicon carbide fiber filter cartridge.**

Researchers at Industrial Ceramic Solutions have developed a ceramic filter system that meets specifications provided by DaimlerChrysler, Ford, and General Motors. The system features a ceramic-fiber filter that can be automatically cleaned through the use of microwave power. During FY 2000, the prototype filter system was evaluated on a 1.2-liter DIATA diesel engine in a Ford test cell, a 1.9-liter Volkswagen TDI engine in an ORNL test cell, and a 7.3-liter International engine at the University of Tennessee. During the three tests, the filter system demonstrated 80 to 95% particulate removal efficiency and a microwave regeneration efficiency of over 95% at engine idle. The data indicated that the filter on a 1.9-liter Volkswagen engine operating at cruising speed would need to be regenerated only once every 6 hours, and the fuel efficiency penalty would be less than 0.5 mpg. Additional testing proved that the time between regenerations could be extended significantly by the addition of particulate matter catalysts to the filter cartridge.

**Uniform heating of cartridge in microwave cycle.**

The exhaust filter system developed by Industrial Ceramic Solutions signifies a breakthrough in emission control technology. If successful, this filter system could be applied to a wide variety of diesel engines that generate very fine particulate matter. Beyond the application in diesel-powered automobiles, this technology could be applied to diesel engines used in pick-up trucks, sport utility vehicles, and large trucks.

***Awards and Achievements***

| | |
|---|---|
| **Carbon Foam Thermal Management** *(ORNL)* | ✔ R&D 100 Award Winner—2000<br>✔ Commercialization of Carbon Foam ahead of schedule (POCO Graphite)<br>✔ Brian Kelly Award (Presented at the International Carbon Conference by the British Carbon Group)—2000 |
| **Near-Frictionless Coating** *(ANL)* | ✔ ASME Innovative Research Award—1999<br>✔ Patent Application Submitted |

## Future Directions

The Automotive Propulsion Materials Program will continue to work closely with PNGV partners and industry to understand propulsion materials-related requirements. Building upon the recent advances in materials technologies, many of this year's projects will be moved out of the laboratory and over to industry for testing. The development of the microwave-regenerative exhaust filter will move from engine test cell evaluations toward vehicle testing. In addition, prototype particulate filters and carbon foam heat sinks will be fabricated for testing by industry partners. The scale-up and commercialization of carbon foam for thermal management applications will continue so that quantities of material can be purchased from POCO Graphite by year's end. Other projects will continue to refine manufacturing requirements and necessary characteristics to meet the challenges of the PNGV program.

A promising new activity in the Automotive Propulsion Materials Program for FY 2001 was the initiation of the MEA microstructural and microchemical characterization project. The project will make available to all membrane and MEA developers an important tool with which they can study the structure, catalyst distribution, and degradation of their MEAs. The initial experiments have indicated that the catalyst layer is far from optimal and can be improved significantly. This tool will play a significant role in that development process.

As advanced automotive technology developments uncover new challenges, the Automotive Propulsion Materials Program will continue to provide breakthrough technology solutions through collaboration with industry, PNGV partners, national laboratories, and small businesses.

## Project Abstracts

The remainder of this report communicates the progress achieved during FY 2000 under the Automotive Propulsion Materials Program. It consists of 17 abstracts of national laboratory projects—five that address power electronics, four that address combustion and emission technologies, and eight that address fuel cells. The abstracts provide an overview of the critical work being conducted in order to improve these systems, reduce overall cost, and maintain component performance. In addition, these abstracts provide insight into the challenges and opportunities associated with advanced materials for high-efficiency automobiles.

Patrick B. Davis

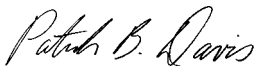

Program Manager
Energy Conversion Team
Office of Advanced Automotive Technologies
Office of Transportation Technologies

# 2. POWER ELECTRONICS

## A. Carbon Foam Thermal Management Materials for Electronic Packaging

*J. W. Klett, R. D. Ott, and A. D. McMillan*
*Oak Ridge National Laboratory, P.O. Box 2008, MS 6087, Bldg. 4508*
*Oak Ridge, TN 37831-6087*
*(865) 574-5220; fax: (865) 576-8424; e-mail: klettjw@ornl.gov*

*DOE Program Manager: Patrick Davis (202) 586-8061; fax: (202) 586-9811; e-mail: patrick.davis@hq.doe.gov*
*ORNL Technical Advisor: David Stinton (865) 574-4556; fax: (865) 574-6918; e-mail: stintondp@ornl.gov*

---

*Contractor: Oak Ridge National Laboratory, Oak Ridge, Tennessee*
*Prime Contract No.: DE-AC05-00OR22725*

---

### Objectives

- Collaborate with automotive partners to develop carbon foam heat exchanger and heat sink designs to dissipate 30 W/cm$^2$ using current cooling fluids, achieving a targeted heat flux/weight ratio of >30% over current standards.
- Expand on mathematical model for prediction of pressure drop and heat transfer in graphite foam.

### OAAT R&D Plan: Section 3.5: Task 4; Barriers B, C, D

### Approach

- Vary processing conditions and characterize foam structures to gain understanding of the effects of processing conditions on structures that affects thermal properties, as well as strength, durability, and toughness.
- Develop a methodology to evaluate the heat sink designs using the foams.
- Compare results to existing data on heat sinks and current heat exchanger designs.
- Collaborate with automakers on the design and testing of unique carbon foam heat sinks.

### Accomplishments

- Built and demonstrated a test rig to evaluate heat sink designs.
- Evaluated five different geometries of carbon foams in heat sinks using water cooling as well as air cooling.
- Showed carbon foam heat sinks appear to be much more efficient than current designs.
- Showed air-cooled carbon foam heat sinks appear to be as efficient as conventional water-cooled heat sinks.

### Future Direction

- Test and evaluate different designs of heat sinks for the effect on heat transfer.

- Continue evaluating different joining techniques for the durability and cost.
- Collaborate on functional designs with automakers and advanced integrated power module contractors.
- Verify mathematical model using experimental results.

## Introduction

The components necessary for the high-fuel-economy, low-emission PNGV vehicles require high-power electronics to be smaller and lighter in weight. Overheating and failure of the vehicle electronics becomes a real problem when electronics are reduced in size because the same amount of heat must be dissipated from a smaller volume. A unique graphite foam developed at the Oak Ridge National Laboratory (ORNL) and licensed to Poco Graphite, Inc., promises significant advances in thermal management technology. This unique graphite foam (Figure 1) has a density of between 0.4 and 0.6 g/cm$^3$ and a bulk thermal conductivity of between 150 and 187 W/m·K. Because the foam has a very high and accessible surface area (>4 m$^2$/g) and is open-celled, the overall heat transfer coefficients of foam-based heat exchangers can be up to two orders of magnitude greater than those of conventional heat exchangers. As a result, foam-based heat exchangers could be dramatically smaller and lighter, yet dissipate equal amounts of heat.

Contemporary thermal management has centered around aluminum and copper heat sinks and substrates because of the very high thermal conductivity of those metals (180 W/m·K for aluminum 6061 and 400 W/m·K for copper). However, in automotive applications where weight is a real concern, a lighter-weight thermal management material would be beneficial.

Mesophase pitch-derived graphitic foam can be considered as an interconnected network of graphitic ligaments and thus should exhibit isotropic material properties. More important, such a foam will exhibit extremely high thermal conductivities along the ligaments of the foam (up to 5 times better than copper) and therefore will exhibit high bulk thermal conductivities. Metallic foams, because of their lighter weight, are also being explored as a potential thermal management material. However, the thermal conductivities are still low, 5–50 W/m·K (1). Existing carbon foams are typically reticulated glassy carbon that exhibits thermal conductivities of less than 1 W/m·K.[1–4] The pitch-derived graphitic foams reported here (Figure 1) exhibit a spherical morphology, and they present a unique solution to this problem by offering high thermal conductivity with a low weight.

## Experimental

In order to characterize the behavior of the foam as a heat sink, a test chamber (Figure 2) was built to quantify its power dissipation capacity. As shown in Figure 2, the foam is mounted to an aluminum plate (usually by brazing) and placed in a cavity where the cooling fluid flows. The system is designed with no

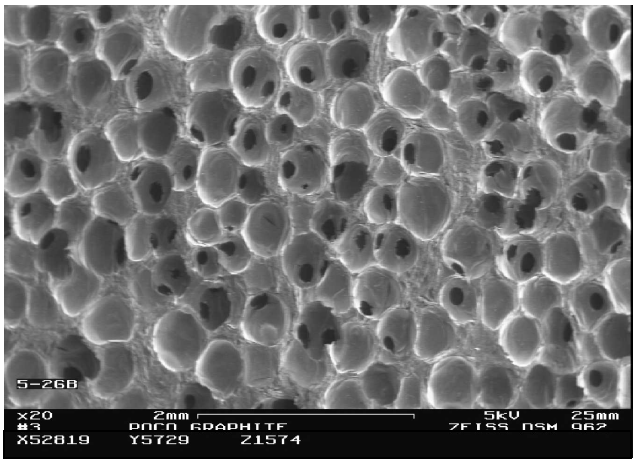


**Figure 1.** High thermal conductivity graphite foam.

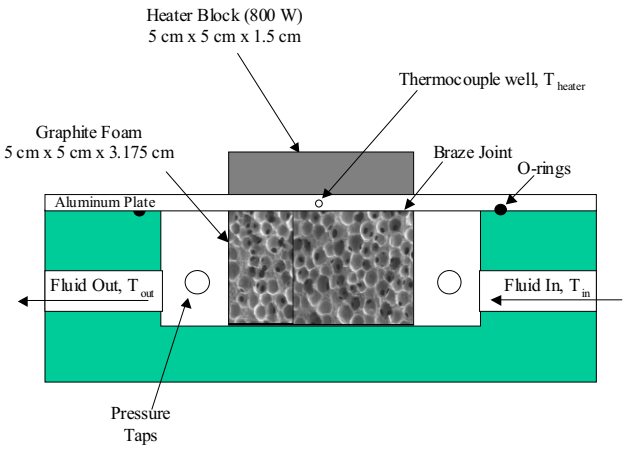


**Figure 2.** Schematic of test rig.

gap around the foam, thereby forcing the fluid to pass through the pores of the foam. The system is sealed with O-rings, and pressure taps are inserted into the chamber to measure the pressure drop of the system. A simulated power inverter (cartridge heaters in a 5 × 5 × 2 cm aluminum block) is mounted to the aluminum plate; it is capable of generating up to 800 W (32 W/cm$^2$). As the cooling fluid passes through the system, the temperatures of the heater and of the inlet and outlet fluid are measured. The overall heat transfer coefficient ($U_o$) is calculated from Eq. (1) where $\Delta T_{LM}$ is the log mean temperature difference, $A$ is the area (foot print) of foam attached to the aluminum plate, and $q$ is the heat dissipated to the cooling fluid.

$$U_o = q/(A \cdot \Delta T_{LM}) \quad (1)$$

To fully investigate the behavior and mechanisms of heat transfer utilizing the graphite foam, several different designs of the foam structure were evaluated. Solid blocks of carbon foam were evaluated initially, but they exhibited significant pressure drops. A number of carbon foam geometries (Figure 3) were evaluated to reduce the pressure drop while maintaining the high heat transfer. The first concept was to mimic current finned heat sinks, which was expected to result in the lowest pressure drop. The second design was a pin-finned heat sink, which should exhibit better performance than the finned design, but at a slightly higher pressure drop. The third design was to incorporate holes perpendicular to the fluid flow and intended to reduce the volume of foam, thereby reducing the pressure drop. The last design (not shown) was to incorporate blind holes parallel to the fluid flow and was intended to reduce the pressure drop further than did the previous example.

## Results

In the first experiment, a solid block of foam (5 × 5 × 3.175 cm) at a density of 0.47 g/cm$^3$ was brazed to the aluminum using SuperBraze® low-temperature braze. Ambient air was passed through the foam at 140, 280, and 420 L per minute. The overall heat transfer coefficient versus airflow is plotted in Figure 4. As can be seen, the overall heat transfer coefficient is very high compared with that of standard heat sinks (70 W/m$^2$·K) and continues to increase with increasing air flow.

The experiment was repeated with process water instead of air as the coolant (0.5 to 0.8 gpm) (Figure 5). The results indicate a dramatic improvement over conventional systems (heat transfer coefficient of ~250 W/m$^2$·K). Following this test, the modified heat sink designs were tested with both air

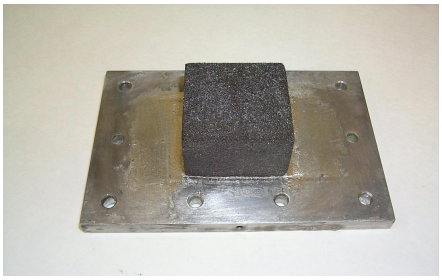

**Solid foam**

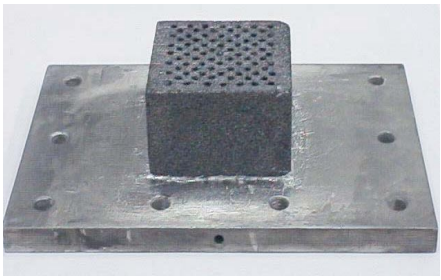

**Vertical blind holes**

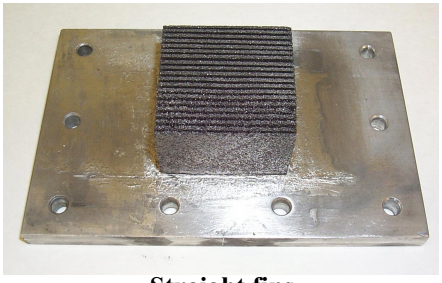

**Straight fins**

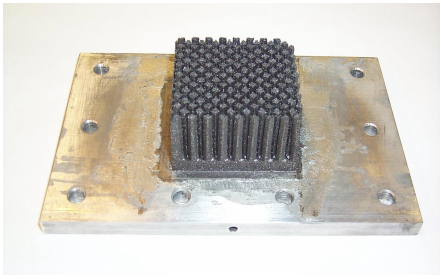

**Pin-fin**

**Figure 3.** Designs of foam substrates evaluated for heat transfer and pressure drop.

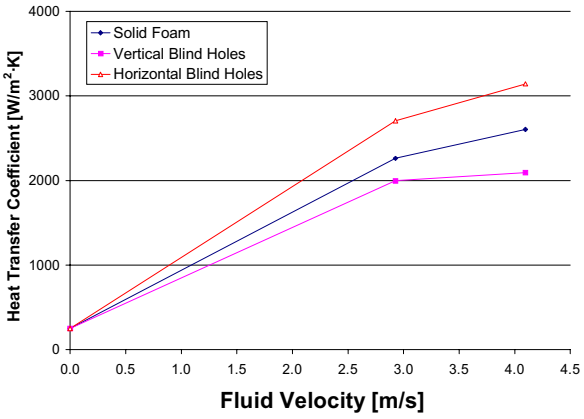


**Figure 4.** Heat transfer coefficient versus air velocity through the foam.

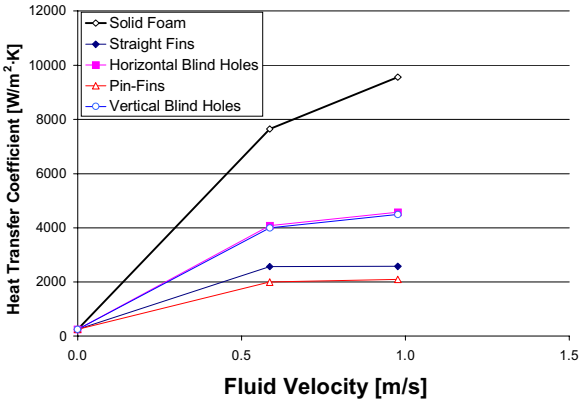


**Figure 5.** Heat transfer coefficient versus water velocity through the foam.

and water cooling (Table 1). As expected, machining fins into the foam reduced the pressure drop to a manageable level; however, the heat transfer also dropped. The heat transfer coefficients of the finned heat sinks were still more than an order of magnitude greater than those of existing systems. At this time, we do not understand why foams with blind holes parallel to the air flow increased their performance in air while reducing heat transfer with water.

It is noteworthy to compare these results with those obtained using conventional systems for power electronics cooling. For a typical system using water as a cooling fluid, and with a power density of 6.2 W/cm$^2$ on the heat sink, the temperature of the heater was 86°C. It is remarkable that similar results were attained using air as the cooling fluid and using the graphite foam. The most desirable design is to use air and eliminate the need for recycling cooling liquids, thereby reducing the overall size and weight of the radiator.

Finally, a mathematical model for the prediction of heat transfer in the foam to a cooling fluid was developed in collaboration with the University of Tennessee. This model utilized the physical parameters of the foam and standard fluid dynamics to predict heat transfer coefficients in the graphite foams. The model has been verified at only one data point and will be verified at many different operating conditions in the coming year.

**Table 1.** Correlated results of heat sink testing with air and water cooling

| | Heat Transfer Coefficient h (W/m²·K) | | P/L (psi/in) | Thermal Resistance °C/W |
|---|---|---|---|---|
| Solid Foam | Air | 2600 | 2 | 0.13* |
| | Water | 9000 | 1 | 0.04 |
| Finned | Air | 1000 | <0.05 | 0.38* |
| | Water | 2100 | 0.5 | 0.19 |
| Pin-Fin | Air | 1500 | 0.05 | 0.26* |
| | Water | 2500 | 0.5 | 0.15 |
| Blind-holes (pin fin negative) | Air | 2000 | 1 | 0.19* |
| | Water | 4600 | 0.5 | 0.09 |
| Blind-holes (parallel to air flow) | Air | 3100 | 0.35 | 0.13* |
| | Water | 4500 | 0.5 | 0.09 |

## Conclusions

The high-conductivity graphite foam presents a unique solution to the increasing cooling demands of power electronics and other automotive components. Novel carbon foam heat sinks were proved to be much more efficient (an order of magnitude increase in heat transfer coefficient) than conventional copper or aluminum heat sinks. These carbon foam heat sinks appear to be able to cool electronics adequately with less than half the water flow rates used in conventional designs. The increased efficiency will be realized in weight savings because the heat sinks will be smaller, they will utilize less cooling water, and the carbon foam is approximately 1/15 the density of aluminum and 1/18 the density of copper. These novel heat sinks are so efficient that air cooling may be adapted, which would simplify and further reduce the size and weight of the cooling system.

## References

1. L. J. Gibson, M. F. Ashby, *Cellular Solids: Structures & Properties* , Pergamon Press, New York, 1988.
2. L. R. Glicksman, M. Schuetz, and M. Sinofsky, *A Study of Radiative Foam Heat Transfer through Foam Insulation,* a report prepared by Massachusetts Institute of Technology under subcontract No. 19X-09099C, 1988.
3. Ultramet Product Literature, 1998.
4. D. Doermann and J. F. Sacadura, *J. of Heat Transfer* **118**, 88–93, 1996.

## FY 2000 Publications

J. W. Klett, C.-C. Tee, D. P. Stinton, and N. A. Yu, "Heat Exchangers Based on High Thermal Conductivity Graphite Foam," in *Proceedings of the 1st World Conference on Carbon* , July 9–13, Berlin, Germany (2000).

J. Klett, A. McMillan, and R. Ott, "Heat Exchangers for Heavy Vehicles," in *Proceedings of the Society of Automotive Engineering Government/ Industry Meeting* , Washington, D.C., June 19–21, 2000.

J. Klett, L. Klett, T. Burchell, and C. Walls, "Graphitic Foam Thermal Management Materials for Electronic Packaging," in *Proceedings of the Society of Automotive Engineering Future Car Congress* , Crystal City, Washington, D.C., April 2–6, 2000.

J. Klett and B. Conway, "Thermal Management Solutions Utilizing High Thermal Conductivity Graphite Foams," in *Proceedings of the 45th International SAMPE Symposium and Exhibition* , Long Beach, California, May 21–25, 2000.

J. Klett, R. Hardy, E. Romine, C. Walls, and T. Burchell, "High-Thermal-Conductivity, Mesophase-Pitch-Derived Carbon Foams: Effect of Precursor on Structure and Properties," *Carbon*, **32**(8), 2000.

C. C. Tee, J. W. Klett, D. P. Stinton, and N. Yu, "Thermal Conductivity of Porous Carbon Foam," in *Proceedings of the 24th Biennial Conference on Carbon*, July 11–16, Charleston, South Carolina (1999), p. 130.

## Awards

2000 B. T. Kelley Award, British Carbon Group

R&D 100 Award, "High Thermal Conductivity Carbon Foam"

## Patents Issued

"Process for Making Carbon Foam," U.S. Serial Number 6,033,506, Oak Ridge National Laboratory.

"Pitch-Based Carbon Foam Heat Sink with Phase Change Material," U.S. Serial Number 6,037,032, Oak Ridge National Laboratory.

# B. dc Buss Capacitors for PNGV Power Electronics

*B. A. Tuttle, D. Dimos, D. Wheeler, G. Jamison, P. G. Clem, and P. Yang*
*MS 1411, Sandia National Laboratories, P.O. Box 5800*
*Albuquerque, NM 87185-1411*
*(505) 845-8026; fax: (505) 844-9781; e-mail: batuttl@sandia.gov*

*DOE Program Manager: Patrick Davis (202) 586-8061; fax: (202) 586-9811; e-mail: patrick.davis@hq.doe.gov and David Hamilton (202) 586-2314; fax: (202) 586-9811; e-mail: david.hamilton@hq.doe.gov*
*ORNL Technical Advisor: David Stinton (865) 574-4556; fax: (865) 574-6918; e-mail: stintondp@ornl.gov*

---

*Contractor: Sandia National Laboratory, Albuquerque, New Mexico*
*Prime Contract No.: 04-94AL85000*

---

## Objectives

- Develop a replacement technology for presently used aluminum electrolytic dc buss capacitors for year 2004 new-generation vehicles.
- Develop a high-temperature polymer dielectric film technology that has dielectric properties technically superior to those of aluminum electrolytic dc buss capacitors and is of comparable or smaller size. The projected high-volume manufacturing cost for a 500-microfarad 600-volt polymer film capacitor is on the order of $30.
- Develop a low-cost multilayer ceramic technology that results in capacitors that are technically superior to presently used aluminum electrolytic capacitors. Cost targets for ceramic capacitors are approximately $100.

## OAAT R&D Plan: Section 3.5: Task 4; Barriers A, B, C, D

## Approach

- Work with automobile design and component engineers, dielectric powder and polymer film suppliers, and capacitor manufacturers to determine state-of-the-art capabilities and to define market-enabling technical goals.
- Develop a project plan with General Motors (GM) engineers to develop a polymer film dielectric material worthy of large-scale commercialization and to deliver sufficient dielectric material to meet 2004 PNGV requirements.
- Synthesize unique conjugated polyaromatic chemical solution precursors that result in dielectric films with low dissipation factors (DFs) and excellent high-temperature dielectric properties.
- Use a molecular engineering approach to create higher polarizabilities in polymer films leading to higher dielectric constants (K): In FY 2000, four different polymer structural families were investigated.
- Fabricate, microstructurally analyze, and electrically characterize barium titanate and lead-based ceramic dielectrics in layers of suitable thickness.

## Accomplishments

- Developed chemical synthesis procedures that resulted in polyfilms of K = 6 and DFs of 0.013 at 25$^{o}$C and suffered no loss in dielectric constant at 1 MV/cm fields. While the dielectric constants of the films fabricated at Sandia National Laboratory are a factor of 2 greater than those of state-of-the-art polyphynelene sulfide and are satisfactory, the DF is just slightly above the DF <0.01 requirement for commercialization.

- Synthesized and evaluated four different structural polymer families to obtain high-K polyfilm dielectrics. These structural polymer families were
  - — Sol-gel siloxane films
  - — Silicone modifications to polyaromatic backbone
  - — Push-pull donor–acceptor groups
  - — Bis-imide chemistry
- Fabricated ultra-low-fire ceramic dielectrics with high permittivity that met or exceeded manufacturer's specifications and that were compatible with low-cost 90/10 Ag electrodes. Used electron paramagnetic resonance to determine site occupancy in base metal electrode dielectric formulations.

## Future Direction

- Enhance dielectric constant of polymer film dielectrics to greater than 6 and keep DF below 0.01. High-volume capacitor manufacturers have stated that these properties would initiate commercial development.
- Perform extensive electric field and temperature characterization to determine that the Sandia polyfilm dielectrics will meet the PNGV requirements (K = 6, DF < 0.01) for temperatures up to 110°C and fields of 1 to 2 MV/cm.
- Interface with the appropriate scale-up company to fabricate 10-kg to 20-kg lots of polyfilm dielectrics that are suitable for fabrication into multilayer capacitors (>200 μF) by AVX/TPC. The scale-up company chosen will depend on the polymer film chemistry.
- Complete evaluation by GM and Sandia, in simulated electric hybrid vehicle environments, of large-value (greater than 200 μF) capacitors fabricated by AVX/TPC.
- Develop more cost-effective synthesis routes for polymer film dielectrics that meet 2004 PNGV requirements.

---

## Results

### *Strategy and Interactions*

Sandia has actively interacted with a number of representatives from the automobile industry to obtain their perspective on what is needed for PNGV automobiles.

The two most viable replacement technologies for the electrolytic dc buss capacitors by 2004 are multilayer polymer film capacitors and multilayer ceramic capacitors. Reduction in the size of the polymer capacitors was most often cited by automobile design engineers as a needed enabling technology. For polymer film dielectrics, a goal for commercialization of a dielectric constant of 6 and a DF of less than 0.01 has been agreed to by AVX/TPC and GM. Once the film technology has been developed by Sandia, 10-kg to 20-kg batches will be synthesized and fabricated into 3-μm-thick polymer films. AVX/TPC has agreed to fabricate 200-μF capacitors from 10-kg lots of our polymer film dielectrics.

The greatest concern for the multilayer ceramic capacitors (Figure 1) was cost. The electrodes comprise roughly 95% of the total cost of a ceramic multilayer capacitor. The industry would like to have higher field operation for low-cost multilayer ceramic technologies, such as base metal (BME) and ultra-low-fire (ULF) dielectrics. Both the BME and ULF technologies substantially reduce the cost of multilayer ceramic capacitors by permitting the use of lower-cost nickel or silver electrodes instead of high-palladium-content electrodes.

Inverter designs and operating conditions for dc buss capacitors vary from manufacturer to manufacturer. Frank Zollner of GM has presented 2- to 5-year and 10-year goals for dc buss capacitors that other auto manufacturers feel are satisfactory milestones for the PNGV program. Specific goals for 2004 commercialization include (1) –40 °C to 110°C operation, (2) greater than 2-μF/cm$^3$ capacitance density, and (3) 575 volts dc with a 600-volt peak for 50-ms operation. In addition, GM has requested fail-safe operation; Ford and Daimler-Chrysler have

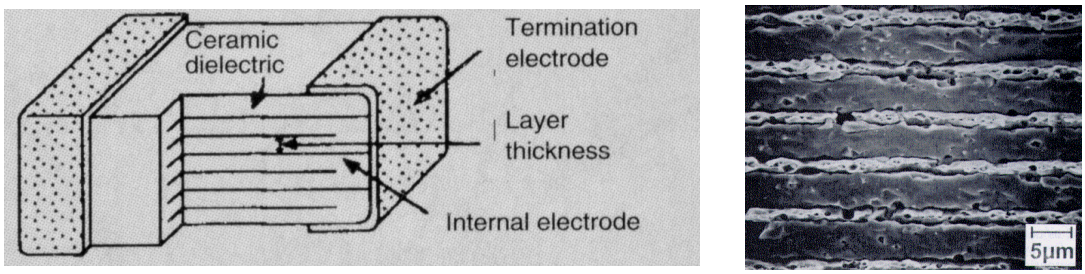


**Figure 1.** Multilayer ceramic capacitor schematic and micrograph of cross-sectional view.

not voiced as strong an opinion regarding the fail-safe criterion. The fail-safe criteria are analogous to soft breakdown of the dielectric, rather than catastrophic electrical discharge and mechanical failure that can be observed in bulk ceramic dielectrics. Soft breakdown results from the vaporization of the thinner electrode layers of the polymer dielectric near electrical breakdown sites.

Based on these criteria, an individual dielectric layer thickness of approximately 3 µm for polyfilm and 40 µm for ceramic capacitors is projected. These thickness values are based on operating field strengths of 2 MV/cm and 150 kV/cm for newly developed polyfilm and ceramic dielectric capacitors, respectively. Based on these assumptions and on measurement of presently available commercial capacitors, size comparisons and capacitance densities of 500 µF dc buss capacitors for different technologies were obtained (Figure 2). While size and outstanding temperature performance are advantages for the ceramic technologies, soft breakdown behavior and lower cost are assets for polymer film capacitors. The projected polymer film capacitor volume is calculated assuming there is 40% non-active capacitor space and 200-nm-thick electrodes are used. Note that the volumetric capacitance efficiency for a K = 6 polyfilm capacitor of 3.2 µF/cm$^3$ exceeds the 2004 commercialization goal of 2 µF/cm$^3$.

## Polymer Film Dielectric Development

SNL polymer film dielectric development has been based on the request from manufacturers that the new polyfilm dielectrics have voltage and temperature stability equivalent to those of present polyphenylene sulfide technology. Thus a structural family of polymer dielectrics has been designed and synthesized to meet two of the most stringent PNGV requirements: (1) low dielectric loss and (2) extremely good temperature stability. Figure 3 shows a schematic diagram of Sandia's conjugated, polyaromatic-based structure and indicates the large number of molecular modifications to this structure that are possible. Our present effort emphasizes molecular engineering of higher-polarizability structures that will enhance dielectric constants, yet retain acceptable dielectric loss characteristics. A patent disclosure[1] has been initiated covering the design and synthesis techniques for this polymeric family. Three initial molecular modifications to the base structure were made: (1) propyl bridge substitution, (2) sulfur bridge substitution, and (3) replacement of R-side groups with high-electronegativity fluorine ions to enhance polarizability.

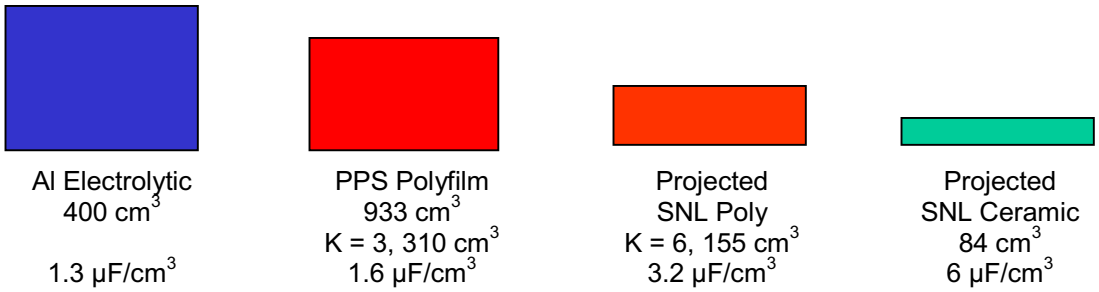


**Figure 2.** Size diagram of 500 µF dc buss capacitors of different technologies.

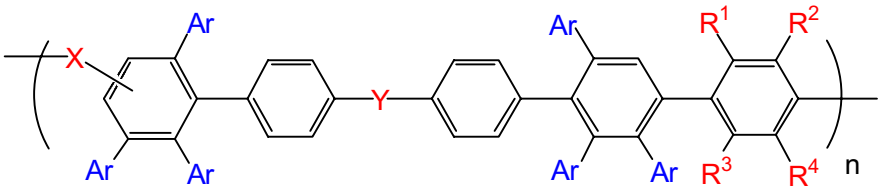


**Figure 3.** Schematic diagram of Sandia conjugated polyaromatic film base structure.

The dielectric properties of a series of films from this structural family resulted in films that were stable with respect to voltage and temperature as shown in Figures 4 and 5. We increased the dielectric constant compared with industry standard PPS from K = 3 to K = 4, while maintaining similar loss and breakdown field characteristics. However, the dielectric constants were below the desired value of 6.

For FY 2000, we have investigated four different polymer film structural families to enhance K. Figure 4 shows a schematic diagram of the structures of the Sol-gel siloxane structure. The sol-gel siloxane family is typified by a large volume percentage of silicone with limited amounts of electric-field-stable polymer. Figure 5 shows a comparison of the K vs electric field behavior for four different polyfilms fabricated in this program. While the sol-gel siloxane film has a dielectric constant of greater than 6 at low field, as the field increases to PNGV operating levels (1000 to 2000 kV/cm), its dielectric constant decreases below that of the Sandia poly-conjugated aromatic films with a fluorine side group substituted. The Sandia fluorine-side-group polymer had a K = 4.6, which was not of sufficient magnitude for commercialization.

We have recently developed a 3-methyl-4 nitro-anisole side group chemical synthesis route for our polyconjugated base structural family. The anisole modification has the potential for enhanced

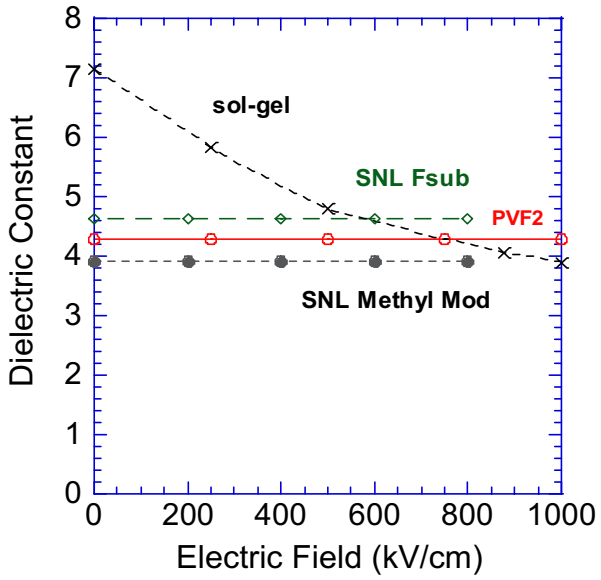


**Figure 5.** Dielectric constant versus field for several polymer film structural types.

polarizability but lower loss. A plot of the dielectric constant and DF vs field of this dielectric is shown in Figure 6. While the dielectric constant remains above 6 as desired, the DF creeps slightly above our 0.01 requirement as field is increased from 0.5 MV/cm to 1 MV/cm fields. Further molecular modifications are being invoked to tie up the molecular groups that cause an increase in high-field DF, while maintaining the polarizability

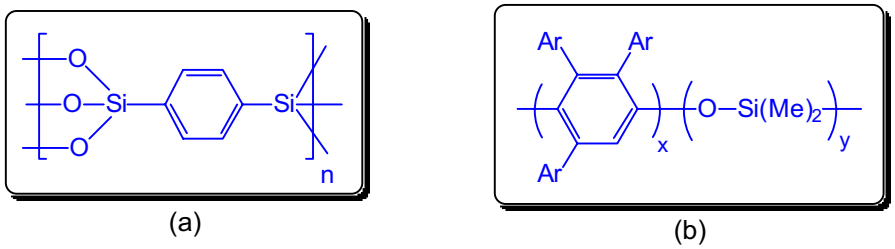


**Figure 4.** Schematic diagrams of (a) sol-gel siloxane chemistry and (b) silicone modified polyconjugated aromatics.

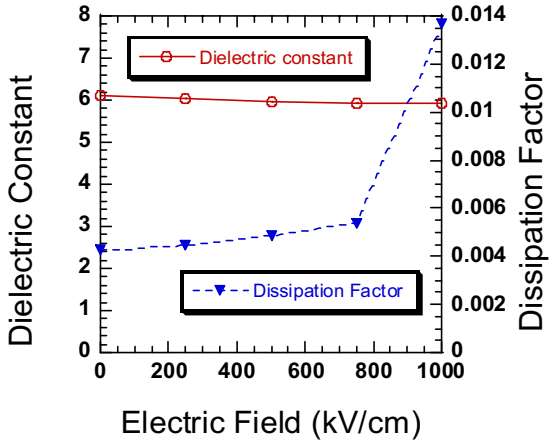


**Figure 6.** Dielectric constant and dissipation factor of SNL anisole push-pull film.

enhancement of the anisole substitution. A slight improvement will lead to polyfilms suitable for commercialization.

## Summary

Critical economic and technical issues for improvement of dc buss capacitors for new generation vehicles were determined through discussions and visits with automobile design engineers and capacitor manufacturers. Polymer film dielectric development has been emphasized in FY 2000, and we have obtained consensus for a project plan for large-scale commercialization of polymer film dc buss capacitors with AVX/TPC and GM. We have been able to fabricate new polymer film dielectrics with a 100% increase in dielectric constant compared with industry standards, while maintaining reasonable electric field and dielectric loss stability to 0.5 MV/cm. Further molecular engineering investigation and electrical testing are necessary to make the slight improvements necessary to meet both voltage and temperature requirements for commercialization. For ceramic dielectrics, we developed low-fire $BaTiO_3$-based (K = 1020) and PZT-based (K = 1270) dielectrics fired at 950 °C, compatible with low-cost Ag/Pd 90/10 electrodes. We also developed a prototype multilayer system with a capacitance volume density of 12 $\mu F/cm^3$ at low field using 20 µm $BaTiO_3$ layers.

## Technical Disclosures

D. Wheeler and G. Jamison, "Novel polymer film synthesis routes of voltage and temperature stable dielectrics," October 5, 1999.

## Presentations

B. A. Tuttle, D. Dimos, G. Jamison, D. Wheeler, P. Clem, P. Yang, and W. Olson, "DC Buss Capacitors for PNGV Power Electronics," Naval Research Laboratory Power Electronics Workshop, Washington, D.C., June 11, 1999 (invited).

P. G. Clem, B. A. Tuttle, P. Yang, and D. Dimos, "Direct Write Fabrication of Multilayer Capacitors and Integrated Passives," ACerS Pacific Coast Regional meeting, Bellevue, Washington, October 26, 1999 (invited).

P. G. Clem, B. A. Tuttle, D. Dimos, and P. Yang, "Direct Write Fabrication of Multilayer Capacitors and Integrated Passives," Center for Dielectric Studies Meeting, November 16, 1999 (invited).

D. Hamilton, D. Stinton, B. A. Tuttle, and coworkers, "Capacitor Materials for Power Electronics," Future Car Congress, Arlington, Virginia, April 2, 2000 (invited).

B. A. Tuttle, D. Dimos, D. Wheeler, G. Jamison, P. G. Clem, and P. Yang "Dielectric Materials for Hybrid Electric Vehicles," Passive Components for Power Electronics Meeting, The Pennsylvania State University, April 27, 2000 (invited).

# C. Mechanical Reliability of Electronic Ceramics and Electronic Ceramic Devices

*M. K. Ferber and A. A. Wereszczak*
*Mechanical Characterization and Analysis Group*
*Oak Ridge National Laboratory, P.O. Box 2008, MS 6069, Bldg. 4515*
*Oak Ridge, TN 37831-6069*
*(865) 576-0818; fax: (865) 574-6098; e-mail: ferbermk@ornl.gov*

*DOE Program Manager: Patrick Davis (202) 586-8061; fax: (202) 586-9811; e-mail: patrick.davis@hq.doe.gov*
*ORNL Technical Advisor: David Stinton (865) 574-4556; fax: (865) 574-6918; e-mail:* stintondp@ornl.gov

*Contractor: Oak Ridge National Laboratory, Oak Ridge, Tennessee*
*Prime Contract No.: DE-AC05-00OR22725*

## Objectives

- Develop testing algorithms that can be used to assess electronic ceramic (EC) and electronic ceramic device (ECD) mechanical reliability.
- Mechanically characterize EC and ECD alternatives that are less expensive and that can be used to promote device miniaturization.

## OAAT R&D Plan: Section 3.5: Task 4; Barriers A, D

## Approach

- Utilize micromechanical testing and ceramic-specific-characterization testing facilities to measure in-situ mechanical properties of ECs in the ECDs.
- Characterize presently used and developmental EC and ECDs supplied from their manufacturers or their end-users.
- Use existing ceramic component prediction codes (whose development was funded by the Office of Transportation Technologies for structural ceramics) and their statistical analysis capabilities in the mechanical strength and fatigue analyses of ECs and ECDs.
- Provide results and insights back to manufacturers that will result in the improved reliability of ECs and ECDs.

## Accomplishments

- Measured the thermal expansion and thermal conductivity as a function of temperature (–50 to 200°C) for monolithic $BaTiO_3$ and a variety of multilayer capacitors (MLCs). These data will be used to model and predict thermal shock susceptibility.
- Completed the mechanical testing of three aluminas during FY 2000; the data will be used by Motorola to design a more thermal-shock-resistant exhaust gas sensor.
- Fabricated special fixturing that will be used in concert with Raman spectroscopy to non-destructively measure the in-situ residual stresses of MLCs.
- Extended the mechanical testing algorithms, which were developed to characterize the mechanical robustness and reliability of small capacitors, to larger dc-buss capacitors.

### Future Direction

- Develop the Raman spectroscopy technique to measure residual stresses as a function of position in MLCs.
- Develop quantifiable thermal shock methodology for MLCs to establish guidelines concerning soldering conditions and maximum allowable temperature excursions.
- Develop micromechanical tests to directly assess the strength of MLCs.

---

## Introduction

A lack of mechanical reliability of ECs in ECDs will limit the life of their electronic functioning. The primary effort in FY 2000 involved the thermal property characterization of $BaTiO_3$ ECs in power electronic capacitor ECDs. Work was completed as well in FY 2000 on oxide ECs for automotive exhaust gas sensor ECDs. The service life of both these ECDs can be limited by their mechanical reliability, so it is essential that that limitation be understandable and predictable.

## Ceramic MLCs for Automotive Power Electronics

Manufacturers must exercise caution during their fabrication of MLCs because these ECDs are relatively large (Figure 1), and experience has taught manufacturers that MLCs can be susceptible to thermal failure if thermal gradients become sufficiently high. Likewise, end-users of these ECDs must minimize the possibility of thermal excursions to avoid producing failures induced by thermal shock. A goal of this project is to help MLC manufacturers quantify thermal properties so that they and their customers may quantitatively predict allowable thermal excursions that do not produce thermal fracture.

To understand and predict thermal shock susceptibility, three property sets must be known as a function of temperature: thermal expansion, thermal conductivity, and mechanical strength. Thermal expansion and thermal conductivity were measured between –50 and 200°C (a temperature range of interest to the automotive industry). Their dependencies on temperature are shown in Figures 2 and 3. In both graphs, the thermal expansion and conductivity of monolithic $BaTi0_3$ are compared with apparent values of some capacitors shown in Figure 1. Thermal expansion of the SM02 MLC (the largest capacitor shown in Figure 1) and that of $BaTi0_3$ are arguably equivalent. The thermal

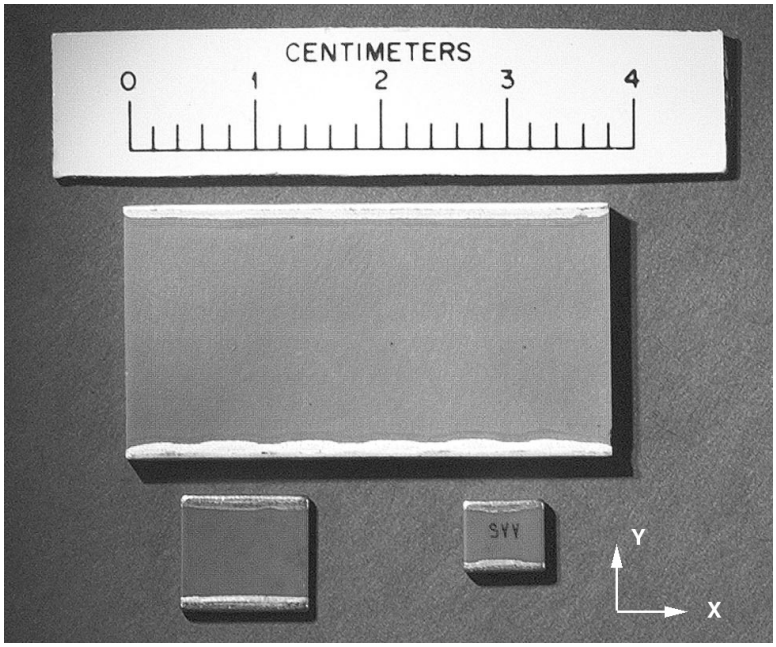


**Figure 1.** Example of multilayer capacitors of various sizes.

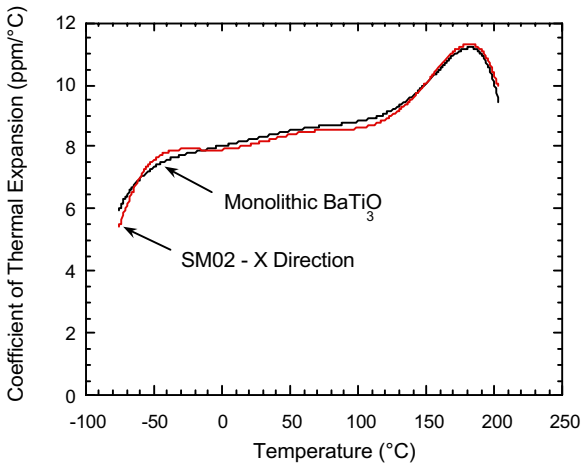


**Figure 2.** Variation in coefficient of thermal expansion with temperature for $BaTi0_3$ and SM02 MLC.

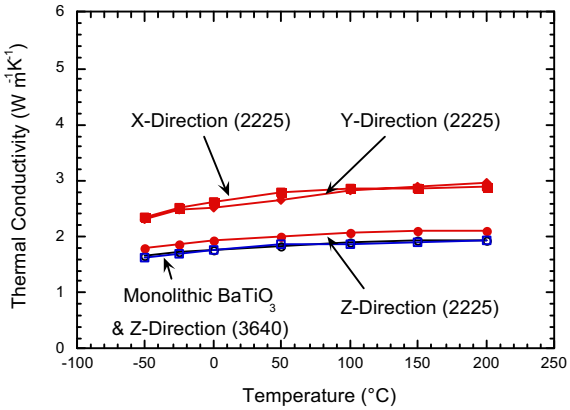


**Figure 3.** Directional dependence of the thermal conductivity.

conductivity of 2225 and 3640 MLCs (right and left, respectively, in Figure 1) in the Z-direction is equivalent to that of monolithic $BaTi0_3$, while it has a higher value in the X and Y directions. The explanation resides with the effects of the electrode metal in these MLCs. The electrode is an overall small volume fraction (≈5%) of these MLCs, so its higher thermal expansion compared with that of monolithic $BaTi0_3$ is insignificant. Even though the thermal conductivity of the electrode metal is approximately 2 orders of magnitude larger than that of $BaTi0_3$, its small volume fraction and transversely isotropic orientation within the MLC contribute little to the apparent thermal conductivity in the Z direction, while slightly increasing the apparent thermal conductivities in the X and Y directions. These data may now be used to model and predict thermal shock susceptibility (once the mechanical strength is known).

Residual stresses in these ECDs are an important consideration in assessing their mechanical reliability. To enable measurement of the residual stresses, special fixturing was fabricated that will be used in concert with Raman spectroscopy. $BaTiO_3$ specimens will be loaded in compression, using the fixture, while a Raman spectrum is generated. As the specimens are loaded to known, higher stresses, a spectrum will be generated for each. The spectra will then be analyzed to examine peak shifts as a function of stress, and a "calibration" curve will result. That calibration curve will then be used with subsequent Raman analyses on MLCs to in-situ (and nondestructively) measure their residual stresses. These residual stresses superimpose on the thermal stresses arising from the thermal expansion and conductivity effects measured above, so acknowledgment of their effects is important to the overall understanding of the mechanical reliability of these MLCs.

## Strength and Fatigue of Alumina for Automotive Exhaust Gas Sensors

Motorola is developing a hydrocarbon exhaust gas sensor, and this project has assisted in its development. The sensor is a multilayer design and will be using alumina as a matrix; however, an alumina with optimum strength and fatigue (that also is inexpensive) has not yet been identified. The mechanical testing of three aluminas was initiated during FY 1999 to measure their strength as a function of temperature, as well as their fatigue performance, and was completed in early FY 2000. The highest purity of alumina examined had the lowest strength at room temperature, while the least pure alumina had the highest strength. However, the strength of the highest-purity alumina was the greatest of the three at 1000°C, and its fatigue resistance was also the highest of the three at room temperature. The thermal expansion and thermal conductivity behaviors of the three were equivalent, suggesting that their strength differences (along with their relative costs of manufacture) must serve as the focus in the choice of which to use for the sensor.

## Conclusions

The mechanical reliability of MLCs has been evaluated from measurements of strength and

thermal properties and by numerical analysis of the residual stresses. This information is currently being used by MLC manufacturers to quantitatively predict allowable thermal excursions that do not produce thermal fracture.

## Publications

A. A. Wereszczak, L. Riester, J. W. Hill, and S. Cygan, "Mechanical and Thermal Properties of Power Electronic Ceramic Multilayer Capacitors," *Ceramic Transactions, Proceedings of the American Ceramic Society*, 2000, in press.

A. A. Wereszczak, K. Breder, L. Riester, T. P. Kirkland, and R. J. Bridge, "In-Situ Mechanical Property Evaluation of Dielectric Ceramics in Multilayer Capacitors," SAE Paper 00FCC-116, SAE 2000 World Congress, Arlington, Virginia, April 2000.

A. A. Wereszczak, A. S. Barnes, and K. Breder, "Probabilistic Strength of {111} n-Type Silicon," *Journal of Materials Science: Materials in Electronics*, **11**, 291–303 (2000).

A. A. Wereszczak, T. P. Kirkland, K. Breder, H.-T. Lin, and M. J. Andrews, "Biaxial Strength, Strength-Size-Scaling, and Fatigue Resistance of Alumina and Aluminum Nitride Substrates," *International Journal of Microcircuits and Electronic Packaging*, **22**(4), 446–458 (1999).

K. Breder, A. A. Wereszczak, L. Riester, and T. P. Kirkland "Determination of Strength for Reliability Analysis of Multilayer Ceramic Capacitors," pp. 565–72 in *Ceramic Engineering and Science Proceedings*, Vol. 20, 1999.

A. A. Wereszczak, R. A. Scheidt, M. K. Ferber, and K. Breder, "Probabilistic Thermal Shock Strength Testing Using Infrared Imaging," *Journal of the American Ceramic Society*, **82**, 3605–08 (1999).

A. A. Wereszczak, K. Breder, L. Riester, T. P. Kirkland, and R. J. Bridge, *Toward the Assessment of Mechanical Robustness of Ceramic Multilayer Capacitors (MLCs)*, ORNL/TM-1999/202, Oak Ridge National Laboratory, October 1999.

# D. Low-Cost, High-Energy-Product Permanent Magnets

*Tom M. Mulcahy and John R. Hull*
*Energy Technology Division, Argonne National Laboratory, Bldg. 335*
*Argonne, IL 60439*
*(630) 252-61451; fax: (630) 252-5568; e-mail: mulcahy@anl.gov*

*DOE Program Manager: Patrick Davis (202) 586-8061; fax: (202) 586-9811; e-mail: patrick.davis@hq.doe.gov*
*ORNL Technical Advisor: David Stinton (865) 574-4556; fax: (865) 574-6918; e-mail: stintondp@ornl.gov*

---

*Contractor: Argonne National Laboratory, Argonne, Illinois*
*Prime Contract No.: W-31-109-Eng-38*

---

## Objectives

- Develop a low-cost process to fabricate NdFeB permanent magnets with up to 25% higher strengths. The higher-strength magnets will replace ones made by traditional powder metallurgy and enable significant size and weight reductions in traction motors for hybrid vehicles.
- Use high-strength superconducting magnets to improve the magnetic alignment of grains prior to pressing and sintering, therefore producing higher-strength permanent magnets.

## OAAT R&D Plan: Section 3.5: Task 3; Barriers B, C, D

## Approach

- Develop facilities to align magnetic domains of NdFeB powders within a high-strength magnetic field, created by a superconducting solenoid, during forming operations.
- Collaborate with ORNL to characterize, compare, and correlate engineering and microscopic magnetic properties of magnets processed under varying conditions, including some in current production.
- Use a reciprocating feed to automate insertion of loose and compacted magnet powder into and out of the steady field of a superconducting solenoid.

## Accomplishments

- Established facilities at Argonne National Laboratory to handle pyrophoric NdFeB powder during its processing into green compacts, which the industrial partners will sinter into permanent magnets.
- For the first time, made axial-die-pressed permanent magnets that used a superconducting solenoid [9-Tesla (T)] for magnetic alignment of the powder.
- Characterized magnetic properties of the first permanent magnets made in the Axial-Die Press Facility and those provided by the industrial partners.

## Future Direction

- Report on the optimization of the fabrication processing and powders using axial-die pressing in batch mode operation.

- Design, fabricate, and operate a reciprocating press in a continuous mode to demonstrate the feasibility of competitive factory operation.
- Optimize fabrication processing and powders from different industrial partners, using transverse-die pressing and a reciprocating press.
- Provide design rules for the fabrication of permanent magnets, including knowledge for scale-up to larger magnets at commercial rates of production.

## Introduction

For the first time, a superconducting solenoid (9 T) was used as part of an axial-die press to compact permanent magnets. (Argonne's new facility is shown in Figure 1.) The solenoid aligns the magnetic domains of NdFeB powder during pressing into green compacts for sintering into permanent magnets by industrial partners. Industrial electromagnets are limited to 2 T.

The installation required shielding of sensitive equipment in an adjacent laboratory from stray magnetic fields. Two layers of shielding that now cover the wall between the laboratories are shown in Figure 2.

Magnetic code analysis was helpful in the design of the wall shielding to reduce the level to ~10 Gauss. But to shield below the 5-Gauss threshold sensitivity levels of computer monitors would have been difficult. Shielding enclosures were purchased for two computer monitors.

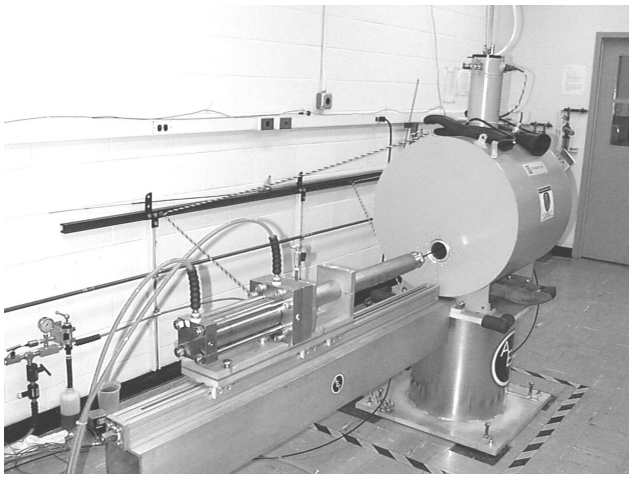

**Figure 1**. The Axial-Die Press Facility. Press tube is remotely moved along a track into the horizontal bore of the 9-T superconducting solenoid.

**Figure 2.** Wall shielding. Press tube fully inserted in bore of superconducting solenoid.

## Results

The innovative press-in-tube device for axial-die pressing magnet compacts in a batch mode was made operational by pressing 25 pure-iron powder compacts. Bronson and Bratton, Inc.'s 5/8-in.-diameter axial-die and punch set, which is similar to the 3/8-in.-diameter set shown in Figure 3, was used. The die/punch set is shown being hand-loaded

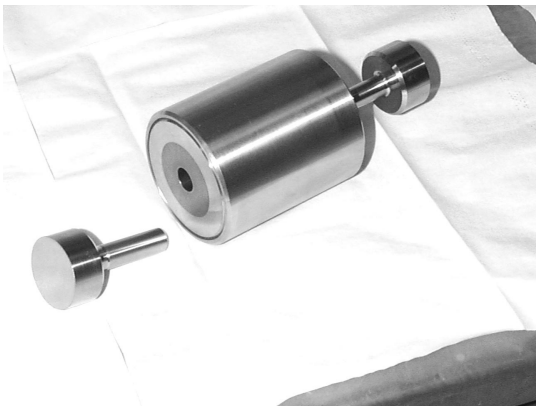

**Figure 3.** One punch removed from 3/8-in. diameter die/punch set.

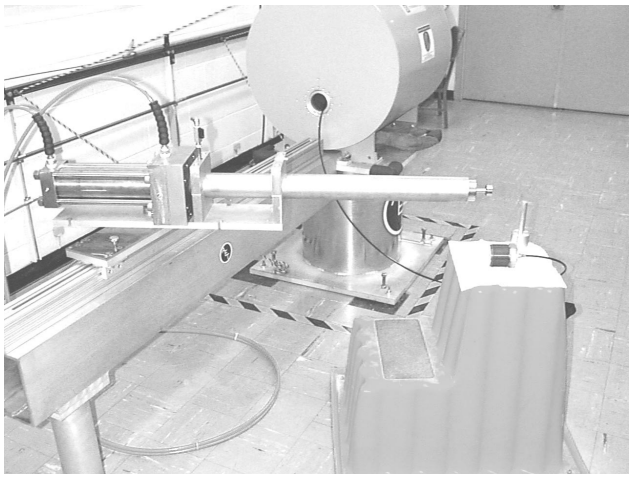

**Figure 4**. Die/punch insertion (right) into press tube, rotated into loading position. Hydraulic cylinder on left end of press tube.

into the press tube in Figure 4, and the press tube is shown in Figures 1 and 2 being moved into the solenoid along the motorized track of the press insertion mechanism. A local manufacturer of die-pressed parts provided the 25-micron-size pure-iron powder, whose grains had no preferred magnetic orientation and were coated with a pressing lubricant. Following procedures developed for processing NdFeB magnet powder, no difficulties were encountered in fabricating compacts over the entire range of expected press and extraction pressures. Pressing operations included extraction of the iron compacts from the superconducting solenoid operating at 8 T, an operation necessary for simulation of compact pressing during automated production using reciprocating feeds. Large extraction forces (up to 750 lb) can occur between the solenoid and compacts.

UGIMAG routinely ships its hazardous NdFeB magnet powder in vacuum-sealed metal pouches. However, requirements for storing the powder at Argonne and shipping the compacts back to UGIMAG for sintering had to be established, using Argonne specialists in waste management and transportation. Material handling of the powder is of critical importance because it can oxidize readily. Oxidation not only is hazardous, but also reduces the percentage of hard magnetic material in the compact and therefore the strength of the sintered magnet. In factory operation, the powder is made into compacts and sintered within two days, all the while being handled in an argon atmosphere.

Since Argonne operations with a batch of powder would extend over weeks, additional handling procedures were identified and implemented in consultation with UGIMAG. Also, press operation in the superconducting solenoid could take tens of minutes, instead of an instant, because of the slow ramp times of the superconducting solenoid's magnetic field. A powder-handling facility to load and eject the compact from the die/punch set with the pyrophoric NdFeB powder was established using a glove box built to fabricate fuel elements for breeder reactors. (See Figures 5 and 6.) During compaction, the press tube is maintained under an argon atmosphere.

Originally, the glovebox was intended for use at oxygen levels of less than 10,000 ppm and with a

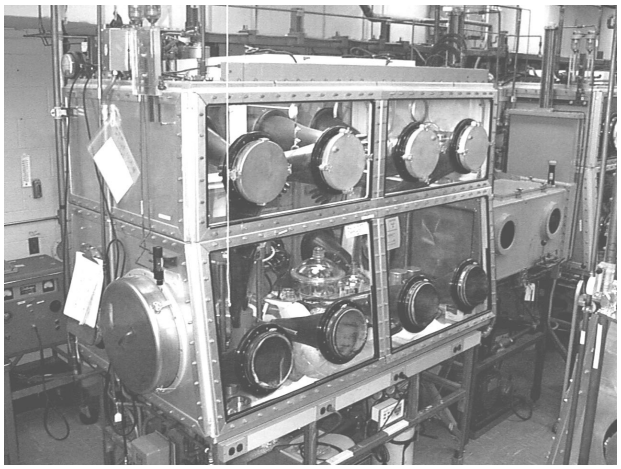

**Figure 5**. Glovebox to store and load magnet powder in die, then eject compact.

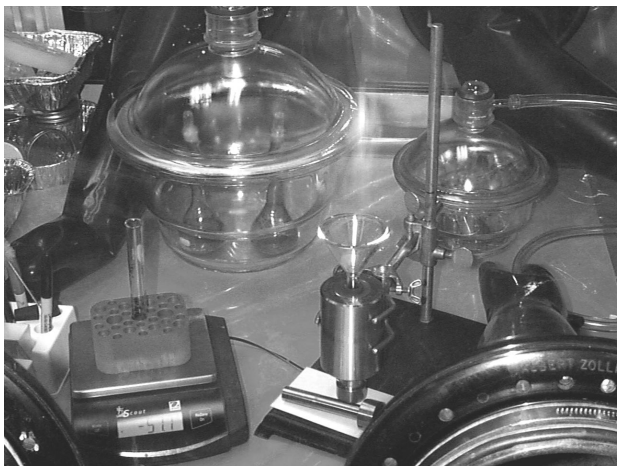

**Figure 6.** Glovebox powder weighing and die filling. Vacuum storage desiccators in rear.

nitrogen cover gas. It was overhauled and improved with a new oxygen sensor that extends measurement capability to 1 ppm. Now the glovebox operates at 350–600 ppm during powder handling operation. To avoid an oxidation buildup over time, the magnet powder and compacts are stored in the vacuum (~30 in. mercury) containers (dry-seal desiccators; Figure 6) during processing and before sintering.

Although no problems were encountered in pressing the pure iron powder, many unexpected hurdles had to be overcome in pressing the smaller 5–10 µm powder into green compacts. Magnetically anisotropic powder was found to be difficult to process because the grains tend to form in chains. The negative magnetic pole of one grain is attracted to the positive pole of another grain. The magnetic bonding between grains inhibits pouring and creates bridging during filling operations, which results in voiding that is difficult to remove prior to pressing. Exacerbating the bridging phenomenon are lubricants added to the powder to facilitate rotation of the grains (easy magnetic axes) into alignment with the orienting magnetic field that is applied during pressing. If gas is trapped in voids as the powder is pressed into a compact, elevated gas pressures may cause internal cracking and promote end capping.

End capping begins at the die wall under the punch when pressure on the punch is reduced to zero, usually as part of the compact ejection process. Friction between the die wall and the compact, developed during pressing, may exceed the forces of elastic rebound during punch unloading and initiate a crack that causes a thin lens of the compact to delaminate under the punch. End capping is not an uncommon problem in the industry, but it is not one of which Argonne was made aware of during the design of the press-in-tube device. The industrial solution of maintaining some pressure on the punches as the compact is ejected from the die cannot be accomplished with the current press design. Control of the other processing parameters was investigated to eliminate compact cracking.

A study was made to identify useable ranges of more than 12 processing parameters. The compaction pressure, rate of loading and unloading, load hold time, and amount of die lubricant were found to be the most sensitive parameters for the control of cracking. The rate of loading was greatly reduced and load times increased by installation of velocity control and shut-off valves in the hydraulic circuit of the press. Success was achieved when the thickness of the die and punch lubrication (1% stearic acid in IPA) was reduced to nearly zero by careful buffing. All these modifications can be interpreted as improving the venting of air during compaction.

Higher magnetic alignment fields may improve the integrity of the compact, but the study results are hard to interpret because the hold time of the load increased, as well. Ramping up and down of the superconducting magnet to 8 T took 90 min, and the load was held during ramping down. Lower field strength took proportionally shorter ramping-down times.

Whole compacts can now be made in any diameter-to-length ratio. However, all of the first 65 compacts made had some end capping and hairline cracking. Fortunately, 38 were long enough for UGIMAG to sinter, slice, and determine their standard B-H curves and magnetic properties. Seven compacts were sintered for each of five different strength alignment fields: 0, 2, 4, 6, 8 T. Table 1 shows selected measurement results for ten of the compacts.

**Table 1.** Magnetic measurements of PMs

| Sample | H(T) | Br(kG) | MGOe | g/cm$^3$ |
|---|---|---|---|---|
| 2-4/25 | 0 | 7.24 | 10.72 | 7.583 |
| 1-5/2 | 0 | 7.28 | 10.82 | 7.582 |
| 2-5/2 | 0 | 7.32 | 10.95 | 7.593 |
| 3-5/12 | 2 | 11.47 | 29.94 | 7.558 |
| 4-5/12 | 2 | 11.19 | 28.15 | 7.561 |
| 5-5/12 | 2 | 11.76 | 31.58 | 7.553 |
| 1-5/15 | 4 | 11.86 | 32.14 | 7.580 |
| 2-5/15 | 4 | 12.25 | 34.73 | 7.587 |
| 1-6/5 | 8 | 12.15 | 33.91 | 7.557 |
| 1-6/6 | 8 | 12.67 | 37.19 | 7.583 |

## Conclusions

For the first time, a facility has been established for pressing permanent magnets in the high fields (9 T) of a superconducting solenoid. The energy product (MGOe) and remnant field Br(kG) showed a strong dependence on the magnitude of the alignment field H(T). Improvements in permanent magnet strength of 25% were found by increasing the alignment field to 8 T from the 2 T typically used in industry. The 8-T magnet strengths are comparable to those obtained in industry. The density (g/cm$^3$) of

the sintered magnets is typical of those produced in the factory and is an indication that oxidation during Argonne's longer processing times is not a problem. Now that compacts can be made in shorter lengths, whose shape effect creates large distortions in alignment at current industrial fields (2 T), improvements of alignment in the higher fields of the superconducting solenoid will be evaluated next.

# E. Low-Cost High Energy-Product Permanent Magnets: Characterization of Microstructure at Texture

*E. A. Payzant*
*Oak Ridge National Laboratory, P.O. Box 2008, MS 6064, Bldg. 4515*
*Oak Ridge, TN 37831-6064*
*(865) 574-6538; fax: (865) 574-3940; e-mail: payzanta@ornl.gov*

*DOE Program Manager: Patrick Davis (202) 586-8061; fax: (202) 586-9811; e-mail: patrick.davis@hq.doe.gov*
*ORNL Technical Advisor: David Stinton (865) 574-4556; fax: (865) 574-6918; e-mail: stintondp@ornl.gov*

*Contractor: Oak Ridge National Laboratory, Oak Ridge, Tennessee*
*Prime Contract No.: DE-AC05-00OR22725*

## Objectives

- Quantify the relationship between processing parameters and the crystal chemistry and microstructure of NdFeB permanent magnets fabricated at Argonne National Laboratory and by commercial suppliers.

## OAAT R&D Plan: Section 3.5: Task 3; Barriers B, C, D

## Approach

- Use advanced electron microscopy and X-ray diffraction techniques at ORNL to precisely determine the effect of processing conditions on microstructure and degree of preferred orientation of product.

## Accomplishments

- Received commercial samples of highly oriented magnets produced by uniaxial and/or isostatic pressing of magnetically oriented powders from Crumax, Inc. (Elizabethtown, Kentucky).
- Undertook an investigation of the microstructure and orientation using electron microscopy and X-ray diffraction; report is in progress.

## Future Direction

- Using the Crumax samples as a baseline of the industry standard, evaluate the benefits of the superconducting magnet processing system under development at Argonne National Laboratory. Samples from Argonne are expected to be received now that the system has been made operational.

## Introduction

High-energy permanent magnets are an important component of the electric motors required to meet the goals of the PNGV program. A higher-energy-product permanent magnet will reduce the weight of the electric motor for a given torque. Energy products in permanent magnets are currently limited by manufacturing processes and are considerably below the theoretical potential.

The best commercial permanent magnets are those made from NdFeB that are prepared using powder metallurgy techniques. Because the crystal structure of NdFeB is tetragonal, the properties are quite anisotropic; that is, the magnitude of the magnetic properties vary as a function of the

crystallographic orientation of a particular crystallite. Going to large single crystals is not an option because a fine grain size is required which limits the size of the magnetic domains and increases the energy product. However, the remanent field, which is an important factor in determining the energy product, can be significantly increased by aligning the individual NdFeB particles before the permanent magnet is sintered into a polycrystalline solid. In an ideal permanent magnet, the bulk magnet would consist of very fine grains all oriented in precisely the same direction.

One method to accomplish this orientation is to orient the NdFeB powder with a high magnetic field during the pressing process before sintering. The stronger the magnetic field, the greater the restoring torque and the less particle misalignment there is likely to be. This phenomenon is well recognized by permanent magnet manufacturers who use the sintering process. They use the largest magnetic fields available in a manufacturable process. These magnetic fields are limited in present manufacturing processes by the cooling and structural requirements of pulsed electromagnets. To obtain higher magnetic fields, the use of superconducting magnets will be required. This approach is being developed by our collaborators Tom Mulcahy and John Hull at Argonne National Laboratory.

Additionally, the oriented powder must be pressed and then sintered. The pressing and sintering steps both can contribute to lowering the final energy product by reducing the preferred orientation or by permitting grain growth. Therefore, the influence of pressing and sintering variables on the microstructure must be considered in order to fully understand the final magnetic properties.

## Approach

The crystal structure, microstructure, texture, and morphology of samples are examined systematically by optical and electron microscopy and diffraction methods during each stage of the production process to identify the critical variables and their optimum values. Through John Hull at Argonne, teaming with U.S. permanent magnet manufacturers Crumax and UGIMAG has been initiated; these companies have supplied initial sintered samples to provide a "present state of the art" baseline for material characterization.

Scanning electron microscopy is another useful technique for determining grain size and morphology (Figure 1). It also permits elemental analysis to look for grain boundary impurities and minor phases that may impact the magnetic properties. It is very important that the NdFeB samples are not magnetized for this study, as any permanent magnetic field will significantly distort the electron beam and defocus the image.

The most important characterization tool for these materials is X-ray diffraction pole figure analysis, by which the magnitude of preferred orientation can be quantitatively determined for NdFeB samples (Figure 2). This technique permits a detailed comparison of the preferred orientation with magnetic property measurements made at Argonne or elsewhere, in order to quantify the impact of the degree of orientation on the magnetic properties.

We have opted to use a chromium X-ray source in order to limit the amount of fluorescent radiation from the NdFeB samples. The wavelength of chromium k-alpha radiation is 2.29Å, which better resolves the diffraction peaks than lower wavelength X-rays. This is important, as the diffraction patterns of NdFeB have a large number of closely-spaced peaks, and overlapping peaks can lead to over estimated intensities in the pole figure spectra.

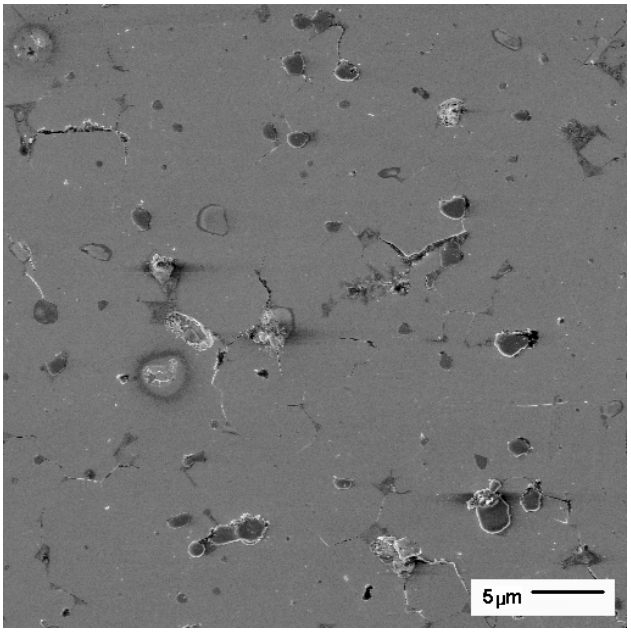


**Figure 1.** Scanning electron micrograph of typical Nd-Fe-B sample from Crumax used to determine grain size and morphology, porosity, and grain boundary phases.

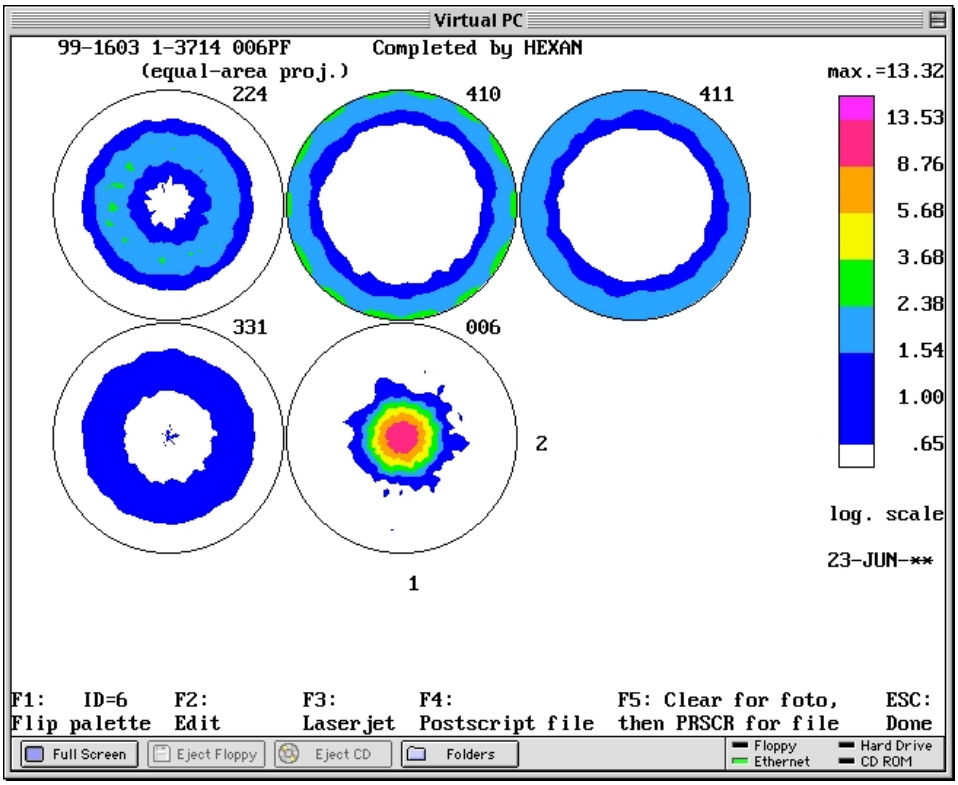


**Figure 2.** Five pole figures of an NdFeB sintered sample (#1-3714) prepared by Crumax using an axial magnetic field that yields a strong c-axis orientation (13 times random for the 006 pole figure) in the direction normal to the examined surface. The three digits to the upper right of each pole figure indicate the Miller indices of the diffracting planes.

Collected pole figures are subsequently analyzed using the best available software packages—PopLA and BEARTEX.

## Results

A detailed characterization of production process effects on the orientation texture in permanent magnets has been undertaken on samples provided from industry. A large set of samples prepared from different powder grades and under different processing conditions were supplied by Crumax.

## Conclusions

The experiments conducted on the Crumax samples have been particularly useful in establishing a "state-of-the-art" baseline with which to evaluate the samples now under production at Argonne. We are fully prepared for this phase of the project.

## Publications/Presentations

None to date.

# 3. FUEL CELLS

## A. Nanopore Inorganic Membranes as Electrolytes in Fuel Cells

*Marc A. Anderson and Flavio M. Vichi*
*Water Chemistry Program, University of Wisconsin–Madison, 660 N. Park St.*
*Madison, WI 53706*
*(608) 262-2674; fax: (608)262-0454; e-mail: nanopor@facstaff.wisc.edu*

*DOE Program Managers: Patrick Davis (202) 586-8061; fax: (202) 586-9811; e-mail: patrick.davis@hq.doe.gov and JoAnn Milliken (202) 586-2480; fax: (202) 586-9811; e-mail: JoAnn.Milliken@hq.doe.gov*

---

*Contractor: University of Wisconsin–Madison*
*Prime Contract No.: DE-FC02-99EE50583*

---

### Objectives

- Develop microporous inorganic membranes of $TiO_2$ with high proton conductivity that are capable of operating at temperatures above 100°C with minimal water management problems.
- Develop methods for depositing platinum on mesoporous ceramic electrolytes.
- Deposit crack-free films of ceramic electrolyte membranes on mesoporous electrodes.
- Fabricate and test an entire proton exchange ceramic membrane fuel cell (PECMFC).

### OAAT R&D Plan: Section 3.3: Task 13; Barriers A, B

### Approach

- Phase 1: (a) Determine conditions under which nanoparticle $Al_2O_3$ and $TiO_2$ sols yield microporous xerogels; (b) Measure proton conductivities of these xerogels as a function of temperature, relative humidity, and membrane thickness; (c) Chemically adsorb anionic or cationic functional groups onto oxide particles contained in xerogels or membranes in order to enhance proton conductivity.
- Phase 2: (a) Develop methods for depositing platinum on asymmetric mesoporous electrodes; (b) Deposit crack-free films of ceramic electrolyte membranes on mesoporous electrodes; (c) Characterize permeabilities of $H_2$ and $O_2$ through the resulting supported membranes under desired conditions of relative humidity and temperature; (d) Fabricate and test an entire PECMFC.

### Accomplishments

- Developed inorganic membranes with high proton conductivity, both as self- standing monoliths and as supported thin films.
- Achieved deposition of platinum on these electrolyte membranes.
- Modified the materials chemically to further enhance their proton conductivity.
- Determined the gas permeation properties for the supported membranes.
- Performed initial crossover studies on the supported membranes.

### Future Direction

- Conclude the crossover studies.
- Send prototype supported membranes for testing at Los Alamos National Laboratory.
- Assemble and test a complete PECMFC.

---

## Introduction

Polymer electrolyte membrane (PEM) fuel cell technologies based on organic polymer membranes (perfluorosulfonated polymer—sold under the trade name of Nafion) may have trouble meeting certain requirements for PEM fuel cell systems. First, the lower operating temperatures required for using these perfluorosulfonic membranes lead to increased costs because of significant platinum requirements and the tendency of the anodes in these cells to foul from CO poisoning. In addition, as operating temperatures are raised, organic polymer membranes are not able to retain water, leading to poor proton conductivity.

The overall objective of this research is to develop fuel cells that incorporate novel ceramic electrolyte membranes based on nanoparticulate oxides, specifically $Al_2O_3$ and $TiO_2$. As we will demonstrate, these high-surface-area porous oxide membranes should be capable of operating at temperatures above 100°C while displaying minimal water management problems. The intrinsic proton conductivities of these materials are expected to be of at least the same order of magnitude as, or better than, those of their organic counterparts.

Inorganic PEMs represent a fundamental departure from the polymer-based PEMs currently used in hydrogen fuel cells. Therefore, fuel cells built using inorganic PEMs will require a significantly different fabrication method. In particular, inorganic PEMs are not free standing, but rather need to be supported on a strong, porous substrate because they are inherently ultra-thin and brittle. Hydrogen electrode substrates for these membranes are being produced by Dr. Mark Janney at ORNL (see the following article in this section). We foresee a multilayer system built upon the hydrogen electrode (anode) substrate (see Figure 1). A sandwich layer having a similar porosity is deposited on top of the electrode foil. The sandwich layer provides an appropriate surface upon which to deposit the nanoparticle membranes.

## Approach

Perfluorosulfonic polymers [1] currently serve as electrolytes in PEM fuel cells because of their high protonic conductivity at low temperatures. The protonic conductivity of these polymers under high (80%) relative humidity ranges between $2.8 \times 10^{-2}\ \Omega^{-1}cm^{-1}$ for Nafion 117 (Ref. 2) and

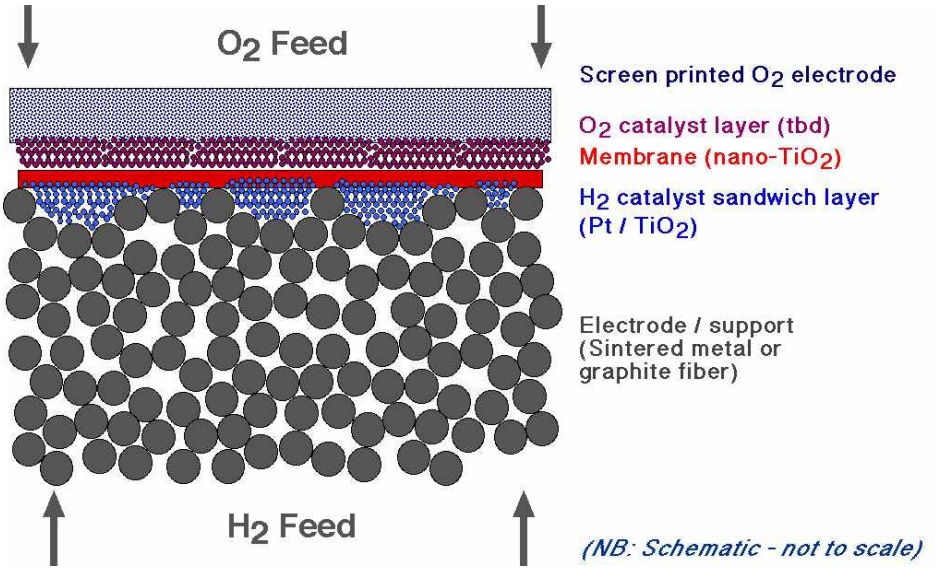


**Figure 1.** The inorganic PEM fuel cell assembly is envisioned as a multilayer structure built upon a mechanically robust hydrogen electrode.

$8.8 \times 10^{-2}\ \Omega^{-1}cm^{-1}$ for Dow membranes.[1,3] Presently, Nafion is one of the few materials that deliver the set of chemical and mechanical properties required to perform as a good PEM.[4] However, it is unable to retain water at higher temperatures and limits the fuel cell operation to approximately 80 °C. Also, Nafion membranes are very expensive.

In recent publications,[5,6] we have shown that, under the right conditions, proton conductivity for porous $SiO_2$ and $TiO_2$ materials can reach values similar to that of Nafion. Moreover, we have shown that the conductivity of such materials is highly dependent on the chemistry of their pore walls. The surface chemistry of these pores can be modified in a series of ways, and in some cases improvements of more than one order of magnitude can be observed in conductivity.

The ratio of five coordinated $Ti^{4+}$/two-coordinated $O^{2-}$ groups was modified by treating the porous $TiO_2$ with an acidic solution at pH 1.5. We also changed the state of surface protonation by equilibrating this material with aqueous solutions of different pH levels. In addition, we modified the surface by phosphate adsorption. These changes are aimed at investigating the influence of surface site density and charge density, as well as surface acidity and interfacial dipolar charge distribution, on the water adsorption of $TiO_2$.

In some cases, the increase in conductivity is of orders of magnitude, as seen in Figure 2, where we show the effect of treatment at different pH levels on the conductivity. The effect of relative humidity is observed in Figure 3, where the resistance of $TiO_2$ decreases dramatically with increasing relative humidity, a behavior typical of proton conductors.

We have prepared very thin (ca. 0.2 to 0.5 microns thick) membranes, supported on conductive porous membranes prepared by Dr. Mark Janney at ORNL. We are currently testing gas permeability and crossover across the assembly.

We are also producing some prototype membrane-electrode assemblies, which will be sent to the Los Alamos National Laboratory for testing.

## Conclusions

The surface chemistry of the pore walls of mesoporous $TiO_2$ wafers is a determining factor in the water adsorption behavior of these materials. The uptake of physisorbed water is a two-regime process. At lower relative humidity, the water forms a layer of clusters along the walls (interfacial layer) of a matrix of interconnected pores. At higher relative humidity, new water molecules start filling the remaining pore space through capillary condensation. The capacity of the interfacial layer of water is strongly influenced by the chemistry of the pore wall. However, uptake by capillary condensation is independent of the surface chemistry of the pore wall. Therefore, the pore water density is different

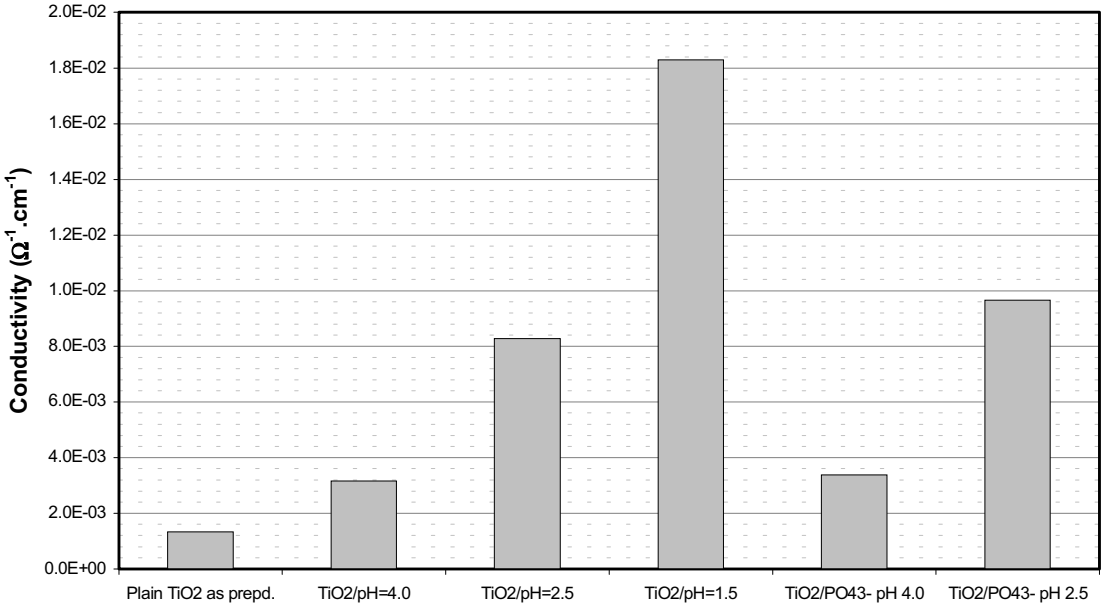


**Figure 2.** Effect of surface modification on the conductivity of $TiO_2$.

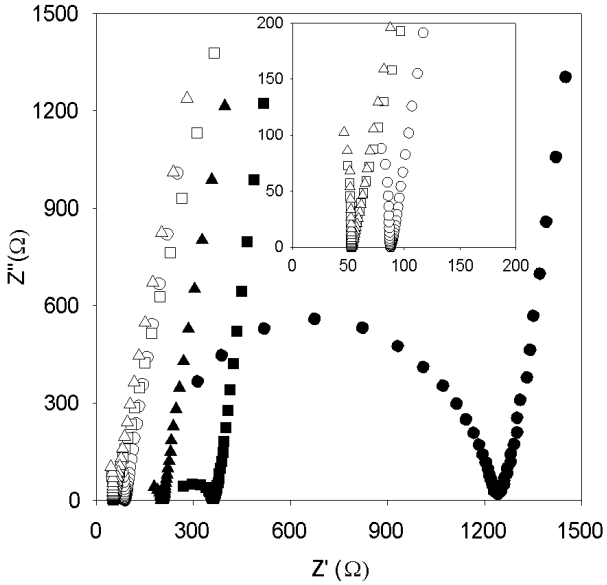


**Figure 3.** Effect of relative humidity on the impedance spectra of $TiO_2$ equilibrated at a pH of 1.5; (●) 33%; (■) 53%; (▲) 62%; (○) 75%; (□) 81%; (Δ) 92%.

for each of the studied materials, and in every case larger than that of water at 40 °C.

The proton conductivity values for these materials increase with increasing water content. Moreover, in the first regime of hydration, the activation energy decreases with increasing water content; whereas, in the capillary condensation regime, activation energy increases, to a limit, with increasing water content. Although differences in the proton conductivity of these materials are related to their differences in water adsorption behavior, the values for proton conductivity do not totally correlate with the water content of a sample. This fact indicates existing differences in both proton concentration and proton mobility in the pore water.

## References

1. S. Gottesfeld and T. A. Zawodsisnki, *Polymer Electrolyte Fuel Cells, in Advances in Electrochemical Science and Engineering* , Alkire, R. C.; H. Gerischer, D. M. Kolb, and C. W. Tobias, eds., Wiley-VCH, Weinheim, 1997, Chapter 5, pp. 245–63.
2. J. J. Summner, S. E. Creager, J. J. Ma, and D. D. DesMarteau, *J. Electrochem. Soc*. **145** (1998), p. 107.
3. T. A. Zawodsisnki, M. Neeman, L. Sillerud, and S. Gottesfeld, *J. Phys. Chem*. **95** (1991), p. 6040.
4. K. D. Kreuer, *Solid State Ionics* **97** (1997), p. 1.
5. F. M. Vichi, M. T. Colomer, and M. A. Anderson, *Electrochem. Solid State Lett*. **2** (1999), p. 313.
6. F. M. Vichi, M. I. Tejedor-Tejedor, and M. A. Anderson, *Chemistry of Materials,* 2000, in press, available online at http://pubs.acs.org/cgi-bin/doilookup?10.1021/cm9907460.

# B. Inorganic Polymer Electrolyte Membrane Electrode/Support Development

*M. A. Janney*
*Oak Ridge National Laboratory, MS 6087, P.O. Box 2008*
*Oak Ridge, TN 37830-6087*
*(865) 574-4281; fax: (865) 574-8271; e-mail: janneyma@ornl.gov*

*DOE Program Manager: Patrick Davis (202) 586-8061; fax: (202) 586-9811; e-mail: patrick.davis@hq.doe.gov*
*ORNL Technical Advisor: David Stinton (865) 574-4556; fax: (865) 574-6918; e-mail: stintondp@ornl.gov*

---

*Contractor: Oak Ridge National Laboratory, Oak Ridge, Tennessee*
*Prime Contract No.: DE-AC05-00OR22725*

---

## Objectives

- Develop electrically conducting hydrogen electrode substrates containing catalytically active ceramic sandwich layers for use in ceramic polymer electrolyte membranes (PEMs) based on nanoparticles of $TiO_2$ and $Al_2O_3$. This project is being conducted in coordination with Marc Anderson's project on microporous inorganic membranes at the University of Wisconsin (UW). The membrane substrates developed at ORNL are being evaluated at UW.
- Investigate methods for high-volume fabrication of inorganic membrane electrode assemblies (MEAs) using a multilayer system built upon a hydrogen electrode substrate that uses screen printing or other appropriate "off-the-shelf" technologies to apply the $O_2$ catalyst layer, the oxygen electrode, and the interconnects.

## OAAT R&D Plan: Section 3.3: Task 13; Barriers A, B

## Approach

- Base the initial electrode/substrate on a tape-cast, sintered porous nickel foil.
- Develop follow-on substrates based on carbon fiber paper and other conductors.
- Supply substrates to UW in a timely fashion to allow them to test their nanoparticle $TiO_2$ membranes.

## Accomplishments

- Developed a new process for applying a sandwich layer on top of the nickel substrate having a particle size appropriate to act as a bridge between the substrate and the membrane.
- Developed a substrate with sandwich layer that has low gas permeability, with a high ratio of Knudsen to Pousille flow.
- Developed initial substrates based on carbon fiber paper.

## Future Direction

- Develop a viable substrate based on a material that can withstand the long-term fuel cell environment, such as carbon or a surface-treated metal powder.

- Develop methods for high-volume, low-cost fabrication of inorganic MEAs. Use "off-the-shelf" multilayer manufacturing technologies (e.g., screen printing) to apply the $O_2$ catalyst layer, the oxygen electrode, and the interconnects.

## Introduction

Microporous inorganic membranes are being developed at UW as PEMs for fuel cells. These new membranes can operate at temperatures in excess of 100°C, retain water at these elevated temperatures, and provide proton conductivities of the same order of magnitude as the presently employed Nafion ® membranes. More important, these membranes should reduce the cost of the membrane by substantially reducing the amount of platinum catalyst required to operate a fuel cell, and should minimize CO poisoning of the platinum by operating at elevated temperatures.

$TiO_2$ membranes must be supported on a structural substrate because these membranes are thin (≤200 nm), porous (~40 vol % void space), and brittle (an inherent characteristic of ceramic membranes). The porous substrate provides both electrical conductivity and gas distribution. Because the membrane is composed of 5–10 nm particles, an intermediary sandwich layer (particle diameter of 50 to 500 nm) is required to provide geometric compatibility.

## Objectives

The goal of this project is to develop electrically conducting hydrogen electrode substrates containing a catalytically active ceramic sandwich layer. These substrates will be used as supports for ceramic PEMs based on nanoparticles of $TiO_2$ and $Al_2O_3$. This project is being conducted in coordination with Marc Anderson's project on microporous inorganic membranes at UW (see the preceding paper, 3.A). The substrates are being evaluated at UW.

Inorganic PEMs represent a fundamental departure from the polymer-based PEMs currently used in hydrogen fuel cells because they are supported membranes, not free-standing ones. Therefore, a significantly different manufacturing approach will be required in fabricating inorganic MEAs. We foresee a multilayer system built upon the hydrogen electrode substrate. Such a system would use screen printing or other appropriate "off-the-shelf" technologies to apply the $O_2$ catalyst layer, the oxygen electrode, and the cell interconnects. Therefore, a *future goal* is to investigate methods for high-volume, low-cost fabrication of integrated, multilayer inorganic MEAs.

## Results and Discussion

The initial electrode/support is based on a tape-cast, sintered porous nickel foil. The sintered nickel support is not a long-term solution. It has, however, allowed us to provide a usable substrate to UW in a timely fashion, allowing UW to manufacture and test its membranes on a substrate suitable for electrochemical and fuel cell tests.

The sintered nickel foil has a porosity of about 55 vol % and an average pore size of about 2–5 μm. A sandwich layer having a similar porosity and a pore size of about 0.1 μm is deposited on top of the electrode foil. The small pore size of the sandwich layer provides an appropriate surface upon which to deposit the nanoparticle membrane. An example of the supports is shown in Figures 1 and 2. In addition, the sandwich layer can be platinized. The platinum is deposited on the sandwich layer from an aqueous solution of chloroplatinic acid or aminoplatinum.

The substrates that were produced using the combined tape-cast nickel with the sandwich layer

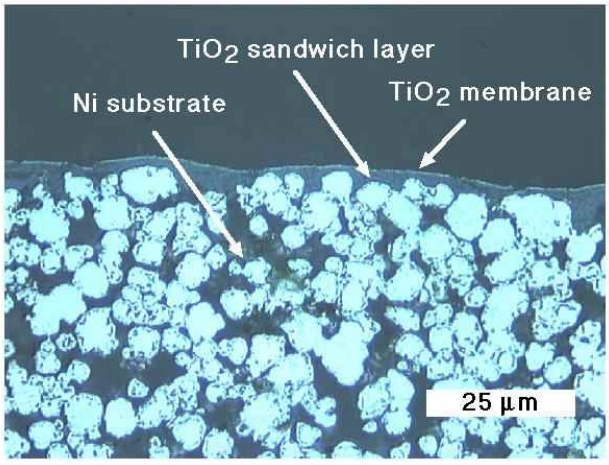


**Figure 1.** A novel sandwich layer was developed to permit deposition of the $TiO_2$ membrane.

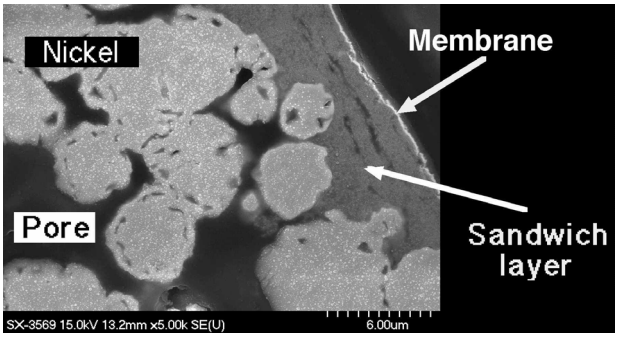


**Figure 2.** The sandwich layer does not penetrate deeper than the surface roughness of the substrate.

exhibited excellent gas permeability. Figure 3 shows the permeability of three supports—one coated with a 0.25-µm titania (designated HP02), one coated with a 50-nm titania (designated P25), and one coated with P25 followed by coating with a 5–10-nm titania membrane layer. Permeability was measured using both He and $N_2$, which can be used to give a measure of the relative contributions of Knudsen and Pouisille flow. For pure Knudsen flow, a figure of merit of 2.65 is predicted for the

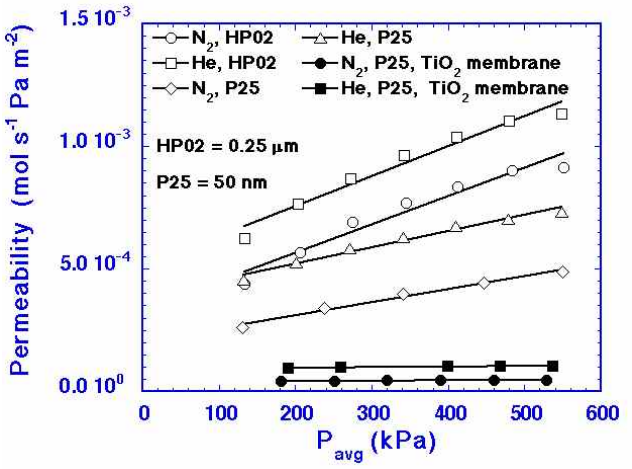


**Figure 3.** Low permeability was achieved in $TiO_2$-coated nickel substrates by controlling $TiO_2$ particle size in the sandwich layer.

ratio of He to $N_2$ flow through the samples. For our best samples, ratios of as high as 2.5 were obtained. Even lower gas permeability was demonstrated when tests were conducted in moist air (Figure 4). Under these conditions, essentially pure Knudsen flow was obtained.

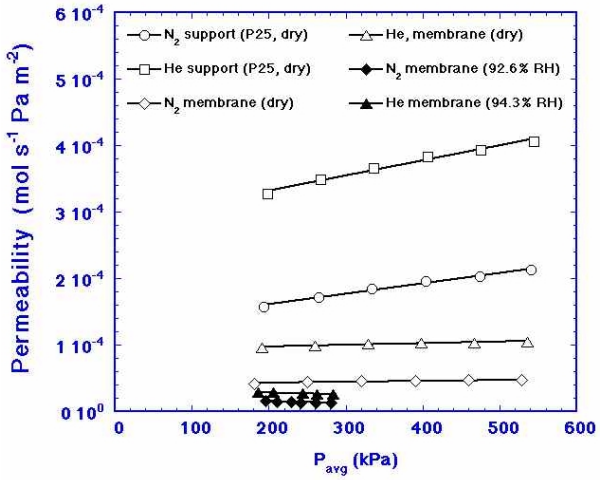


.

**Figure 4.** High relative humidity substantially reduced the permeability of the nickel-supported $TiO_2$ membrane.

## Summary

- Inorganic, microporous titania membranes were fabricated on porous, electrically conducting nickel substrates with a ceramic sandwich layer.
- A novel method was developed for applying ceramic sandwich layer to nickel substrate, which is useful in other membrane applications.
- We are progressing toward a graphite-fiber-based substrate having the requisite chemical compatibility with the PEM environment.
- PEM fuel cell assembly using multilayer technology manufacturing will be investigated using standard, industrial technologies.

# C. Low-Friction Coatings for Fuel Cell Air Compressors

*George R. Fenske (primary contact), Oyelayo Ajayi, John Woodford, and Ali Erdemir*
*Argonne National Laboratory, ET-212, 9700 South Cass Avenue*
*Argonne, Illinois 60439*
*(630) 252-5190; fax: (630) 252-4798; email: gfenske@anl.gov*

*DOE Program Manager: Patrick Davis (202) 586-8061; fax: (202) 586-9811; e-mail: patrick.davis@hq.doe.gov*
*ORNL Technical Advisor: David Stinton (865) 574-4556; fax: (865) 574-6918; e-mail: stintondp@ornl.go*

---

*Contractor: Argonne National Laboratory, Argonne, Illinois*
*Prime Contract No.: W-31-109-Eng-38*

---

## Objectives

- Develop and evaluate the friction and wear performance of low-friction coatings and materials for fuel cell air compressor/expander systems. Specific goals are these:
  - 50 to 75% reduction in friction coefficient
  - One order-of-magnitude reduction in wear
- Transfer the developed technology to DOE's industrial partners.

## OAAT R&D Plan: Section 3.3: Task 13; Barrier D

## Approach

- Identify critical compressor components requiring low friction.
- Apply and evaluate Argonne's near-frictionless carbon (NFC) coatings to the components.
- Develop and evaluate polymer composite materials containing boric acid solid lubricant.

## Accomplishments

- Identified the radial air bearings and thrust bearings of Meruit's turbocompressor as components that require both low friction and low wear rate for satisfactory performance.
- Conducted thrust washer wear tests that showed that Argonne's NFC coating reduced friction by about four times and wear rate by two orders of magnitude. Both exceeded the project goals.
- Conducted tests that showed NFC coatings increased the scuffing resistance of a steel surface by about 10 times.
- Completed coating a set of Meruit's turbocompressor bearing components for friction and wear testing in the air bearing test rig.
- Completed initial friction and wear testing of Nylon-12 polymer with $B_2O_3$ addition. Significant reduction in wear was observed with the addition of $B_2O_3$, especially under high relative humidity.
- Achieved 50% reduction in friction for application in a Variex variable displacement compressor/expander using Hitco C/C composite and anodized aluminum contact pairs.

### Future Direction

- Conduct bearing test of NFC-coated air bearing parts.
- Pursue commercial fabrication and tribological evaluation of injection-molded polymer and boric acid composite material.
- Assess Mechanology's TIVM (toroidal intersecting vane machine) components. Develop and evaluate appropriate coating and/or material to meet needs.

## Introduction

A critical need in fuel cell systems for vehicles is an efficient, compact, and cost-effective air management system (compressor/expander) to pressurize the fuel cell systems to about 3 atmospheres. Pressurization of fuel cells will result in higher power density and lower cost. Several compressor/expanders are currently being developed; and their efficiency, reliability, and durability depend on effective lubrication or friction and wear reduction in critical components such as bearings and seals. The objective of this project is to develop and evaluate low-friction coatings and/or materials for critical components of air compressor/expanders being developed for vehicle fuel cell systems.

## Approach

Over the years, the Tribology group at Argonne has developed low-friction and low-wear coatings and materials. Most notable is the discovery of an amorphous carbon coating with extremely low friction coefficients (<0.001 in dry nitrogen) and very low wear. One approach in the present project is the application of the carbon coating to fuel cell compressors. Another approach is the development of a polymeric-boric acid composite material. Critical components requiring low-friction and low-wear surfaces in the various compressor/expander designs will be identified. The NFC coatings and polymer composite materials will be evaluated under conditions expected to be typical for the components.

## Results

The previous report presented the effects of the NFC coating on friction and wear in a thrust washer test. The coating reduced the friction coefficient by a factor of 4, thus increasing efficiency. It also reduced the wear rate by more than 10 times, ensuring higher durability.

A major failure mode that will compromise the reliability of fuel cell air compressors is scuffing or seizure. All poorly lubricated sliding components are susceptible to this failure mode. The impact of the NFC coating on the scuffing performance of steel surfaces under dry contact condition was evaluated in laboratory bench top tests by using a reciprocating sliding-contact configuration. During each scuffing test, the load was held constant while the sliding speed was increased in discrete steps of two-minute duration. Each test was terminated when scuffing occurred, as indicated by a sudden rise in friction coefficients (see Figure 1).

As measured at the scuffing point by the contact severity index (defined as the product of friction coefficient ($\mu$), sliding velocity ($V$) and contact pressure ($P$), $\mu PV$, the scuffing or seizure resistance of NFC-coated surfaces is about 10 times that of an uncoated surface (Figure 2). Of the three variations of NFC that we evaluated, NFC-2 showed the highest scuffing resistance. The much higher scuffing resistance provided by the NFC coatings will translate to higher reliability for NFC-coated compressor/expander components. It also means that coated components can operate under more severe contact conditions without catastrophic failure.

Based on the excellent performance of the NFC coating during the benchtop tests, we tested an NFC-coated air bearing in a bearing test rig. Four sets of Meruit's turbocompressor air bearing components have been coated with NFC. A set of coated components is shown in Figure 3. These parts are scheduled for testing soon at Meruit.

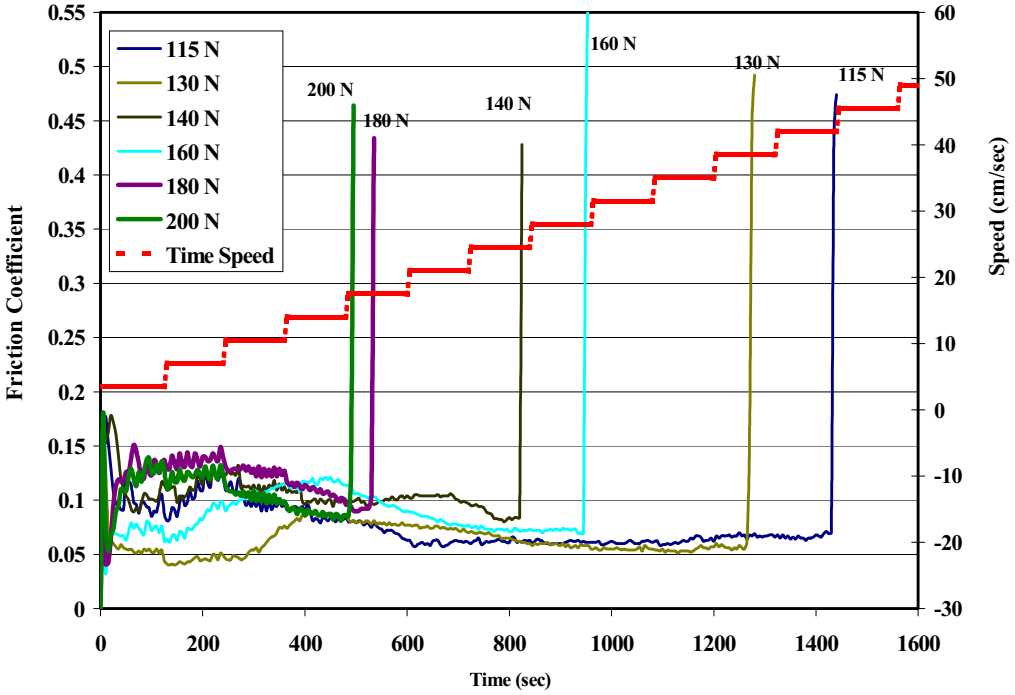


**Figure 1.** Variation of friction coefficient over time during scuffing test of NFC-coated steel surfaces.

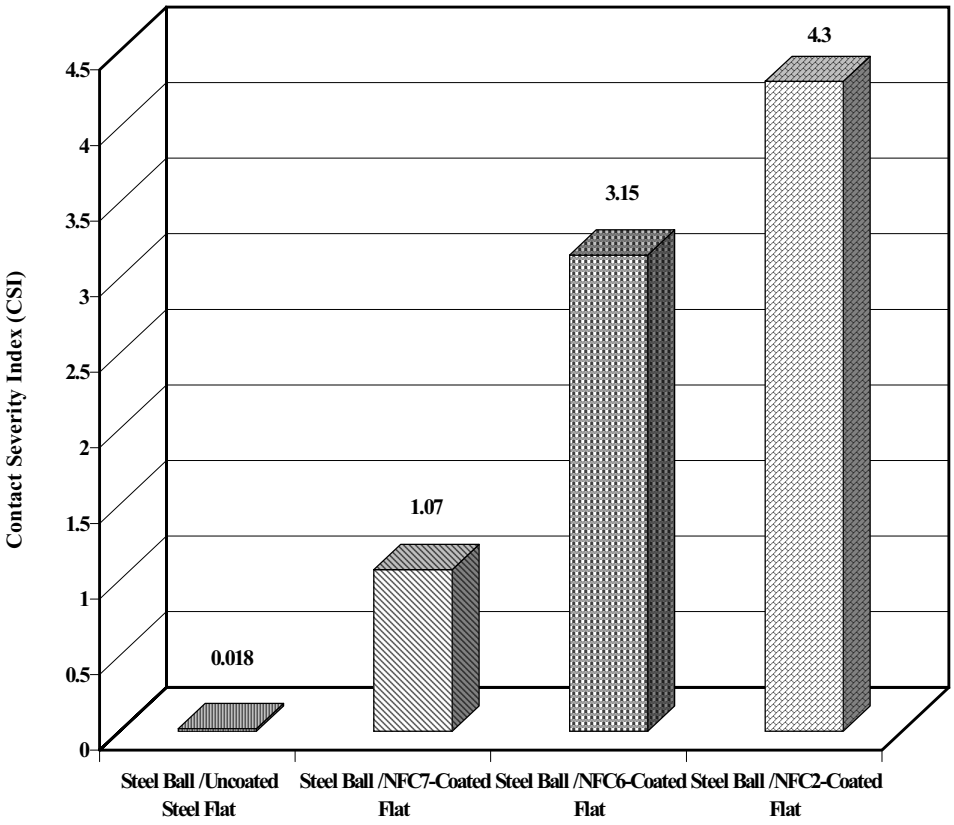


**Figure 2.** Contact severity at scuffing for uncoated and NFC-coated steel surfaces.

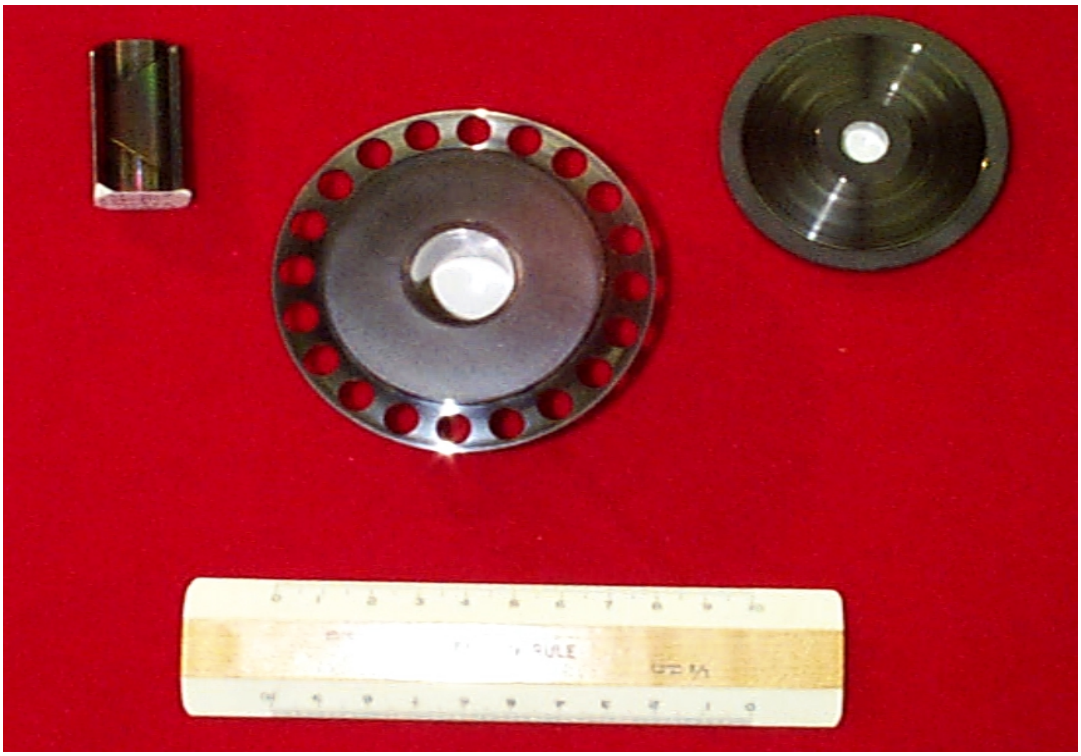

**Figure 3.** NFC-coated components of Meruit's turbocompressor air bearings.

## Conclusions

NFC-coated steel surfaces showed very good tribological behavior in terms of reduced friction, reduced wear, and improved scuffing resistance compared with the uncoated surface. Therefore, this material is indeed a good candidate for application in fuel cell compressor/expander components. Four sets of turbocompressor air bearings are NFC-coated and will be tested in a bearing test rig.

## Publications

O. O. Ajayi, G. R. Fenske, A. Erdemir, J. Woodford, J. Sitts, K. Elshot, and K. Griffey, "Low-Friction Coatings for Air Bearings in Fuel Cell Air Compressors," in SAE Paper 2000-01-1536, Society of Automotive Engineers, Warrendale, Pennsylvania.

A. Erdemir, O. L. Eryilmaz, I. B. Nilufer, and G. R. Fenske, "Synthesis of Superlow Friction Carbon Films from Highly Hydrogenated Methane Plasmas," presented at the International Conference on Metallurgical Coatings and Thin Films, April 9–14, 2000, San Diego.

# D. Microstructural Characterization of PEM Fuel Cells

*D. A. Blom and T. A. Nolan*
*Materials Analysis User Center (MAUC)*
*Oak Ridge National Laboratory, P.O. Box 2008, MS 6064, Bldg. 4515*
*Oak Ridge, TN 37831-6064*
*(865) 241-3898; fax: (865) 576-5413; e-mail: blomda@ornl.gov*

*DOE Program Manager: Patrick Davis (202) 586-8061; fax: (202) 586-9811; e-mail: patrick.davis@hq.doe.gov*
*ORNL Technical Advisor: David Stinton (865) 574-4556; fax: (865) 574-6918; e-mail: stintondp@ornl.gov*

---

*Contractor: Oak Ridge National Laboratory, Oak Ridge, Tennessee*
*Prime Contract No.: DE-AC05-00OR22725*

---

## Objectives

- Optimize the catalyst microstructure and distribution in membrane electrode assemblies (MEAs) for low cost and high performance.
- Understand the effects of microstructure and microchemical composition on the performance and aging characteristics of the fuel cell.

## OAAT R&D Plan: Section 3.3: Task 13; Barriers A, B

## Approach

- Develop a technique to produce thin samples of MEAs suitable for characterization in a transmission electron microscope (TEM).
- Investigate cross-sections through an entire MEA, from the cathode to the anode, to understand the microstructure and chemistry on an atomic level for usable MEAs.
- Maintain spatial relationships in thin sections of the catalyst layer and throughout the MEA. This is a key requirement for understanding the real systems.
- Characterize unused, "fresh" MEAs and MEAs after use in a fuel cell test stand to investigate atomic-scale changes in composition and microstructure that may occur during fuel cell operation.

## Accomplishments

- Successfully produced thin sections of a commercially available MEA suitable for high-resolution TEM imaging and energy-dispersive X-ray spectroscopy (EDX). Specimens were suitably thin over a wide area that the interfaces between both catalyst layers and the membrane were amenable to analysis.
- Obtained X-ray spectra to characterize elemental distributions in fresh vs aged MEAs.

### Future Direction

- Complete analysis of changes in chemistry and microstructure that occurred during the fuel cell testing.
- Perform more stringent aging tests to understand the link between fuel cell performance degradation and MEA microstructure and chemistry.

## Introduction

Polymer electrolyte membrane (PEM) fuel cells hold great promise for use as an environmentally friendly power source for automobiles. One of the key hurdles in making PEMs commercially viable is to reduce the cost by reducing the amount of precious metal catalyst necessary to provide high power density operation at low temperature. For efficient catalysis to occur, gas molecules must be able to interact easily with the surface of the catalyst particles. A pathway for diffusion of protons must exist in close proximity to the active sites on the catalyst, and an electrically conductive pathway from the catalyst to the electrodes is required for electron transport. Finally, water (the by-product of the fuel cell reaction) has to be transported away from the catalyst for reactions to continue. These requirements show the complexity of building an efficient PEM fuel cell and clearly indicate the opportunity for atomic-scale microstructural and chemical characterization to provide feedback on the geometry and distribution of the various components for optimum performance.

## Approach

A new specimen preparation technique was developed to allow PEM fuel cell MEAs to be characterized in a TEM. MEAs consist of a proton-conducting polymer membrane (which is gas-tight) sandwiched between two catalyst layers that are surrounded by two porous electrodes for gas diffusion and electrical conductivity. Specimens for TEM study must be extremely thin, on the order of 100 nm or less in thickness. Preparing thin specimens without disturbing the geometry and distribution of the components of an MEA was the initial challenge of this project. To provide reliable information on the microstructure, the MEA must be disturbed as little as possible so we can be sure that we are characterizing the microstructure as it exists during operation.

Following the development of the specimen preparation technique, a commercially available MEA was studied prior to use in a fuel cell. The first question addressed was the distribution and quantity of precious metal catalyst in the catalyst layers. The second question addressed was the relationship between the catalyst layer and the membrane. High-resolution electron microscopy provided atomic-level microstructural information about the components of the MEA. Energy-dispersive X-ray spectroscopy (EDX) provided chemical information about the MEA at a nanometer-level spatial resolution. W. L. Gore and Associates, Inc., agreed to provide fuel cell testing and aging of a third-party MEA. Gore ran the MEA continuously for 325 hours at 75ºC in fully humidified ambient pressure hydrogen and air at a constant voltage of 0.6 V. With these test conditions, minimal change in cell performance was recorded over the duration of the test.

## Results

Figure 1 shows the interface between the catalyst layer and the PEM for the unused MEA. The catalyst

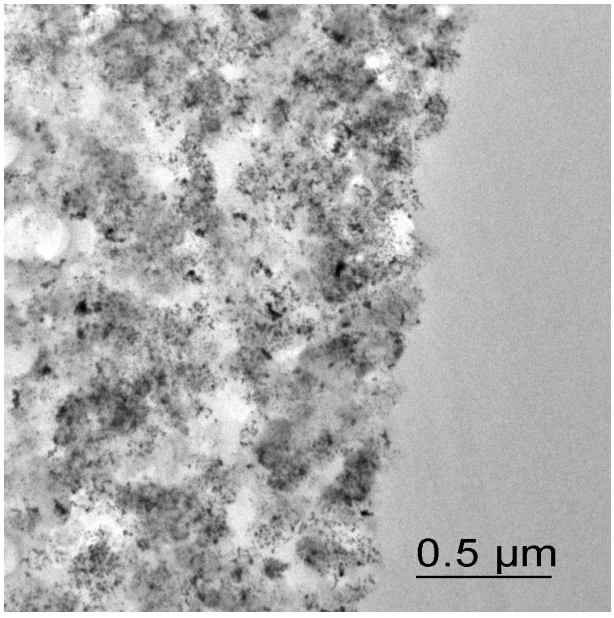


**Figure 1.** TEM micrograph of the interface between the PEM and catalyst for an unused MEA. The small dark particles are platinum.

layer is on the left in the figure. Note the good bonding between the catalyst layer and the membrane. Figures 2 and 3 are EDX spectra from the catalyst layer and membrane, respectively. The copper peaks in all the EDX spectra shown are from the copper grid used to support the MEA specimens. The catalyst layer clearly contains large numbers of platinum (Pt) catalyst particles, seen as the small, uniformly distributed dark particles. The membrane contains significant amounts of fluorine (F) and sulfur (S). Figure 4 is a high-resolution micrograph

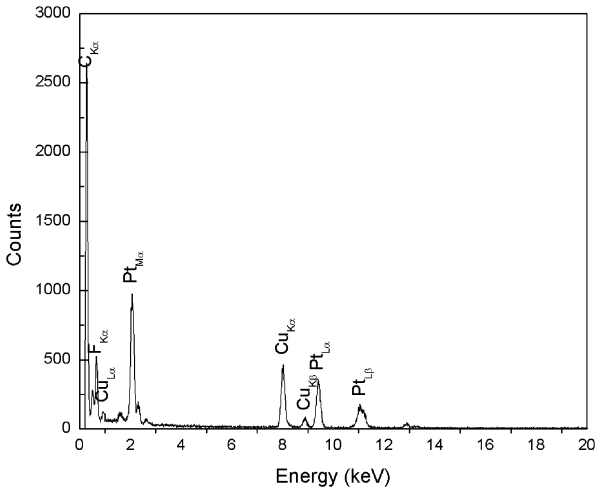


**Figure 2.** Chemical composition of the catalyst layer as measured by EDX. The copper signal is from the support grid. The catalyst layer contains carbon, fluorine and platinum.

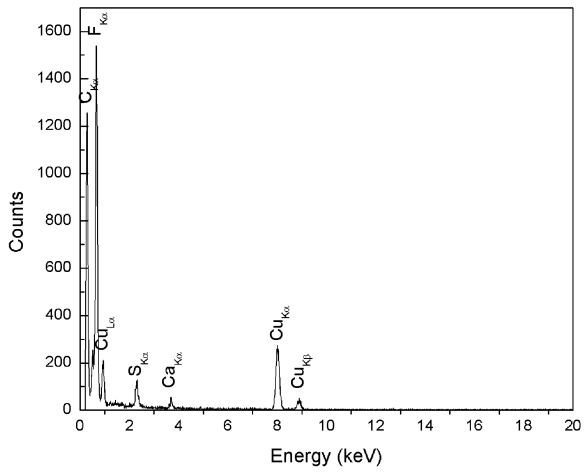


**Figure 3.** The membrane shown in the right hand side of Figure 1 contains carbon, fluorine, sulfur and calcium.

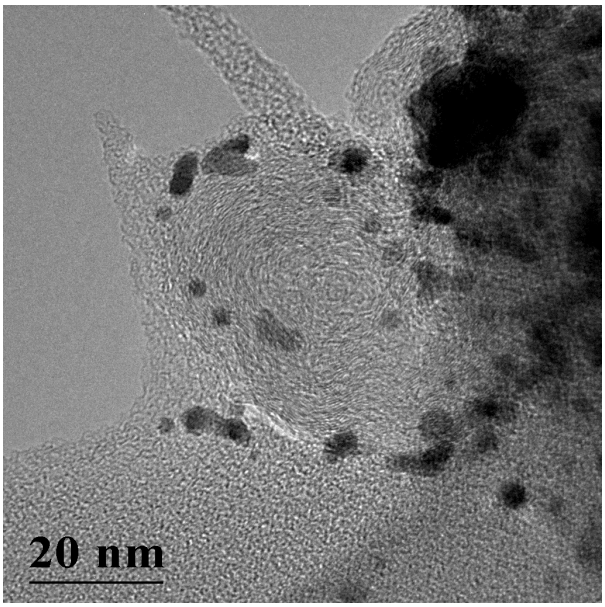


**Figure 4.** High-resolution micrograph of carbon-black-supported platinum catalyst in an MEA.

of the catalyst (Pt supported on carbon black) in the MEA. The carbon black particle is oval with a major axis of ~50 nm and a minor axis of ~30 nm. The smaller, darker particles are individual Pt catalyst particles. This MEA has a high loading of Pt catalyst spread non-uniformly throughout the thickness of the catalyst layer. Possible improvements in processing may decrease the Pt requirements while maintaining or improving the performance.

An MEA identical to the untested MEA described above was tested at W.L. Gore and then prepared for TEM characterization. Figure 5 shows the interface between the cathode catalyst layer and the PEM for the used/aged MEA. Note the appearance of the membrane directly adjacent to the catalyst. Figure 6 is a higher-magnification micrograph of the same area. The membrane appears to have begun crystallizing during the fuel cell testing. Initial observations of the catalyst distribution and size indicate no significant changes have occurred as a result of the testing. Figures 7 through 9 are EDX spectra from the various areas indicated in Figures 5 and 6. Figure 7 is the EDX spectrum from the catalyst layer, which confirms the presence of Pt. Figure 8 is the spectrum from the membrane showing the crystallization effect, while Figure 9 is the spectrum from the membrane directly adjacent to the catalyst layer. Comparing Figures 8 and 9, it is clear that there has been a composition change in the

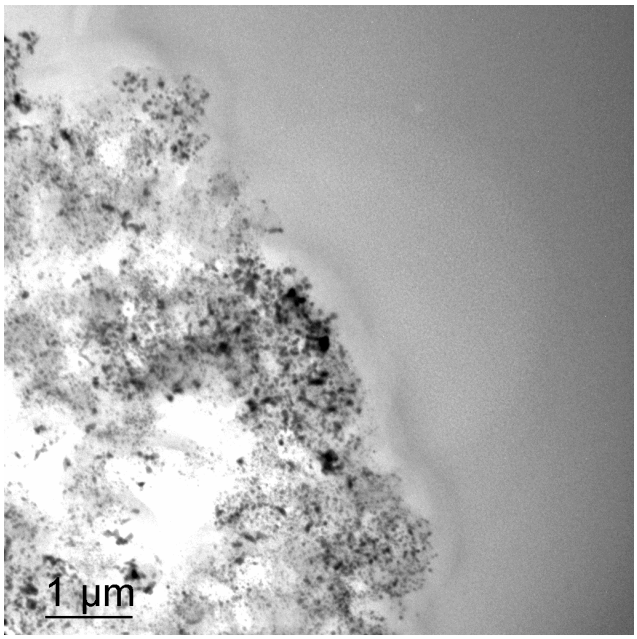


**Figure 5.** TEM micrograph of the interface between the cathode catalyst and the PEM after 325 hours of fuel cell testing. Note the visible difference in the membrane directly in contact with the catalyst layer.

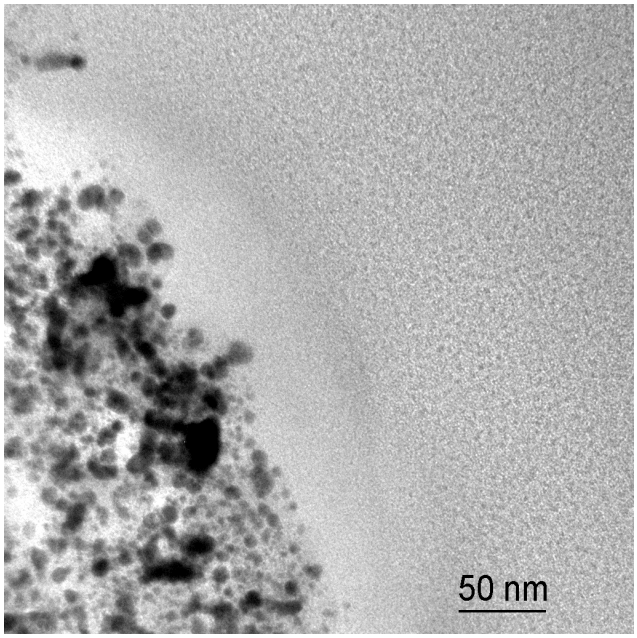


**Figure 6.** Higher magnification micrograph of the same area shown in Figure 5. The interfacial layer between the catalyst and the rest of the membrane is more clearly visible.

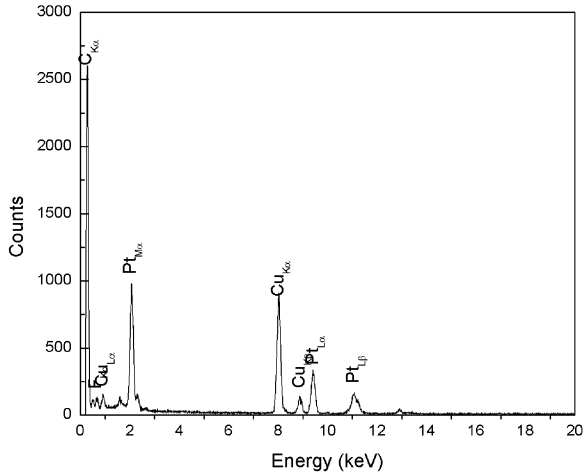


**Figure 7.** EDX spectrum from the cathode catalyst layer seen in Figures 5 and 6. The copper peaks are from the TEM specimen support grid.

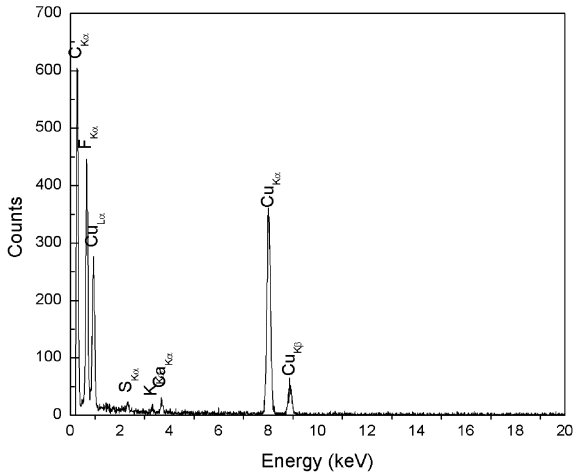


**Figure 8.** EDX spectrum from the membrane far from the catalyst layer. The membrane contains carbon, fluorine, sulfur, potassium and calcium.

membrane. The area closest to the catalyst layer is enriched in sulfur relative to the rest of the membrane. As previously noted, only minimal performance degradation was noted in this MEA relative to the unused MEA. Additional MEA testing is planned in order to study the correlations between the chemistry and microstructure of the MEA and its

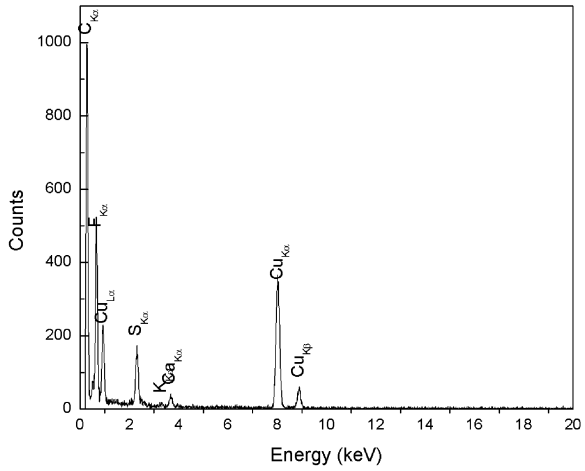


**Figure 9.** EDX spectrum from the PEM in direct contact with the catalyst layer. Note the increase of sulfur relative to fluorine compared with Figure 8.

performance in a fuel cell. Figure 10 shows the anode side of the MEA corresponding to the images in Figures 5 and 6. No readily visible changes are seen in the microstructure or chemistry of the used MEA. EDX spectra corresponding to the membrane and catalyst layer are shown in Figures 11 and 12, respectively.

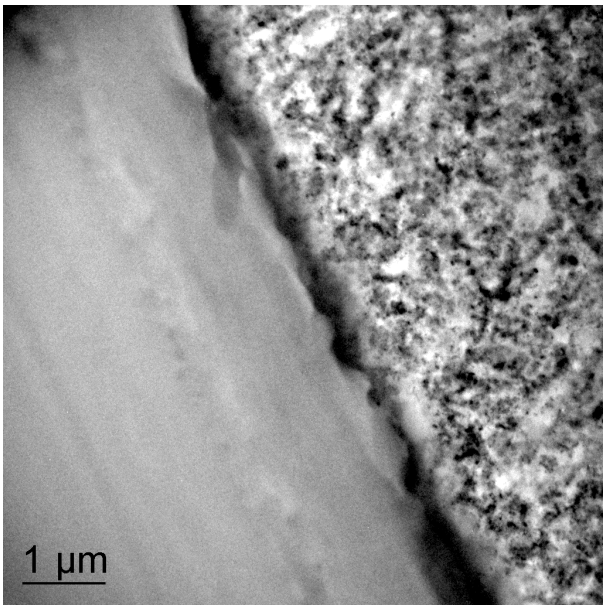


**Figure 10.** TEM micrograph of the interface between the PEM and the anode catalyst layer corresponding to that seen in Figures 5 and 6. The microstructure is essentially the same as that of the unused MEA shown in Figure 1.

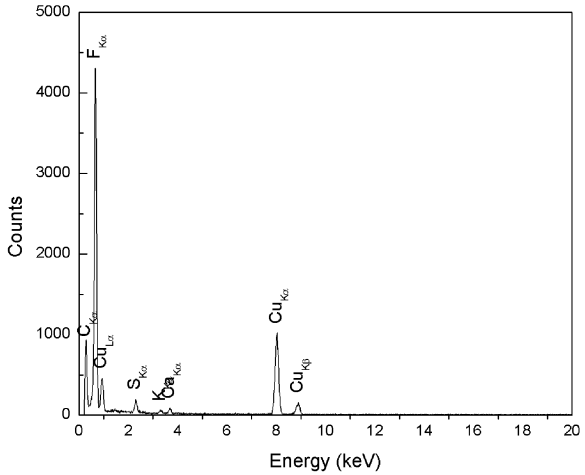


**Figure 11.** EDX spectrum from the PEM seen in Figure 10. No significant chemical composition changes have occurred relative to Figure 3, the unused MEA.

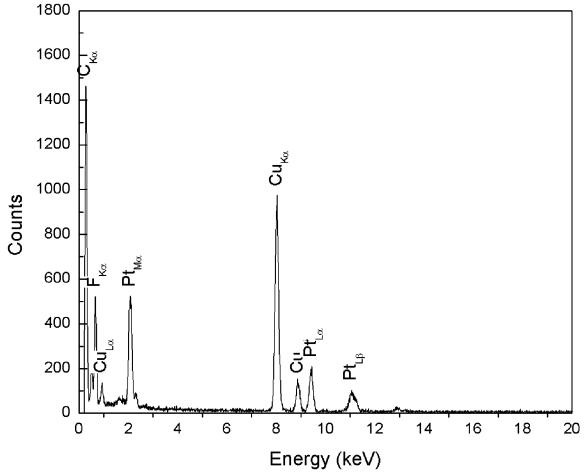


**Figure 12.** EDX spectrum from the anode catalyst layer of the used MEA; essentially identical to the spectrum in Figure 2 from the unused MEA.

## Conclusions

A new specimen preparation technique has been developed and demonstrated that produces thin cross-sections of PEM fuel cell MEAs suitable for microstructural and micro-chemical characterization in a TEM. Initial observations of precious metal catalyst content and distribution indicate that the microstructure of the catalyst layer is far from optimized in a commercially available PEM MEA. Cross-sections have been produced that preserve the

geometry and distribution of the MEA components and are thin over wide areas, allowing for the simultaneous study of the microstructure and chemical composition representative of the cathode, membrane, and anode of an MEA as it existed during use in a fuel cell. By carefully maintaining the spatial relationships in the real system, it becomes possible to correlate the fuel cell performance and performance changes with TEM microcharacterization. Initial aging/use studies were conducted. Negligible performance degradation was observed for the given test conditions over 325 hours of continuous use. However, microstructural and chemical composition changes were found at the interface of the PEM and the cathode catalyst layer. A sulfur-rich interfacial region ~50 nm in width was observed. Further MEA testing will be conducted to attempt to understand the correlations among microstructure, atomic level chemical composition, and MEA performance.

## Presentation

D. A. Blom and T. A. Nolan, "Microstructural Characterization of Proton Exchange Membrane Fuel Cells," DOE 2000 Review, OTT Fuel Cells Program, Pacific Northwest National Laboratory, June 7–8, 2000.

# E. Carbon Foam for Radiators for Fuel Cells

*J. W. Klett, Ron Ott, April McMillan, and Bret Conway**
*Carbon and Insulation Materials Technology Group*
*Oak Ridge National Laboratory, P.O. Box 2008, MS 6087, Bldg. 4508*
*Oak Ridge, TN 37831-6087*
*(865) 574-5220; fax: (865) 576-8424; e-mail: klettjw@ornl.gov*

**(Performance Research, Inc., Denver, NC)*

*DOE Program Manager: Patrick Davis (202) 586-8061; fax: (202) 586-9811; e-mail: patrick.davis@hq.doe.gov*
*ORNL Technical Advisor: David Stinton (865) 574-4556; fax: (865) 574-6918; e-mail: stintondp@ornl.gov*

---

*Contractor: Oak Ridge National Laboratory, Oak Ridge, Tennessee*
*Prime Contract No.: DE-AC05-00OR22725*

---

## Objectives

- Develop compact, lightweight, and more-efficient radiators for fuel-cell-powered vehicles utilizing Oak Ridge National Laboratory's (ORNL's) unique high-conductivity carbon foam.
- Investigate key property-structure relationships in ORNL's carbon foam, leading to the optimization of the foam structure for ultra-efficient compact radiators.

## OAAT R&D Plan: Section 3.3: Task 13; Barrier C

## Approach

- Conduct a fundamental study of heat transfer mechanisms, including thermal transport in the carbon foam, and transport phenomena associated with the moist air/foam interface.
- Develop appropriate testing protocols for carbon foam properties and for the evaluation of compact, high-efficiency fuel-cell radiators.

## Accomplishments

- Developed a methodology for testing carbon foam core radiators.
- Elucidated key materials-related issues for carbon foam.
- Constructed and tested a prototypical radiator. Operated the device successfully under a 7-kW thermal load.
- Conducted preliminary brazing and joining studies. Demonstrated the importance of joining in heat transfer applications of the carbon foam.

## Future Direction

- Develop a mathematical model that incorporates the heat transfer characteristics of carbon foam and apply it to optimize radiator design.

- Evaluate optimized radiator designs for ruggedness and durability, including test rig evaluations for vibration behavior, reliability, etc.
- Study brazing/joining methodologies for carbon foams.
- With vehicle manufacturers, conduct on-vehicle trials of compact, efficient, fuel cell radiators.

## Introduction

Dissipation of heat from fuel cells is more difficult than for internal combustion (IC) engines because they operate at lower temperatures. The smaller driving force to disperse the heat results in a design problem, that is, excess size and weight of the radiator. Unless more efficient and compact thermal management systems can be developed, radiators on fuel-cell-powered vehicles will need to be three or four times larger than those on conventional vehicles.

A unique graphite foam developed at ORNL and licensed to Poco Graphite, Inc., has shown great promise as a heat sink for power electronics (see paper 2.A in this report). The unique graphite foam has a density of about 0.5 g/cm$^3$ and a thermal conductivity of about 1500 W/m·K along the ligaments of the foam. Because the foam has a very high and accessible surface area (>4 m$^2$/g) and is open celled, the overall heat transfer coefficients of foam-based heat sinks have been proved to be one or two orders of magnitude greater than those of conventional heat sinks. Therefore, a program was initiated to develop smaller, lighter, and more-efficient radiators for fuel cell vehicles.

The efficiency of carbon foam heat sinks was found to be dependent upon the geometry of the foam used in the device (see paper 2.A. in this report). The heat transfer coefficients shown in Table 1 were achieved with the geometries of foam shown in Figure 1. Very high values were obtained with the solid block of foam, but pressure drop was a concern. The finned and pin-fin heat sink designs dramatically reduced the pressure drops but sacrificed the heat transfer coefficients. Designs that used blind holes to direct the flow of air or water increased the heat transfer coefficients but created more of a pressure drop.

On the basis of our preliminary data, we believe we can develop compact, efficient heat exchangers for fuel-cell-powered vehicles.

**Table 1.** Results of heat sink testing with air and water cooling

| | Heat Transfer Coefficient h (W/m$^2$·K) | | P/L (psi/in) | Thermal Resistance °C/W |
|---|---|---|---|---|
| Solid Foam | Air | 2600 | 2 | 0.13* |
| | Water | 9000 | 1 | 0.04 |
| Finned | Air | 1000 | <0.05 | 0.38* |
| | Water | 2100 | 0.5 | 0.19 |
| Pin-Fin | Air | 1500 | 0.05 | 0.26* |
| | Water | 2500 | 0.5 | 0.15 |
| Blind-holes (pin fin negative) | Air | 2000 | 1 | 0.19* |
| | Water | 4600 | 0.5 | 0.09 |
| Blind-holes (parallel to air flow) | Air | 3100 | 0.35 | 0.13* |
| | Water | 4500 | 0.5 | 0.09 |

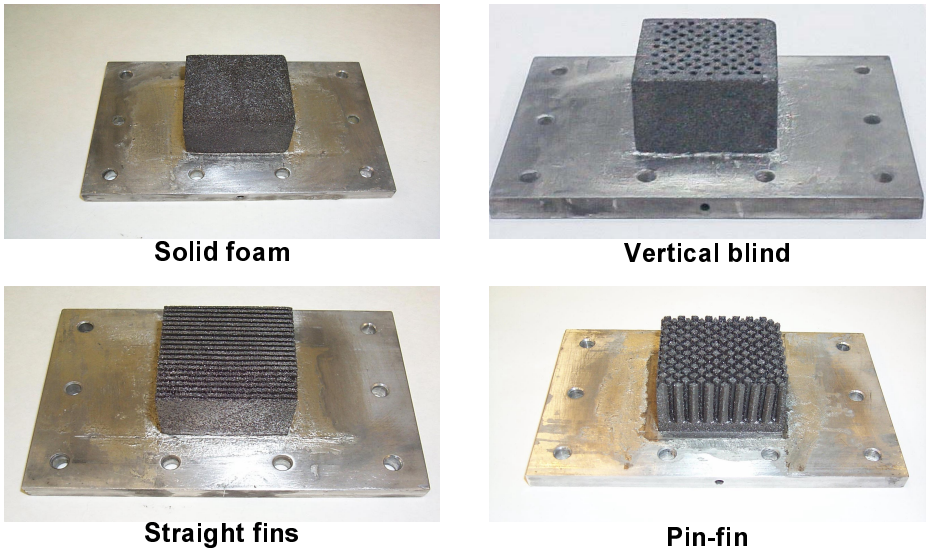


**Figure 1.** Designs of foam substrates evaluated for heat transfer and pressure drop.

## Results

In a demonstration test of a carbon foam heat exchanger, a block of foam 10.2 cm square by 2.54 cm thick was fitted with three aluminum tubes (0.635 cm diameter), as shown in Figure 2. The foam had a density of approximately 0.5 g/cm$^3$ and a thermal conductivity of approximately 150 W/m·K. Water was pumped through the tubes at 11.34 L/min and 80°C, and ambient air at 560 L/min at 25°C was forced through the foam (in a duct-type arrangement). The temperature drop of the water was measured at approximately 3°C, and the temperature change of the air was recorded. The temperature of the ambient air passing through the foam increased by up to 30°C (much more than for typical heat exchangers).

The overall heat transfer coefficient was calculated at between 6,000 and 11,000 W/m$^2$·K and was dependent upon humidity. This result is different from the performance of most air/water heat

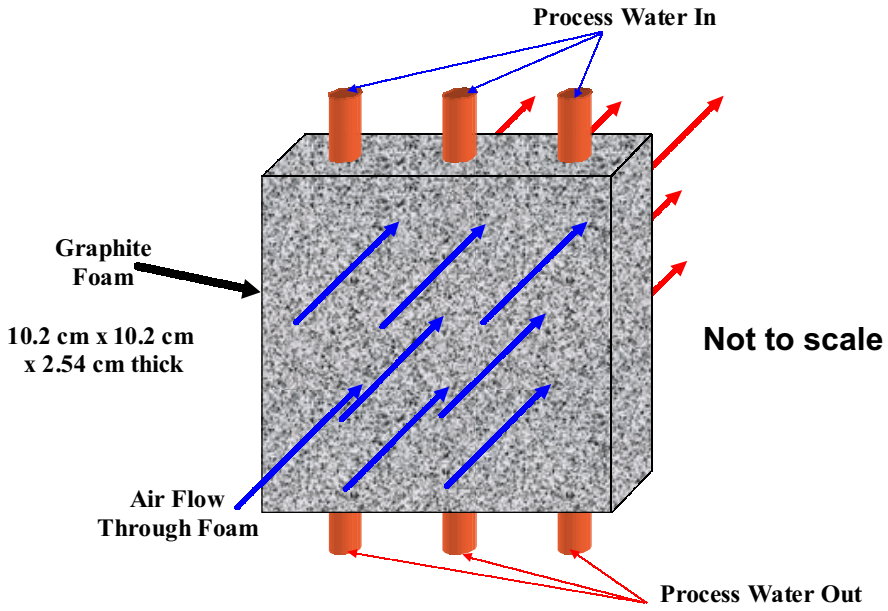


**Figure 2.** Schematic representation of heat exchanger with cooling air forced through pores of foam. Overall heat transfer coefficient measured at 11,000 W/m$^2$·K.

exchangers, where humidity does not affect heat transfer coefficient significantly. Most air/water heat exchangers, such as car radiators, exhibit an overall heat transfer coefficient of about 20–30 W/m$^2$·K. While this test demonstrates a remarkable increase in heat transfer coefficient and provides the tool to reduce the size of heat exchangers dramatically, the pressure drop through the foam was approximately 5.4 kPa/cm. This is not unreasonable for land-based systems in which developing a pressure head is feasible. However, in an automobile or airplane, where weight and power are significant concerns, this large pressure drop presents a potential problem for an efficient design.

To address the issue of pressure drop, another design was tested. A block of foam approximately 20.3 cm square by 2.54 cm thick was fashioned with eight 0.635-cm-diam. tubes press-fit through the foam (similar to Figure 3). However, unlike in the previous test, through-holes were machined in the foam to allow the passage of the cooling air and reduce the pressure drop. While the specific size and number of holes are proprietary, the total surface area of the holes was 948 cm$^2$. This radiator was placed on a NASCAR Winston Cup racing car, with an 800-hp, V8, gasoline high-performance engine. An electric fan forcing approximately 5663 L/min through the heat exchanger (radiator) was ducted to the system. The engine pumped approximately 56.8 L/min of coolant (pure water) through the radiator at a temperature of 210°C. The radiator reduced the temperature of the water by only 1.2°C and therefore rejected approximately 4.0 kW of heat to the ambient air. Unfortunately, the engine requires a heat rejection of approximately 33 kW of heat; hence, the performance of this device was insufficient. However, the overall heat transfer coefficient was calculated to be 943 W/m$^2$·K, based on the external surface area of the through-holes in the foam where the heat is being exchanged.

The calculated heat transfer coefficient is 30% greater than that of the existing conventional engine radiator (68.6 cm × 48.3 cm × 7.6 cm). To test the hypothesis that a compact radiator with an increased surface area could reject substantially more heat than the first prototype radiator, a second heat exchanger (radiator) for a NASCAR racing car was designed and constructed as shown schematically in Figure 4. This new design accounted for the need for a very high surface area of the external foam fins. While the specific design cannot be shown due to its proprietary nature, the total external fin surface area was 7561 cm$^2$. Aluminum 6061 tubes with an internal dimension of 0.782 cm were press-fit through the foam and then the fins and through-holes were machined into the foam. The new design yielded a

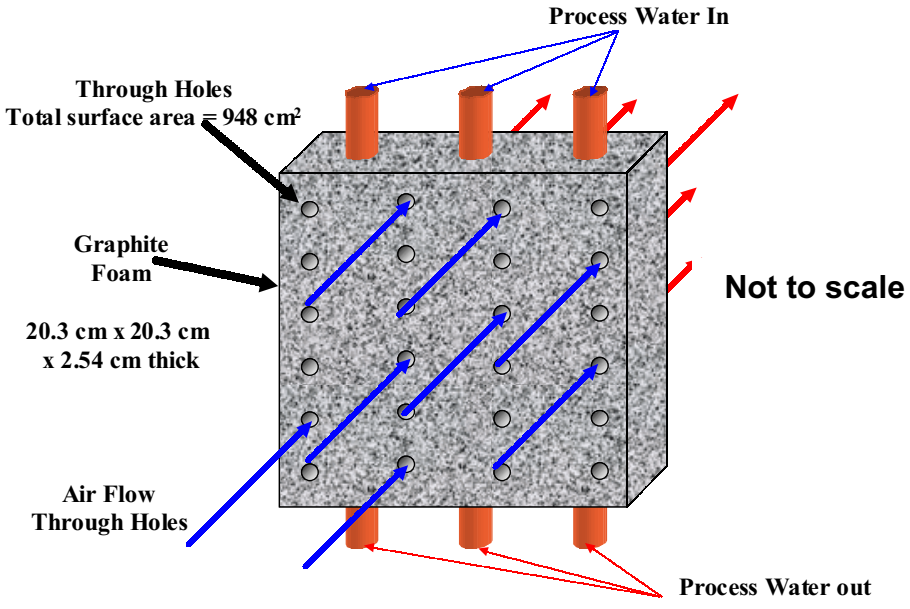


**Figure 3.** Schematic representation of heat exchanger with cooling air forced through channels in foam. Overall heat transfer coefficient measured at 943 W/m$^2$·K.

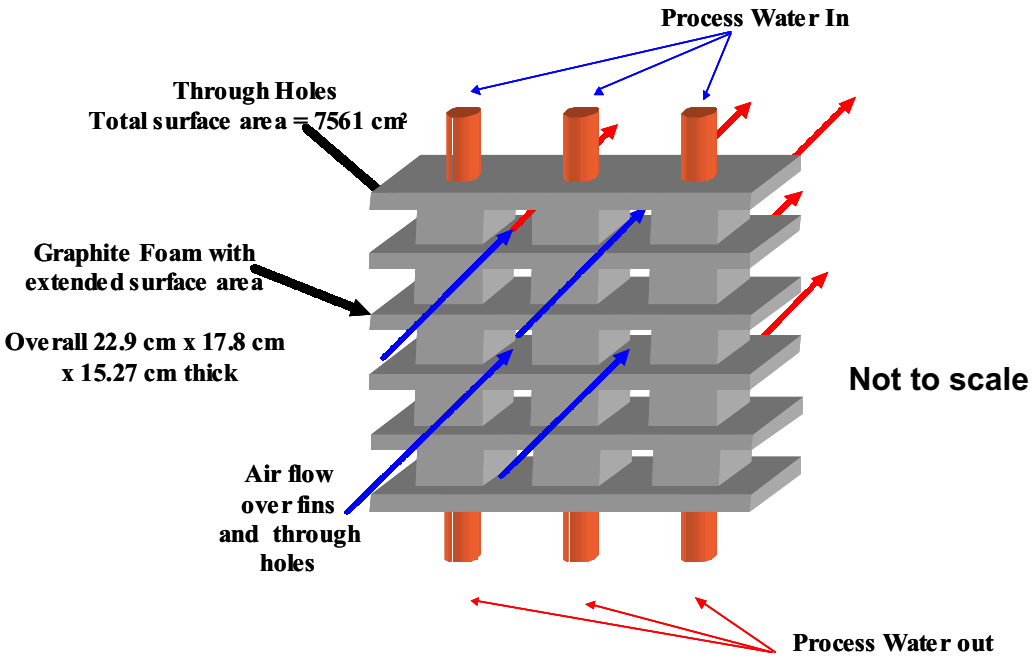


**Figure 4.** Schematic representation of heat exchanger with enhanced surface area machined into foam for enhanced heat transfer and reduced pressure drop. Overall heat transfer coefficient measured at 977 W/m$^2$·K. Note that several rows of this design were employed in the final version.

very small resistance to airflow, with a pressure drop of only 0.03 kPa/cm. Cooling air was ducted to the radiator at the rate of 39,300 L/min (dramatically smaller than the 1.7 million L/min of air at 180 mph at which the cars currently operate). The overall dimensions of the radiator were 22.9 cm × 17.78 cm × 15.27 cm deep, significantly smaller than current radiators. The hot engine coolant (pure water) flow rate was maintained at 57.5 L/min at 99.4°C. Under steady-state conditions, the water coolant temperature dropped from 99.4° to 91°C, which is the desired engine inlet coolant temperature (inlet temperatures below it will reduce engine efficiency). At the given coolant flow rate, this temperature is equivalent to 33.5 kW of heat rejected to the air and an increase from an ambient of 43°C for dry air (41°C for air at 60% relative humidity). The overall heat transfer coefficient was calculated to be 977 W/m$^2$·K. Because the desired inlet coolant temperature was achieved, this was deemed a successful test.

In a final test (see Figure 5), foam was machined into fins and adhesively bonded with epoxy to flat aluminum radiator tubes acquired from a radiator manufacturer. The device was approximately 30 × 7.5 × 4 cm, with eight fins per inch and a fin width of 0.060 in. This design dissipated 7 kW of heat to the air at a water flow rate of 15.1 gpm. The inlet water temp was 92.2°C and the outlet temperature was 90.5°C. These results were very disappointing, largely because of the poor heat transfer of the epoxy. It is clear that the techniques (gluing, brazing, press-fitting) used to assemble radiators have a dramatic effect on the heat transfer.

## Conclusions

High-conductivity graphite foam presents a unique solution to the thermal management problems that face fuel cell vehicles. Because the foam has a very high thermal conductivity and a very high surface area, the overall heat transfer coefficients of foam-based radiators can be orders of magnitude greater than those of conventional radiators. Novel carbon foam radiators of several different designs were fabricated and tested. The initial design produced an extremely high heat transfer coefficient (~2 orders of magnitude greater than those of conventional radiators) but created an unacceptable pressure drop. Alternative designs eliminated the

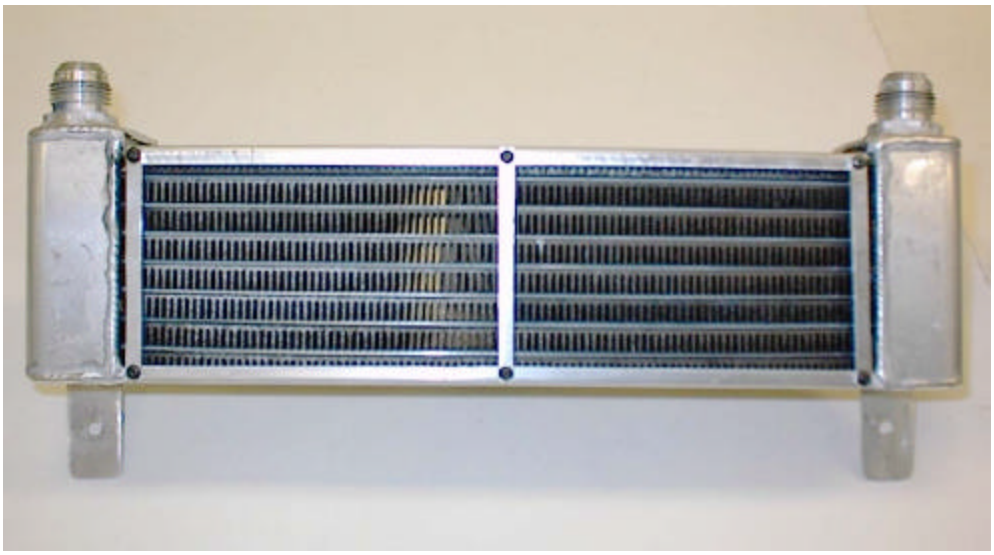

**Figure 5.** Photograph of radiator constructed which dissipates 7 kW of heat. Note that the foam is epoxied to the aluminum tubes, rather than brazed or press-fit.

pressure drop, but the heat transfer coefficients were reduced to about one sixth of the original value.

The data presented here illustrate that high-conductivity carbon foam has great promise for use in fuel-cell radiators; however, much work remains to be done. It appears that the foam will provide the greatest benefit when it is used in innovative designs and not used simply as a replacement for existing thermal management materials. The technique used to join or bond the foam to other materials has been proved to have a dramatic effect on heat transfer.

## References

1. J. Klett, R. Hardy, E. Romine, C. Walls, and T. Burchell, "High-Thermal-Conductivity, Mesophase-Pitch-Derived Carbon Foams: Effect of Precursor on Structure and Properties," *Carbon*, **32**(8) (2000).

2. J. Klett, "High Thermal Conductivity Mesophase Pitch-Derived Graphitic Foams," Composites in Manufacturing, **14** (4) (1999).

3. J. Klett, C. Walls, and T. Burchell, "High Thermal Conductivity Mesophase Pitch-Derived Carbon Foams: Effect of Precursor on Structure and Properties," p. 132 in *Proceedings of the 24th Biennial Conference on Carbon*, July 11–16, Charleston, South Carolina, 1999.

## FY 2000 Publications

J. W. Klett, C.-C. Tee, D. P. Stinton, and N. A. Yu, "Heat Exchangers Based on High Thermal Conductivity Graphite Foam, " in *Proceedings of the 1st World Conference on Carbon*, July 9–13, Berlin, Germany, 2000.

J. Klett, A. McMillan, and R. Ott, "Heat Exchangers for Heavy Vehicles," in *Proceedings of the Society of Automotive Engineering Government/ Industry Meeting*, June 19–21, Washington, D.C., 2000.

J. Klett, L. Klett, T. Burchell, and C. Walls, "Graphitic Foam Thermal Management Materials for Electronic Packaging," in *Proceedings of the Society of Automotive Engineering Future Car Congress*, Crystal City, Washington, D.C., April 2–6, 2000.

J. Klett and B. Conway, "Thermal Management Solutions Utilizing High Thermal Conductivity Graphite Foams," in *Proceedings of the 45th International SAMPE Symposium and Exhibition*, Long Beach, California, May 21–25, 2000.

J. Klett, R. Hardy, E. Romine, C. Walls, and T. Burchell, "High-Thermal-Conductivity, Mesophase-Pitch-Derived Carbon Foams: Effect of Precursor on Structure and Properties," *Carbon*, **32**(8) (2000).

## Awards

2000 B. T. Kelley Award, British Carbon Group

R&D 100 Award, "High Thermal Conductivity Carbon Foam"

## Patents Issued

"Process for Making Carbon Foam," U.S. Serial Number 6,033,506, Oak Ridge National Laboratory.

"Pitch-based Carbon Foam Heat Sink with Phase Change Material," U.S. Serial Number 6,037,032, Oak Ridge National Laboratory.

# F. Nanofluids for Thermal Management Applications

*S. Choi*
*Argonne National Laboratory, ET-335, 9700 South Cass Avenue*
*Argonne, IL 60439*
*(630) 252-6439; fax: (630) 252-5568; e-mail: choi@anl.gov*

*DOE Program Manager: Patrick Davis (202) 586-8061; fax: (202) 586-9811; e-mail: patrick.davis@hq.doe.gov*
*ORNL Technical Advisor: David Stinton (86) 574-4556; fax: (865) 574-6918; e-mail: stintondp@ornl.gov*

---

*Contractor: Argonne National Laboratory, Argonne, IL*
*Prime Contract No.: W-31-109-Eng-38*

---

## Objectives

- Exploit the unique properties of nanoparticles to develop high-thermal-conductivity heat transfer fluids.
- Characterize the thermal conductivity and heat transfer behavior of nanofluids.
- Develop nanofluid technology for increasing the thermal transport of engine coolants and lubricants.

## OAAT R&D Plan: Section 3.3: Task 5; Barrier C

## Approach

- Design and fabricate a hot-wire cell which requires 60 ml of nanofluids to measure the thermal conductivity of nanofluids.
- Characterize presently used coolants and model nanofluids supplied from the industrial partner.

## Accomplishments

- Successfully designed, fabricated, and tested a small hot-wire cell which requires only 60 ml of nanofluids in an effort to reduce the volume of testing samples (~10× reduction).
- In collaboration with Purdue University, characterized the thermal conductivity and heat transfer of present and developmental coolants supplied from the industrial partner.
- Discovered that the thermal conductivity of nanofluids increases as particle size decreases—a major milestone in the development of nanofluid technology.

## Future Direction

- Acquire commercially available nanoparticles of less than 10 nm and measure the thermal conductivity of nanoparticles in collaboration with Purdue University.
- Produce and characterize nanofluids containing nanoparticles of less than 10 nm.
- Produce and characterize nanofluids using new nanoparticle materials.
- Characterize nanofluid through heat transfer and pressure drop experiments.

---

## Introduction

The heat rejection requirement of a fuel-cell-powered vehicle can be significantly greater than that of a conventional automobile. Fuel cells currently operate at temperatures of approximately 80ºC, resulting in a smaller driving temperature difference for heat transfer in the radiator. These requirements lead to an alarming increase in radiator size (at least four times the size of the radiator used in conventional automobiles). It may not be possible to resolve these issues with conventional fan and radiator technology. Improved thermal management systems for vehicles require more compact heat exchangers, innovative heat transfer schemes, and fluids with improved heat transfer properties.

Conventional automotive heat transfer fluids, such as lubricants and engine coolants, are inherently poor heat transfer fluids. There is a strong need to develop advanced heat transfer fluids with significantly higher thermal conductivities and improved heat transfer. Modern fabrication technology provides opportunities for actively processing materials at the nanoscale. The thermal, mechanical, optical, magnetic, and electrical properties of nanophase materials are superior to those of conventional materials with coarse grain structures. Consequently, R&D of nanophase materials has drawn considerable attention from material scientists and engineers alike. Combining nanophase technology with heat transfer technology provides a new class of heat transfer fluids, called nanofluids, that are engineered by dispersing nanometer-size solid particles in traditional heat transfer fluids to increase thermal conductivity and heat transfer performance. [1]

Two techniques are used to make nanofluids: the single-step direct evaporation method, which simultaneously makes and disperses the nanoparticles directly into the base fluid; and the two-step method, which first makes nanoparticles and then disperses them into the base fluid. Although the two-step technique works well for oxide nanoparticles, it is not as effective for metal nanoparticles such as copper. For nanofluids containing high-conductivity metals, it is clear that the single-step direct evaporation technique is preferable to the gas-condensation processing. Argonne National Laboratory has already produced oxide nanofluids by the two-step technique and metal nanofluids by the single-step technique to conduct proof-of-concept tests. [2] In particular, it was demonstrated that stable suspensions can be achieved by maintaining the particle size below a threshold level. Figure 1 is a schematic diagram of the direct evaporation system built at Argonne. The liquid is in a cylinder that is rotated to continually transport a thin layer of liquid above a resistively-heated evaporation source. The liquid is cooled to prevent an undesirable increase in vapor pressure.

The thermal conductivity behavior of nanofluids with low particle concentrations (1–5% by volume) was also studied experimentally. Water and ethylene-glycol-based nanofluids, containing copper oxide and aluminum oxide nanoparticles, were tested. [3] The experimental results show that these nanofluids have substantially higher thermal conductivities than the same liquids without nanoparticles. For example, a 20% improvement in the thermal conductivity of ethylene glycol was observed when 4 vol % copper oxide was dispersed in this fluid. However, recent measurements show that metallic nanoparticles can increase the thermal conductivity by a significant amount over the oxide particles.

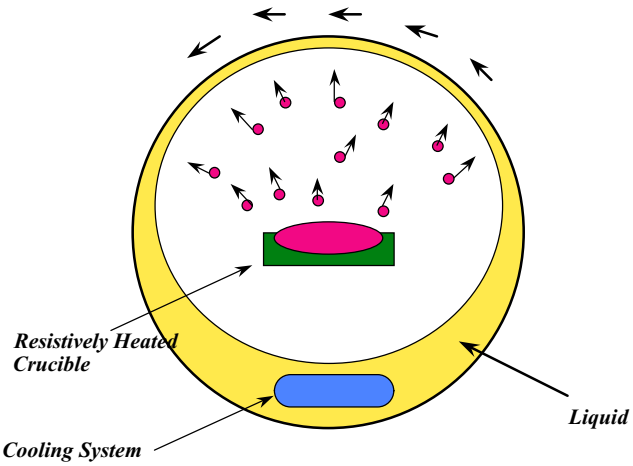


**Figure 1.** Schematic of nanofluid production system for direct evaporation of nanoparticles. The liquid is located in a cylinder that is rotated to continually transport a thin layer of liquid above a resistively-heated evaporation source. The liquid is cooled to prevent an undesirable increase in vapor pressure because of radiant heating during the evaporation.

The potential benefits of using nanofluids include these:

- improved heat transfer of engine coolants and oils
- reduced heat exchanger size and weight
- reduced heat transfer fluid inventory
- reduced coolant jacket size
- reduced emissions
- improved wear resistance
- reduced friction coefficient
- reduced pumping energy in existing system

The objectives of the project are to exploit the unique properties of nanoparticles to develop high-thermal-conductivity heat transfer fluids, to characterize the thermal conductivity and heat transfer behavior of nanofluids, and to develop nanofluid technology for increasing the thermal transport of engine coolants and lubricants.

## Approach

Our approach to overcoming the poor heat transfer rates of conventional automotive heat transfer fluids is to significantly increase the thermal conductivity of the liquids. An attractive method of doing so is the use of a suspension of solid nanoparticles in a liquid. Solids are chosen with thermal conductivities orders of magnitudes higher than those of the liquids. For example, the thermal conductivity of copper at room temperature is about 3000 times greater than that of engine oil. In fact, numerous theoretical and experimental studies of the effective thermal conductivity of dispersions that contain solid particles have been conducted since Maxwell's theoretical work was published more than 100 years ago.[4] However, published studies on thermal conductivity of suspensions have been confined mainly to millimeter- or micrometer-sized particles. A major problem with the use of such large particles is the rapid settling of these particles in fluids. Another is the abrasive nature of the suspension. The use of nanoparticles has the potential to produce the increased thermal conductivity sought in heat transfer fluids without the problems of settling and abrasion.[1] Maxwell's concept of enhancing the thermal conductivity of fluids by dispersing solid particles in them is old, but what is new and innovative regarding the concept of nanofluids is the idea of using the nanoparticles that have become available to us only recently.

To facilitate the development of nanofluid technology, a hot-wire cell that requires less fluid is needed to measure the thermal conductivity of nanofluids. Furthermore, presently used coolants and model nanofluids supplied from the industrial partner should be characterized.

## Results

Argonne has developed a cooperative R&D agreement (CRADA) with the Valvoline Company. The nanofluid project occupies the wide spectrum between the areas of basic science and applied R&D. The CRADA with Valvoline would directly benefit nanofluid technology development, funded jointly by OAAT and the Office of Heavy Vehicle Technologies. The objectives of the CRADA project are to develop our understanding and characterization of nanofluid technology to increase the thermal transport of engine coolants and lubricants, to assess the feasibility of applying the technology to vehicle thermal management systems, and to provide a solid basis for state-of-the-art applications of nanofluid technology to advanced vehicle thermal management systems.

An article by Wang, Xu, and Choi, "Thermal Conductivity of Nanoparticle-Fluid Mixture," was published in the October–December 1999 issue of *Journal of Thermophysics and Heat Transfer* . It was demonstrated that thermal conductivities computed by theoretical models are much lower than the measured data. A more comprehensive theory is needed to explain the behavior of nanofluids.

A hot-wire cell used to measure the thermal conductivity of nanofluids required about 500 ml of nanofluids. In an effort to reduce the volume of testing samples, a small hot-wire cell which requires only 60 ml of nanofluids was successfully designed, fabricated, and used. New, smaller hot-wire cells were used to measure and characterize thermal conductivity as a function of nanoparticle size. Figure 2 shows that the thermal conductivity of oxide nanofluids increases with decreasing particle size. The discovery that "smaller is better" is a major milestone in the development of nanofluid

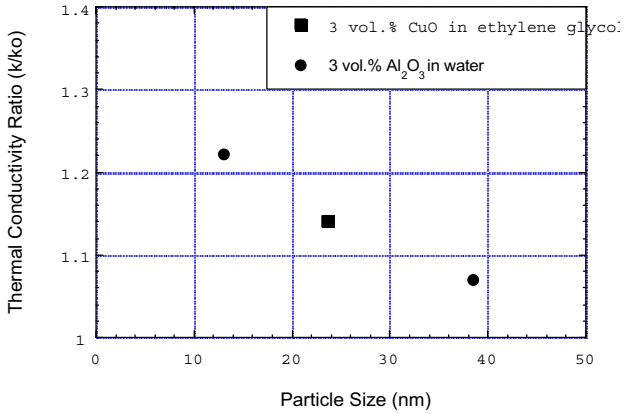


**Figure 2.** Thermal conductivity ratio of oxide nanofluids as a function of particle size.

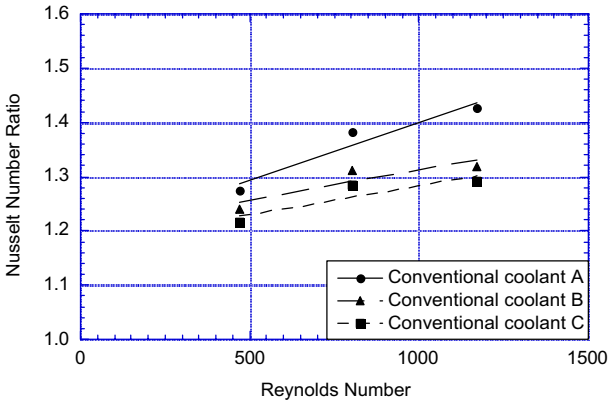


**Figure 3.** Comparative heat transfer of a model nanofluid to conventional cooling fluids.

technology and creates new challenges in manufacturing nanoparticles as small as 1 nm. Also, the discovery will directly impact the fundamentals of nanofluid technology. Therefore, we need to conduct simulations of nanofluids based on nanofluid theory or molecular dynamics because no existing theories consider nanoparticle size as a dominant parameter in enhancing nanofluid thermal conductivity.

Valvoline has produced a model nanofluid. The thermal conductivity measurements and some predictive estimates of heat transfer coefficients and colligative properties, using traditional chemical engineering approaches, were completed for a model nanofluid system. Heat transfer coefficients for laminar flow in the developing region of a circular tube were measured on this model system and on three conventional coolants. A greater than 20% improvement in the Nusselt number was observed, compared with conventional coolants, as shown in Figure 3. The improved heat transfer coefficient of a model nanofluid would allow the use of smaller and lighter heat exchangers in future applications using nanofluids. Future work will focus on further matching of predictions vs measured colligative properties, looking for exceptions to classical behavior. Once the model system is fully characterized, the work will be extended to practical systems.

## Conclusions

Thermal conductivity and heat transfer experiments were performed using commercial and developmental coolants supplied from the industrial partner. Significantly enhanced thermal properties are obtained with nanofluids by successfully exploiting the unique properties of nanoparticles in liquids. In future applications using nanofluids, the improved thermal properties of nanofluids would allow the use of significantly smaller and lighter heat exchangers for fuel-cell powered vehicles, heavy vehicles, hybrid-electric vehicles, and other performance-driven systems.

Characterization of the thermal conductivity of nanofluids as a function of nanoparticle size has led to a discovery that the thermal conductivity of nanofluids increases with decreasing particle size. It should be noted that particle size is of primary importance in the development of nanofluid technology.

## References

1. U. S. Choi, “Enhancing Thermal Conductivity of Fluids with Nanoparticles,” pp. 99–105 in *Developments and Applications of Non-Newtonian Flows*, D. A. Siginer and H. P. Wang, eds., FED–Vol. 231/MD-Vol. 66, American Society of Mechanical Engineers, New York, November 1995.

2. J. A. Eastman, U. S. Choi, S. Li, L. J. Thompson, and S. Lee, “Enhanced Thermal Conductivity through the Development of Nanofluids,” pp. 3–11 in *Proceedings of the Symposium on Nanophase and Nanocomposite Materials II*, Vol. 457, Materials Research Society, Boston, 1997.

3. S. Lee, U. S. Choi, S. Li, and J. A. Eastman, "Measuring Thermal Conductivity of Fluids Containing Oxide Nanoparticles," *ASME Tran. J. Heat Transfer*, **121**, 280–289 (1999).

4. J. C. Maxwell, *A Treatise on Electricity and Magnetism*, 2nd ed., Clarendon Press, 1881, pp. 1, 435.

## FY 2000 Publications/Presentations

X. Wang, X. Xu, and U. S. Choi, "Thermal Conductivity of Nanoparticle-Fluid Mixture," *Journal of Thermophysics and Heat Transfer* , **13**(4), 474–480 (1999).

J. A. Eastman, U. S. Choi, S. Li, G. Soyez, L. J. Thompson, and R. J. DiMelfi, "Novel Thermal Properties of Nanostructured Materials," *Journal of Metastable and Nanocrystalline Materials* , **2–6**, 629–34 (1999), also *Materials Science Forum* , **312–314**, pp. 629–34 (1999).

U. S. Choi and G. Zhang (Valvoline), "Nanofluids," presented at the Workshop on Thermal Management for Heavy Vehicles, October 19–20, Argonne National Laboratory, 1999.

## Awards/Patents

A patent on nanofluids is pending.

# G. Carbon Composite for PEM Fuel Cells

*T. M. Besmann, J. W. Klett, and J. J. Henry, Jr.*
*Surface Processing and Mechanics Group and Carbon and Insulating Materials Group*
*Oak Ridge National Laboratory, P.O. Box 2008, MS 6063, Bldg. 4515*
*Oak Ridge, TN 37831-6063*
*(865) 574-6852; fax: (865) 574-6198; e-mail: besmanntm@ornl.gov*

*DOE Program Manager: JoAnn Milliken (202) 586-2480; fax: (202) 586-9811; e-mail: JoAnn.Milliken@hq.doe.gov*
*ORNL Technical Advisor: David Stinton (865) 574-4556; fax: (865) 574-6918; e-mail: stintondp@ornl.gov*

*Contractor: Oak Ridge National Laboratory, Oak Ridge, Tennessee*
*Prime Contract No.: DE-AC05-00OR22725*

## Objectives

- Develop a slurry-molded carbon fiber material with the surface sealed by chemical-vapor-infiltration (CVI) as a bipolar plate.
- Collaborate with potential manufacturers with regard to testing and manufacturing of such components.

## OAAT R&D Plan: Section 3.3: Task 13, Barrier B

## Approach

- Fabricate fibrous component preforms for the bipolar plate by slurry-molding techniques using carbon fibers of appropriate lengths.
- Fabricate hermetic plates using a final seal with chemical-vapor-infiltrated carbon.
- Develop commercial-scale components for evaluation.

## Accomplishments

- Demonstrated the ability to mold prototypical 100-$cm^2$ active area plate (single- and two-sided).
- Demonstrated freeze and thaw resistance.
- Demonstrated a very low corrosion rate (less than that of the material supplied by Poco Graphite).
- Provided single-sided specimens to industry for evaluation.

## Future Direction

- Scale to 15 × 15-cm plates or other commercial designs.
- Transfer technology to partners such as Plug Power, Honeywell, Porvaire, H Power, and others.

## Introduction

In FY 2000, the ORNL carbon composite bipolar plate effort has achieved several programmatic goals in molding preforms, producing two-sided plates, and demonstrating corrosion and freeze/thaw resistance. Single-sided components 1.5 mm in thickness and two-sided plates 2.5 mm in thickness with 100 $cm^2$ of active area have been produced. Sample components are being tested at Plug Power and Honeywell for their evaluation. Previously it was demonstrated that projected costs would meet program goals, that the material properties met program requirements, and that the component had the substantial advantage of weighing almost 50% less than competing materials.

## Approach

Fibrous component preforms for the bipolar plate are prepared by slurry-molding techniques using 400-µm carbon fibers (e.g., Amoco DKD-x mesophase pitch fiber) in water containing phenolic resin. The approach is such that a vacuum molding process produces a low-density preform material. A phenolic binder is used to provide green strength; it also assists in providing geometric stability after an initial cure. The surface of the preform is sealed using a CVI technique in which sufficient carbon is deposited on the near-surface fibers to make the surface hermetic. The preforms are placed in a furnace that is heated to 1400–1500°C, and methane under reduced pressure is allowed to flow over the components. The hydrocarbon reacts and deposits carbon on the exposed fibers of the preforms; when sufficient deposition has occurred, the surfaces become sealed. Thus the infiltrated carbon provides both an impermeable surface and sufficient electrical conductivity that power can be efficiently obtained from the cell. Processing times are in the range of 4 hours.

The bipolar plates tested to date have been fabricated with machined flow fields. In production, these plates would need to use embossed or otherwise impressed features, as machining would be too costly. A set of brass molds was fabricated with 0.78-mm (31 mil)-deep and -wide channels. The molds were used to impress channels and other features into the preform material.

## Results

Brass molds containing the flow field pattern and other necessary features were fabricated to produce 100-$cm^2$ active area plates of the Los Alamos National Laboratory design (Figure 1). Slurry-molded preforms 2.5 mm in thickness were produced for fabrication into two-sided bipolar plates. These were placed between the brass molds, and the assembly was placed in a heated press. The mold was uniformly compressed to 10 kPa (14 psi) at 200°C and held briefly both to impress the features and to cure the phenolic resin. The molded preforms released readily from the mold (a common release agent is used), and the features were precisely reproduced in the preform (Figure 2).

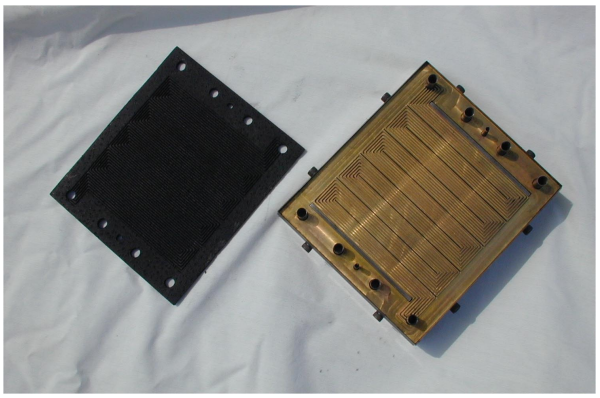

**Figure 1.** A brass mold used to impress the flow field and other features into slurry-molded preforms, along with one of the molded components with a 100-$cm^2$ active area.

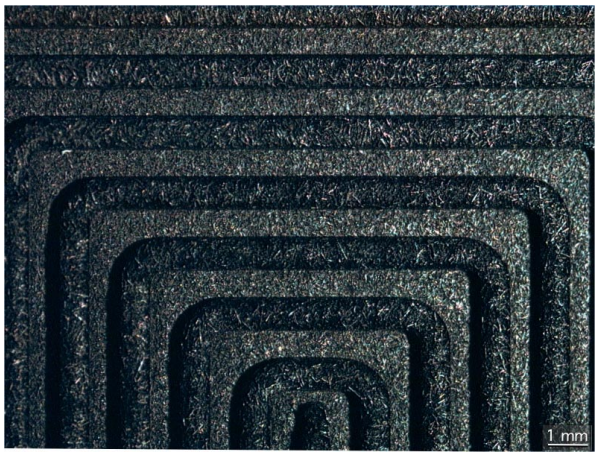


**Figure 2.** Features of the impressed flow-field surface (channels are 0.8 mm deep and wide).

After cooling, the preform is removed and is ready for the CVI step. In collaboration with Brown University, we have been modeling the CVI process to optimize uniformity and reduce processing time. The result has been that higher flows and adjustment of the flow pattern have been found to improve both time and uniformity. A typical infiltrated component is seen in Figure 3.

Dissolution characteristics were determined from voltage curves. These measurements were performed in the following solution: 0.001 N $H_2SO_4$, 2 ppm $F^-$ and a temperature of 80°C with nitrogen purge. Over a period of 60 days, little corrosion was observed and the properties remained constant (Figure 4).

To evaluate the effect of freezing and thawing of water on the bipolar plate structure, a machined flow-field plate was saturated with water and allowed to freeze. The plate was then thawed and dried, and there was no apparent mechanical failure, based on a visual inspection. Measurement of the through-thickness gas leakage rate revealed no deterioration of hermeticity due to freeze/thaw effects.

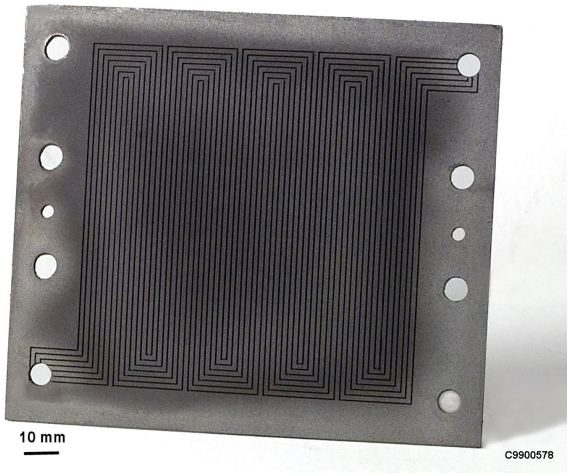


**Figure 3.** Completed carbon composite bipolar plate.

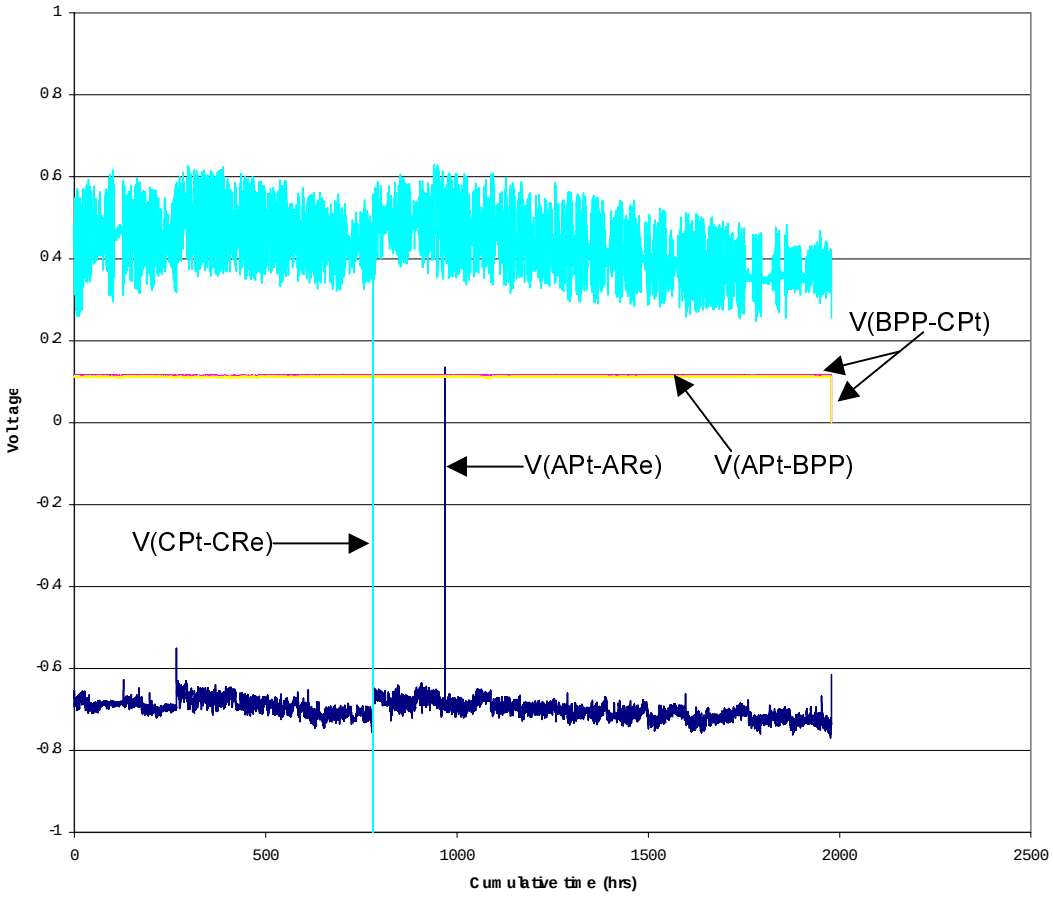


**Figure 4.** Voltage plot from corrosion testing of the carbon composite bipolar plate indicating a low corrosion rate which is invariant over the 60-day test.

## Conclusions

During this period, the molding of the flow field and other features into slurry-molded preforms was demonstrated for two-sided bipolar plates. This process resulted in components that replicated the mold and that were easily prepared for the CVI step. Corrosion testing over a 60-day span revealed little effect on the material—its performance was superior to that of the material supplied by Poco Graphite. Freeze/thaw testing of the components revealed no detrimental effect.

## Patents Issued

"Bipolar Plate/Diffuser for a Proton Exchange Membrane Fuel Cell," U.S. Patent 6,037,073, March 14, 2000.

"Bipolar Plate/Diffuser for a Proton Exchange Membrane Fuel Cell," process patent pending.

# H. Cost-Effective Metallic Bipolar Plates Through Innovative Control of Surface Chemistry

*M. P. Brady and L. D. Chitwood*
*Oak Ridge National Laboratory, P.O. Box 2008, MS 6115*
*Oak Ridge, TN 37831-6115*
*(865) 574-5153; fax: (865) 574-7659; e-mail: bradymp@ornl.gov*

*DOE Program Manager: JoAnn Milliken (202) 586-2480; fax: (202) 586-9811; e-mail: JoAnn.Milliken@hq.doe.gov*
*ORNL Technical Advisor: David Stinton (865) 574-4556; fax: (865) 574-6918; e-mail: stintondp@ornl.gov*

---

*Contractor: Oak Ridge National Laboratory, Oak Ridge, Tennessee*
*Prime Contract No.: DE-AC05-00OR22725*

---

## Objectives

- Develop a metallic alloy capable of forming a defect-free, corrosion-resistant nitride (carbide, boride) surface layer during gas nitridation to enable use as a bipolar plate in polymer electrolyte membrane (PEM) fuel cells. The alloy must meet DOE cost/performance goals related to the $10/kW bipolar plate target.

## OAAT R&D Plan: Section 3.3: Task 13; Barrier B

## Approach

- Form a protective TiN surface on a Ti-containing alloy by elevated temperature exposure in a nitrogen containing gas. The effort will focus on model ductile Nb-Ti-W (the commercial alloy known as Tribocor), Ni-Ti-based, and Ti-based alloys that are amenable to fabrication to final form by rolling/stamping prior to the nitridation treatment.
- Immerse nitrided alloy coupons in 5% HF to qualitatively evaluate the corrosion resistance and protectiveness of the nitrided surface. Characterize nitride layer microstructure and composition by cross-section scanning electron microscopy (SEM) and electron probe microanalysis (EPMA). Determine electrical conductivity by dc four-point probe. Modify alloy composition and processing conditions to optimize the electrical conductivity and protectiveness of the TiN surface.
- Supply initially optimized nitrided coupons to Los Alamos National Laboratory for detailed corrosion testing in simulated fuel cell environments.
- Down-select an alloy nitride protection mode (inward-growing nitrogen gradient zone or discrete TiN scale) for final optimization and assess the potential of this approach to meet DOE bipolar plate performance/cost goals.

## Accomplishments

- Evaluated the nitridation behavior of a series of Ni-Ti, Fe(Ni)-Ti, and Ni(Cu)-Ti –based alloys.
- Demonstrated a bulk electrical conductivity of $1.47 \times 10^4\ \Omega^{-1}\ cm^{-1}$ for nitrided Ni-10Ti-2.5W-0.15Zr wt %. This value surpasses the DOE electrical conductivity target by two orders of magnitude.

- Delivered nitrided Nb-30Ti-20W wt % (Tribocor) and Ni-10Ti-2.5W-0.15Zr wt % coupons to Los Alamos for corrosion testing.
- Evaluated nitrided Nb-30Ti-20W wt % in the Los Alamos Corrosion Test Cell. It exhibited a 5-hour stabilized corrosion current of $6.1 \times 10^{-7}$ A/cm$^2$ at the air electrode potential of 0.98V vs NHE (data of Kirk Weisbrod). This value meets current DOE corrosion goals. The nitrided Ni-10Ti-2.5W-0.15Zr wt % showed evidence of local surface defects after a 5-hour potential hold that resulted in a transition to unacceptably high corrosion rates.
- Down-selected the inward-growing nitrogen gradient zone protection mode (modeled by nitrided Nb-30Ti-20W wt %) over the discrete TiN scale protection mode (modeled by nitrided Ni-10Ti-2.5W-0.15Zr wt %).
- Obtained preliminary findings that suggest that adding zirconium to titanium promotes the formation of a corrosion-resistant inward-growing nitrogen zone. An optimized nitrided Ti-based alloy has the potential to meet DOE performance/cost goals.

### Future Direction

- Optimize composition and nitridation conditions for inward-growing nitrogen gradient zone Ti-Zr–based alloys and evaluate their electrical conductivity and corrosion resistance (deliver coupons to Los Alamos and Plug Power for evaluation). Include examination of alloying additions, such as V, that improve the cold-formability of titanium. Evaluate alloying additions to promote an inward-growing nitrogen gradient zone in Fe-Ti and Fe(Ni)-Ti alloys (much less expensive than Ti-based alloys).
- Obtain industrial input/collaboration with regard to alloy formability and cost to assist in down-selection of the final alloy base.
- Evaluate the performance of optimized 1-in.-diameter nitrided bipolar plate in a single-cell PEM fuel cell test rig at Los Alamos. Initiate scale-up to 4 in.× 4 in. plates and deliver them to industry for in-cell evaluation and feedback.

---

## Introduction and Approach

The bipolar plate is one of the most expensive components in PEM fuel cells. Thin metallic bipolar plates offer the potential for significantly lower cost than the machined graphite bipolar plates that currently are used, and the potential for reduced weight/volume and better performance than developmental carbon fiber and graphite bipolar plates currently under consideration. However, inadequate corrosion resistance can lead to high electrical resistance and/or contaminate the PEM. Metal nitrides, carbides, and borides (e.g., TiN, NbC) offer electrical conductivities of up to an order of magnitude greater than graphite and are highly corrosion resistant. Unfortunately, conventional coating methods leave "pin-hole" defects in the nitride (carbide, etc.) layers that result in accelerated local corrosion and unacceptable performance.

The goal of this effort is to develop a titanium-containing bipolar plate alloy that will form an electrically conductive and corrosion-resistant TiN surface layer during thermal nitriding. There are three advantages to this approach. First, because the nitriding is performed at elevated temperature, pin-hole defects are not expected because thermo dynamic and kinetic factors favor complete conver sion of the metal surface to nitride. Rather, the key issues are nitride layer cracking, adherence, and morphology (discrete internal precipitates vs continuous external scales), which can be controlled through proper selection of alloy composition and nitridation conditions. Second, thermal nitridation is an inexpensive, well-established industrial technique. Third, the alloy can be formed into final shape by inexpensive metal forming techniques, such as stamping, prior to thermal nitridation.

Two protection schemes were identified: (1) a discrete TiN surface layer and (2) an inward-growing nitrogen gradient zone. The discrete TiN surface layer approach is highly amenable to the formation of a corrosion-resistant TiN composition, but it can be sensitive to the presence of surface defects (e.g., porosity, inclusions), edges, and corners. An inward-growing nitrogen gradient zone is formed on

- Delivered nitrided Nb-30Ti-20W wt % (Tribocor) and Ni-10Ti-2.5W-0.15Zr wt % coupons to Los Alamos for corrosion testing.
- Evaluated nitrided Nb-30Ti-20W wt % in the Los Alamos Corrosion Test Cell. It exhibited a 5-hour stabilized corrosion current of $6.1 \times 10^{-7}$ A/cm$^2$ at the air electrode potential of 0.98V vs NHE (data of Kirk Weisbrod). This value meets current DOE corrosion goals. The nitrided Ni-10Ti-2.5W-0.15Zr wt % showed evidence of local surface defects after a 5-hour potential hold that resulted in a transition to unacceptably high corrosion rates.
- Down-selected the inward-growing nitrogen gradient zone protection mode (modeled by nitrided Nb-30Ti-20W wt %) over the discrete TiN scale protection mode (modeled by nitrided Ni-10Ti-2.5W-0.15Zr wt %).
- Obtained preliminary findings that suggest that adding zirconium to titanium promotes the formation of a corrosion-resistant inward-growing nitrogen zone. An optimized nitrided Ti-based alloy has the potential to meet DOE performance/cost goals.

### Future Direction

- Optimize composition and nitridation conditions for inward-growing nitrogen gradient zone Ti-Zr–based alloys and evaluate their electrical conductivity and corrosion resistance (deliver coupons to Los Alamos and Plug Power for evaluation). Include examination of alloying additions, such as V, that improve the cold-formability of titanium. Evaluate alloying additions to promote an inward-growing nitrogen gradient zone in Fe-Ti and Fe(Ni)-Ti alloys (much less expensive than Ti-based alloys).
- Obtain industrial input/collaboration with regard to alloy formability and cost to assist in down-selection of the final alloy base.
- Evaluate the performance of optimized 1-in.-diameter nitrided bipolar plate in a single-cell PEM fuel cell test rig at Los Alamos. Initiate scale-up to 4 in.× 4 in. plates and deliver them to industry for in-cell evaluation and feedback.

---

## Introduction and Approach

The bipolar plate is one of the most expensive components in PEM fuel cells. Thin metallic bipolar plates offer the potential for significantly lower cost than the machined graphite bipolar plates that currently are used, and the potential for reduced weight/volume and better performance than developmental carbon fiber and graphite bipolar plates currently under consideration. However, inadequate corrosion resistance can lead to high electrical resistance and/or contaminate the PEM. Metal nitrides, carbides, and borides (e.g., TiN, NbC) offer electrical conductivities of up to an order of magnitude greater than graphite and are highly corrosion resistant. Unfortunately, conventional coating methods leave “pin-hole” defects in the nitride (carbide, etc.) layers that result in accelerated local corrosion and unacceptable performance.

The goal of this effort is to develop a titanium-containing bipolar plate alloy that will form an electrically conductive and corrosion-resistant TiN surface layer during thermal nitriding. There are three advantages to this approach. First, because the nitriding is performed at elevated temperature, pin-hole defects are not expected because thermodynamic and kinetic factors favor complete conversion of the metal surface to nitride. Rather, the key issues are nitride layer cracking, adherence, and morphology (discrete internal precipitates vs continuous external scales), which can be controlled through proper selection of alloy composition and nitridation conditions. Second, thermal nitridation is an inexpensive, well-established industrial technique. Third, the alloy can be formed into final shape by inexpensive metal forming techniques, such as stamping, prior to thermal nitridation.

Two protection schemes were identified: (1) a discrete TiN surface layer and (2) an inward-growing nitrogen gradient zone. The discrete TiN surface layer approach is highly amenable to the formation of a corrosion-resistant TiN composition, but it can be sensitive to the presence of surface defects (e.g., porosity, inclusions), edges, and corners. An inward-growing nitrogen gradient zone is formed on

metals and alloys with a high nitrogen permeability and, because of the inward nature of the growth front, is not sensitive to surface defects, edges, or corners. However, it can be difficult to form a dense, continuous TiN surface layer to impart the desired degree of corrosion resistance.

## Results and Conclusions

Selected for study were a series of Ni, Ni(Fe), and Ni(Cu)-Ti-based alloys with the potential to form a discrete TiN surface layer, and Nb-30Ti-20W wt %, which forms an inward-growing nitrogen gradient zone. Nickel was selected as an alloy base because it does not form a stable nitride, has a low nitrogen permeability, is reasonably low in cost (≈$3 to 4/lb raw material cost) and is highly formable. Titanium is added because it is a strong nitride former and is also reasonably low in cost (≈$3–4/lb raw material cost). The Nb-30Ti-20W alloy, commercially known as Tribocor, was designed to form a corrosion- and wear-resistant nitrogen gradient zone during thermal nitriding. It is too costly for transportation-related PEM fuel cell applications, but it was selected as a model inward-nitrogen gradient zone-forming alloy.

The alloys were nitrided in $N_2$-$4H_2$ at 1000–1100°C for 24–48 hours. To screen for corrosion resistance and the presence of defects in the protective layer, nitrided coupons were immersed in 5% HF for 24 hours. Post-exposure weight change measurements and cross-section scanning electron microscopy and EPMA were used to gage the protectiveness of the nitrided surface and to provide feedback for modification and initial optimization of alloy composition. Based on these studies, 1-in.-square coupons of nitrided Ni-10Ti-2.5W-0.15Zr wt % (Figure 1) and Nb-30Ti-20W wt % (Figure 2) were sent to Los Alamos for evaluation of corrosion resistance in simulated PEM fuel cell environments.

The nitrogen concentration for both alloys in the near surface region was in the range 46–48 at. %, which is in the range reported for TiN (Figures 1 and 2). The Ti-nitride formed on the Ni-Ti–based alloy was present as a discrete, continuous layer on the order of 5 μm thick (Figure 1). In contrast, the nitrogen gradient zone formed on the Nb-30Ti-20W alloy extended tens of microns into the depth of the alloy (Figure 2). The bulk electrical conductivity of

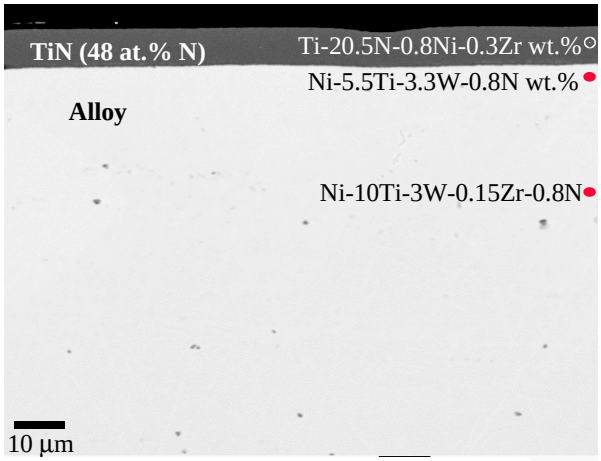


**Figure 1.** SEM cross-section micrograph of Ni-10Ti-2.5W-0.15Zr wt % nitrided for 48 h at 1100°C in $N_2$-$4H_2$.

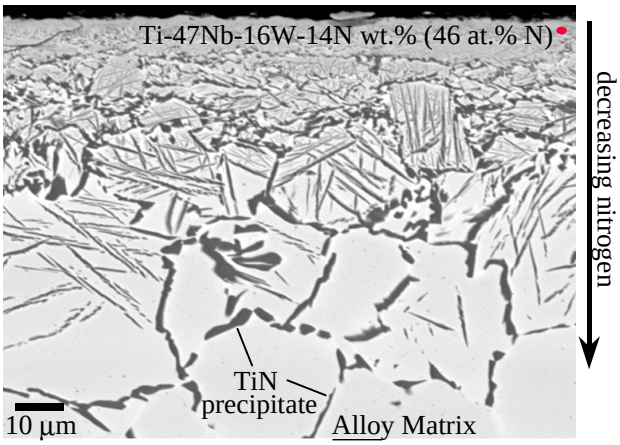


**Figure 2.** SEM cross-section micrograph of Nb-30Ti-20W wt % nitrided for 48 h at 1100°C in $N_2$-$4H_2$.

nitrided Ni-10Ti-2.5W-0.15Zr was $1.47 \times 10^4\ \Omega^{-1}\ cm^{-1}$, which exceeds the DOE goal by two orders of magnitude (measured at room temperature by dc 4-point probe). This value is consistent with the bulk electrical conductivity of TiN, and similar excellent electrical conductivities are expected for all nitrided alloys examined under this program.

Nitrided Ni-10Ti-2.5W-0.15Zr wt % initially exhibited a low corrosion current in a simulated PEM fuel cell environment of 0.001 N $H_2SO_4$ (2 ppm $Fl^-$, 80°C, deaerated with $N_2$) (Figure 3, data of Kirk Weisbrod). However, after a 5-hour hold at the anode and cathode potentials, the corrosion

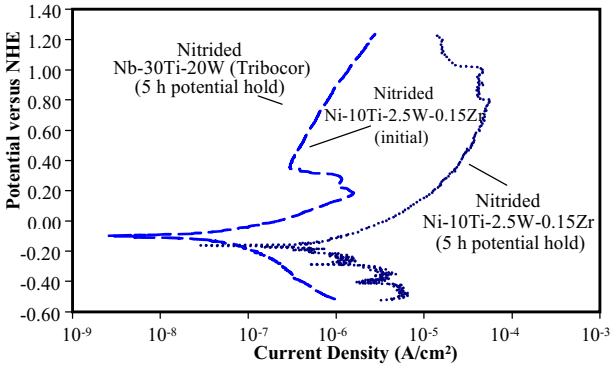


**Figure 3.** Polarization curves: 0.001 N $H_2S0_4$, 2 ppm $Fl^-$, 80°C deaerated with $N_2$ (data from Kirk Weisbrod, Los Alamos National Laboratory).

current increased significantly, which is indicative of the presence of local flaws in the discrete TiN surface layer formed on the Ni-10Ti-2.5W-0.15Zr wt % coupon. The flaws likely result from local inclusions or porosity initially present in the Ni-10Ti-2.5W-0.15Zr wt % casting, or possibly TiN scale cracking at sharp coupon edges and corners (post-exposure characterization is planned). The tendency toward defects makes alloys that form a discrete TiN surface layer, such as Ni-10Ti-2.5W-0.15Zr wt %, unacceptable for use as bipolar plate materials.

In contrast, the nitrided Nb-30Ti-20W wt % coupon exhibited excellent corrosion resistance (both initially and after the 5-hour potential hold), with a corrosion current of $6.1 \times 10^{-7}$ A/cm$^2$ at 0.98 V vs NHE (normal hydrogen electrode). (It should be noted that the Nb-30Ti-20W wt % alloy itself is quite corrosion resistant and may have minimized the effects of any flaws present in the nitrided surface region; post-exposure characterization is planned to check for this possibility.) This degree of corrosion resistance is comparable to the best materials tested to date in the Los Alamos Corrosion Test Cell and meets the current target corrosion performance goal set by DOE. This result strongly suggests that a nitrogen gradient zone formed by thermal nitridation of an alloy can be sufficiently defect-free and corrosion resistant to permit use of the alloy as a PEM fuel cell bipolar plate. Therefore, a down-selection was made to focus solely on alloys that form a nitrogen gradient zone during thermal nitridation.

Unfortunately, niobium-based alloys such as Nb-30Ti-20W wt % are too expensive for transportation-related PEM fuel cell applications. The key to the success of this effort is therefore the development of a less costly alloy that forms a corrosion-resistant nitrogen gradient zone similar to that formed by Nb-30Ti-20W wt %. Work will initially focus on titanium because it forms an inward-growing nitrogen gradient zone during thermal nitridation and offers an attractive combination of low density (4.5 g/cm$^3$ range) and moderate cost and formability sufficient to potentially meet the goals of this effort. Pure titanium is not suitable because its nitrogen permeability is so high that it tends to form an intermixed $Ti_2N$ + TiN surface layer (often cracked) during thermal nitridation. Such a nitrogen gradient zone is not sufficiently corrosion resistant to meet the performance goals.

Preliminary results suggest the corrosion resistance of nitrided titanium can be significantly improved by the addition of zirconium. Nitrided Ti-10Zr-5W-2.5Ni wt % was not attacked during a 4-hour screening immersion in 5% HF, while similarly nitrided pure titanium exhibited a weight loss in excess of 50 mg/cm$^2$. Future work will focus on the optimization of composition and nitridation conditions for Ti-Zr-based alloys that form an inward-growing nitrogen gradient zone, including the examination of alloying additions, such as V, that improve the cold formability of titanium. Alloying additions to promote an inward-growing nitrogen gradient zone in Fe-Ti and Fe(Ni)-Ti-based alloys (much less expensive than Ti-based alloys) will also be evaluated. Industrial input and collaboration will be sought with regard to alloy formability and cost to assist in down-selection of the final alloy base.

# 4. ADVANCED COMBUSTION

## A. Microwave-Regenerated Exhaust Particulate Filter Technology

*Dick Nixdorf*
*Industrial Ceramic Solutions, LLC, 1010 Commerce Park Drive, Suite I*
*Oak Ridge, TN 37830*
*(865) 482-7552; fax: (865) 482-7505; e-mail: nixdorfr@indceramicsolns.com*

*DOE Program Managers: Patrick Davis (203) 586-8061; fax: (202) 586-9811; e-mail: patrick.davis@hq.doe.gov and Ken Howden (202) 586-9811; fax: (202) 586-3631; e-mail: ken.howden@ee.doe.gov*
*ORNL Technical Advisor: David Stinton (865) 574-4556; fax: (865) 574-6918; email: stintondp@ornl.gov*

---

*Contractor: Industrial Ceramic Solutions, Oak Ridge, Tennessee*
*Prime Contract No.: 80X-SZ896V*
*Subcontractor: Microwave Materials Technologies, Inc., Knoxville, Tennessee*

---

### Objectives

- Transfer the FY 1999 bench scale testing to actual engine test cell work on three types of diesel engines.
- Demonstrate 75% efficiency in the removal of exhaust particulate matter.
- Demonstrate a microwave regeneration efficiency to adequately clean the filter to within 90% of the new filter condition while the engine is operating at idle speed.
- Provide data on microwave regeneration power requirements and the frequency of regeneration cycles needed during a normal diesel engine operating condition.

### OAAT R&D Plan; Task 16; Barrier B

### Approach

- Design and fabricate a silicon carbide fiber filter cartridge and microwave regeneration system capable of performing on a PNGV-type diesel engine.
- Test this microwave filter system on a Ford 1.2-L DIATA diesel engine, a Volkswagen 1.9-L diesel engine, and an International 7.3-L diesel engine.
- Analyze the data from the three diesel engine tests to determine particulate removal efficiency, regeneration efficiency, power required for microwave cleaning of the filter cartridge, and approximate cycle time between regenerations.

### Accomplishments

- Demonstrated 80–95% diesel particulate removal efficiency of the microwave filter system over the three engine tests.
- Demonstrated the capability of microwave regeneration of the filter cartridge, at engine idle operating conditions, to return the filter to 95–100% of the exhaust flow capacity of a new filter.

- Obtained data to show that a 1.9-L Volkswagen engine, operating at cruising speed, would require regeneration by the microwave approximately every 6 hours. The regeneration would consume 1.75 kW of power over a 2-min period once every 6 hours (average 0.3% fuel penalty).
- Demonstrated that the microwave-regenerated filter system has the potential to comply with the EPA 2007 Tier II Standards for diesel particulates.

### Future Direction

- Prove the durability of the microwave-regenerated filter system on an operating vehicle.
- Complete product development of the microwave filter system to achieve full compatibility with a particular car and engine type to move toward a commercial application.

---

## Introduction

Current diesel engine particulate filter technologies depend on a catalyst to assist in the regeneration of the filter. Catalyst technology requires an exhaust temperature of approximately 350 °C to be effective. Small diesel engines achieve this exhaust temperature only with extended operation at over 60 mph. The microwave-regenerated particulate filter can achieve acceptable particulate removal efficiencies and regenerate at low exhaust temperatures—from engine startup to idle to speeds below 60 mph. It is the potential answer to problems associated with the urban driving cycle, where the catalyst technologies are ineffective. It may also be a solution to the cold-start issue that is responsible for a significant quantity of both diesel and gasoline engine emissions. Microwave heating of catalyst substrates and other diesel soot traps has been tried. The Industrial Ceramic Solutions (ICS) technology is unique because it is based on a recently discovered special silicon carbide fiber that efficiently converts microwave energy to heat energy. A small mass of these fibers can achieve temperatures of 1200 °C in 9 seconds in a standard household microwave oven. ICS has developed a process to incorporate this discovery into a filter cartridge and microwave regeneration system for use in diesel engine exhaust streams, as shown in Figure 1.

## Approach

Diesel engine test cells provide actual operating diesel exhaust environments with the capability to measure the exhaust particulate emissions before and after the filter system. After FY 1999 bench testing, ICS has advanced to tests on commercial diesel engines. The first trial on a diesel engine for the microwave filter system occurred on the 1.2-L

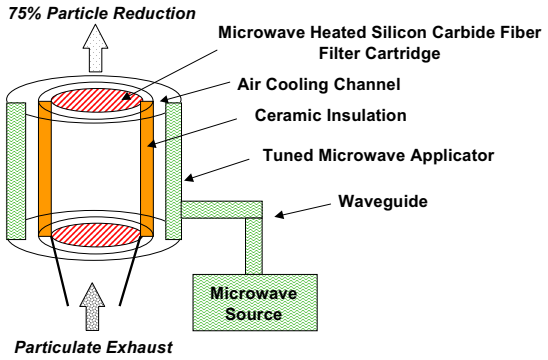


**Figure 1.** Microwave-regenerated ceramic filter system.

DIATA diesel at the Ford Motor Company's Scientific Research Laboratory. Figure 2 shows the entry and exit sides of the silicon carbide filter after a filtration cycle on the DIATA engine, where 86% of the diesel particulate was removed. Data were obtained to demonstrate particulate removal efficiency and regeneration efficiency. Since it takes up to 6 hours to load the ICS filter to the regeneration point on these small engines, a high-soot-generating International 7.3-L diesel engine (mounted in a Ford truck) was run on a chassis dynamometer test at the University of Tennessee. This larger, high-soot production engine allowed multiple loadings and regeneration cycles of the filter system in a relatively short period of time. That test apparatus, which is shown in Figure 3, provided data on filter soot loading capacity, multiple regeneration cycle efficiencies, and the regeneration power requirements. All pressure drop measurements were taken at a constant exhaust flow of 100 kg/hour. A final test to obtain more accurate analytical emissions control data was conducted on a 1997 Volkswagen 1.9-L engine at the Oak Ridge National Laboratory (ORNL) diesel engine test facility. This information

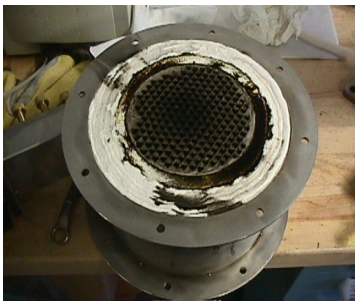

**Ceramic Filter Entry Side**

**Ceramic Filter Exit Side**

**Figure 2.** Entry and exit sides of the silicon carbide filter.

**Figure 3.** Test apparatus at the rear of a Ford F-250 diesel truck.

provided answers to the auto industries' questions on particle size distribution of the soot passing through the filter and on the emissions evolved during microwave regeneration of the filter. ICS was able to combine the results of the three diesel engine tests to calculate the time span between regenerations and the fuel penalty for using the microwave-regenerated particulate filter technology.

## Results

The diesel engine test results exceeded the FY 2000 milestone objectives. Six consecutive exhaust soot loading and microwave regeneration cycles, using the International 7.3-L diesel engine, measured the regeneration efficiency. Regeneration efficiency is calculated as the difference in pressure drop across the filter at maximum particulate loading and after regeneration, divided by the difference in pressure drop at this maximum and the pressure drop across a new filter. The first four microwave regeneration cycles returned the particulate-laden filter cartridge to within 95% of its "new filter condition." The last two regenerations returned the filter to 100% of the clean condition. Figure 4 shows these loading and microwave regeneration cycles of the filter system, as tested at the University of Tennessee. During regeneration, the captured carbon particulates are oxidized and released as harmless $CO_2$ gas. Microwave-regenerated filter particulate removal efficiency was verified on the Volkswagen 1.9-L diesel engine at ORNL. Testing by the ORNL engineers demonstrated an 80–95% removal of diesel exhaust particulate. Particulate removal efficiency was unaffected by transient cycles through idle and high-speed conditions. Exhaust particulate after the filter did not increase as a result of microwave regeneration. The ORNL scientists observed that the backpressure increase across the filter, as a result of soot build-up, was significantly less than for other particulate filter technologies. This factor would extend the time span between microwave regenerations to reduce the energy drain on the diesel engine and the system's fuel penalty. Microwave regeneration will be performed under engine idling conditions and will likely be controlled by engine operating time or backpressure across the filter.

## Conclusions

Three tests on different types of commercial diesel engines continue to show the feasibility of the microwave-regenerated diesel particulate filter system to provide a diesel emissions control solution. The FY 2000 objectives targeted a 75% filter

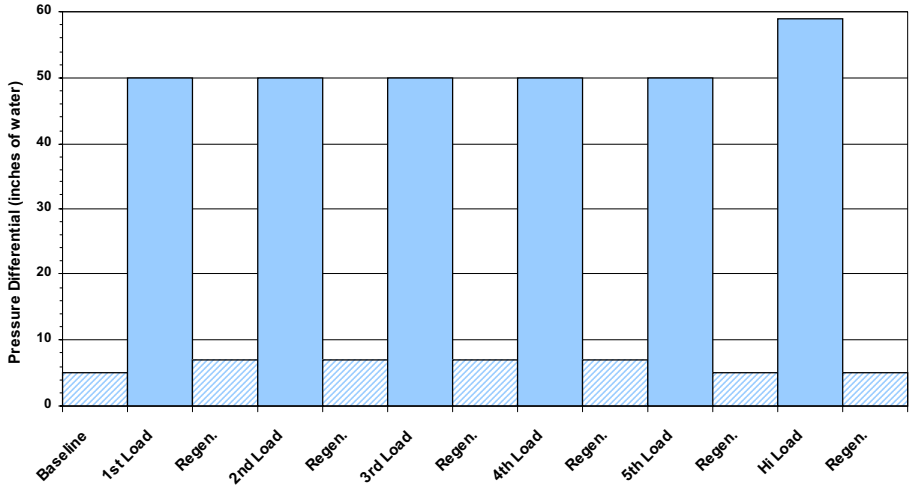


**Figure 4.** Ford F-250 exhaust filter testing. University of Tennessee chassis dynamometer. Loading and regeneration cycles are based on pressure differential.

reduction of diesel particulate. The test results demonstrated 85–95% efficiency. The milestone for filter cleaning by microwave regeneration was 90%. The diesel engine test results attained 95–100% regeneration efficiency by microwave cleaning. Most existing exhaust particulate reduction technologies carry a 5% fuel penalty. The microwave filter system fuel penalty, as calculated from these test results, is 0.3%. Proposed catalyst technologies require expensive adjustments to engine operating conditions and fuel additives to achieve regeneration at temperatures below 350 °C. The microwave filter, with its independent heating source, is able to regenerate at these lower temperatures. Figure 5 shows that the microwave-regenerated filter, as demonstrated by the test results, is capable of compliance

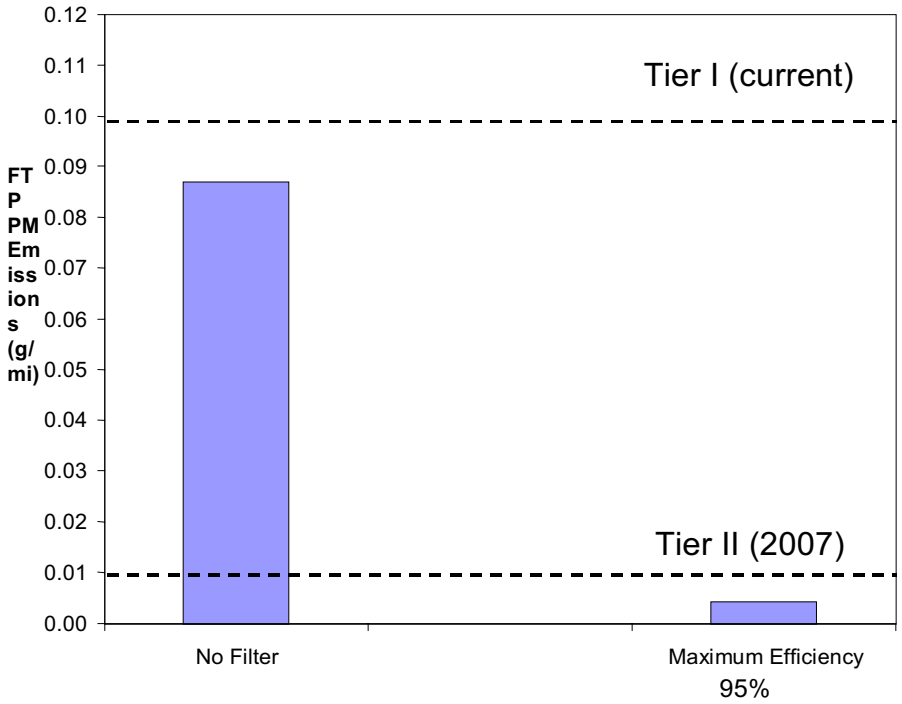


**Figure 5.** 1997 Volkswagen Jetta filter testing compared with EPA Tier II regulations.

with the EPA Tier II Particulate Matter regulations for light-duty vehicles. The next phase of the program will be durability testing, using diesel engine test cells and on-road vehicle demonstrations in conjunction with the auto manufacturers.

# B. NFC Coatings for CIDI Fuel Injection System Components

*George R. Fenske (primary contact), Oyelayo Ajayi, John Woodford, and Ali Erdemir*
*Argonne National Laboratory, ET-212, 9700 South Cass Avenue*
*Argonne, Illinois 60439*
*(630) 252-5190; fax: (630) 252-4798; email: gfenske@anl.gov*

*DOE Program Manager: Patrick Davis (202) 586-8061; fax: (202) 586-9811; e-mail: patrick.davis@hq.doe.gov*
*ORNL Technical Advisor: David Stinton (865) 574-4556; fax: (865) 574-6918; email: stintondp@ornl.gov*

---

*Contractor: Argonne National Laboratory, Argonne, Illinois*
*Prime Contract No.: W-31-109-Eng-38*

---

## Objectives

- Determine the impact of advanced fuel system strategies (advanced designs and low-emission fuels) on the reliability and durability of the materials and surface treatments of critical fuel system components.
- Evaluate the performance of amorphous carbon coatings and other advanced surface treatments subjected to severe contact conditions under fuel or oil lubrication.
- Determine the effect of exhaust gas recirculation (EGR) on the tribological properties of engine lubricants, and characterize the potential of advanced surface treatments to improve the reliability and durability of critical engine components subjected to EGR-contaminated lubricants.

## OAAT R&D Plan: Section 3.2: Task 5; Barriers A, B

## Approach

- Perform benchtop friction and wear tests to characterize the friction and wear properties of baseline materials and coatings subjected to tribological environments prototypical of engine components and systems.
- Deposit near-frictionless carbon (NFC), commercial diamond-like carbon, and other commercial coatings (e.g., CrN, TiN) and evaluate their tribological performance in terms of both reliability-limiting failure (scuffing) and durability in both fuels and lubricants.
- Characterize engine lubricants exposed to various levels of EGR.
- Perform benchtop tests to characterize tribological properties of materials and oil lubricants exposed to EGR.
- Correlate benchtop test results with field results.
- Develop advanced materials and surface treatments for high-EGR levels.

## Accomplishments

- Selected and developed tribological test protocols for the evaluation of different failure mechanisms of materials and coated components (at Argonne National Laboratory).
- Completed preliminary benchtop tribological testing of baseline materials, NFCs, and limited commercial coatings in diesel fuels.
- Completed preliminary analysis of engine lubricants exposed to different levels of EGR.

### Future Direction

- Analyze and compare failure modes and wear modes of baseline and advanced coatings under stringent tribological conditions (low-lubricity fuels and EGR-contaminated lubricants).
- Evaluate the scuffing resistance and wear resistance of NFC-coated and other commercially available coatings.

## Introduction

Reduction of emissions from CIDI engines will require low-sulfur and possibly low-aromatic fuels to minimize degradation of aftertreatment devices, reduce particulate formation, and minimize lubricant degradation. Such fuels, however, have poor lubricity and can increase the occurrence of catastrophic scuffing failure and reduce the long-term durability of critical components. Reducing emissions from CIDI engines may also require the use of low-emission lubricant additive packages that have lower levels of sulfur, phosphorus, and metallic-based compounds critical for anti-wear and low-friction properties. Furthermore, more aggressive engine environments resulting from recirculation of combustion products (particulates and acids) through the use of EGR to reduce $NO_x$, downsized and lighter-weight components, higher injection pressures, and higher speeds will exacerbate the ability of current materials and lubricants to meet reliability and durability requirements. Consequently, there is a need to develop new materials and/or surface modification technologies with superior tribological attributes.

## Approach

The approach at Argonne is the use of tribological coatings—specifically, NFC coatings—to meet the technical challenges.

The development of NFC coatings for advanced CIDI fuel system components requires optimization of the NFC deposition process to minimize catastrophic scuffing and long-term wear. Benchtop friction and wear protocols were employed at Argonne to characterize the scuffing and wear performance of current materials, providing a baseline for comparison with NFC coatings and commercially available coatings (e.g., DLC, CrN, TiN). Commercial coatings applied to benchtop samples were obtained from different suppliers and subjected to the same test protocols as those for the baseline and NFC-coated specimens to obtain information on the scuffing severity index (the product of the critical load, velocity, and friction coefficient at the point where scuffing occurs), as well as on the wear rate.

The process used to deposit the NFC coatings is illustrated in Figure 1. It is a plasma-assisted chemical vapor deposition technique that utilizes a proprietary gas chemistry and plasma potential to form an amorphous carbon coating with unique chemical bonding. Tribological performance studies in dry inert environments have repeatedly demonstrated extremely good properties, with friction coefficients of as low as 0.001 and wear rates in the $10^{-10}$ $mm^3$/N-m range. The current program addresses the properties of NFC coatings in environments prototypical of engines, with emphasis on

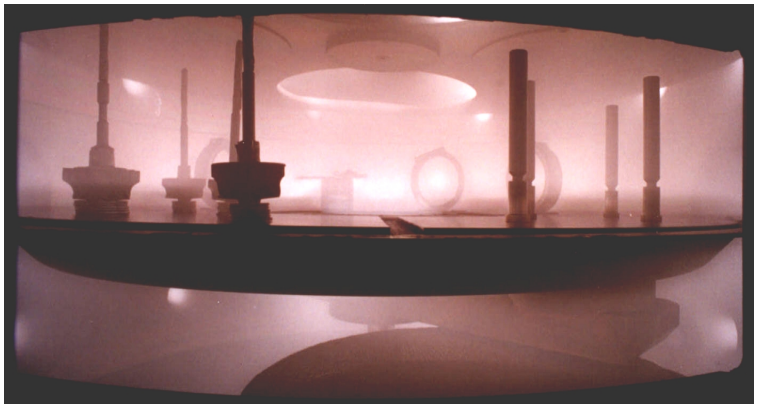

**Figure 1.** Photograph of different engine components being coated with NFC coatings.

assessing the role of sulfur in the fuel on scuffing and wear.

Scuffing resistance was evaluated with a reciprocating pin-on-flat configuration such as that shown in Figure 2. Scuffing tests were conducted at different constant contact loads and with a step-increase in sliding speed until scuffing occurred. Tests were conducted in the load range of 150–400 N, corresponding to an initial Hertzian stress of 1.1–1.8 GPa, 1–15 Hz reciprocating frequency, and a stroke length of about 20 mm, translating to sliding speeds of 0.04–0.6 m/s. The results of a preliminary set of tests are shown in Figure 3, which compares the scuffing resistance of conventional diesel fuel (approx. 500 ppm sulfur) with that of a synthetic diesel fuel with 0 ppm sulfur. The data demonstrate two features: first, the scuffing resistance of the synthetic fuel is less than that of conventional diesel fuel with 500 ppm sulfur; and, second, use of the NFC coating increased the scuffing resistance by one order of magnitude. Microscopic analysis of worn areas indicates that scuffing occurred only after the NFC coating was either worn away or spalled under extremely high loads.

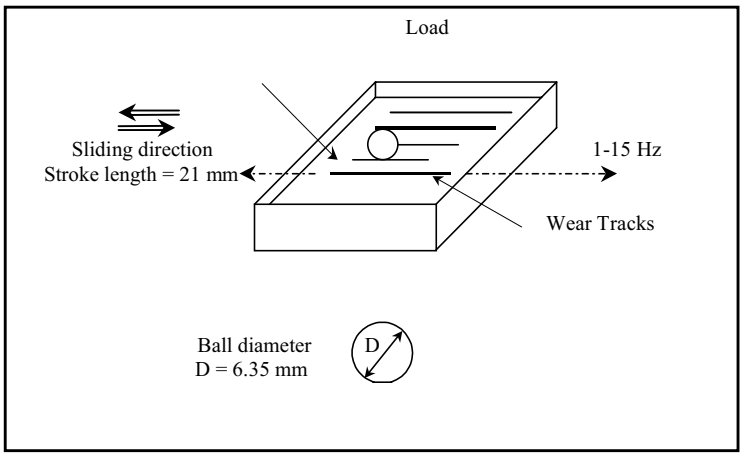


**Figure 2.** Reciprocating pin-on-flat configuration used to evaluate scuffing failure.

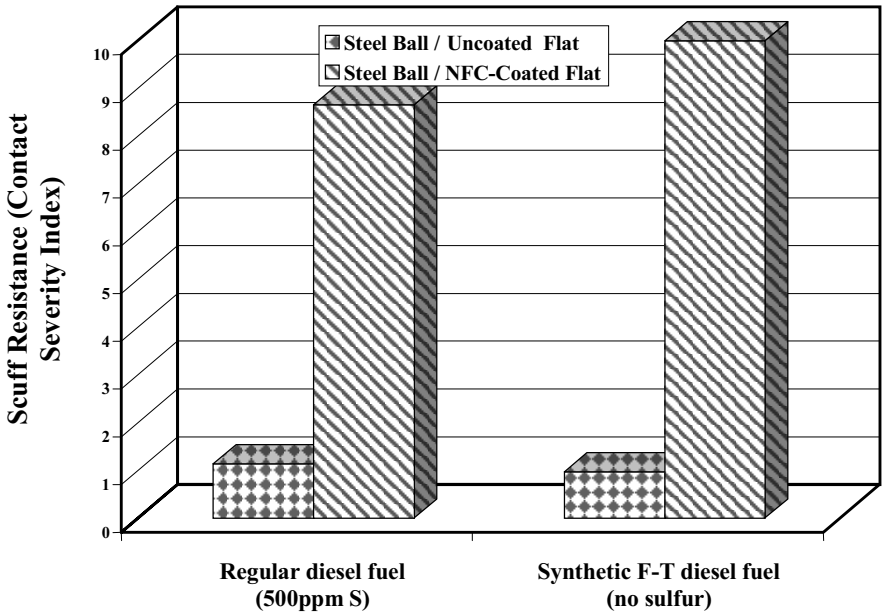


**Figure 3.** Scuffing severity index of uncoated and NFC-coated steel in conventional diesel and synthetic (Fischer Tropsch) diesel fuel.

The durability of the NFC coating and other hard coatings was examined with a high-frequency reciprocating test rig using a ball-on-flat contact geometry. Tests were conducted with uncoated 52100 steel balls sliding on coated flats. Figure 4 shows the effect of various coatings on the long-term wear (durability) of a steel surface sliding in zero-sulfur synthetic diesel fuel (Fischer-Tropsch, or FT). The three variations of NFC evaluated all reduced the wear of both the ball and flat specimens substantially (more than 10 times) compared with other hard coatings and uncoated surfaces.

Because of these exceptional results of NFC coatings in terms of scuffing prevention and durability, several fuel system suppliers are interested in using this technology in production. We are currently collaborating with a number of manufacturers of plasma-assisted chemical vapor deposition original equipment to transfer the NFC process technology in this area, and we anticipate receiving a state-of-the-art unit that will be modified to accept the NFC process.

## Future Direction

Efforts are also being pursued to evaluate the properties of NFC coatings for other engine components; one such program is being conducted in cooperation with a diesel engine original equipment manufacturer. The overall focus of the project is to evaluate the effect of EGR on the lubricating properties of engine lubricants exposed to higher levels of soot and acid. Traditional approaches to solving the EGR problem would be to increase the detergent levels and acid-neutralizing additives in the oil. However, in light of the need to minimize sulfur, phosphorous, and metallic compounds in engine oils because of their deleterious effects on aftertreatment devices, this may not be a viable approach. Consequently, efforts are under way to determine (a) the impact of using higher levels of EGR on the lubricating properties of engine lubes and (b) the role of advanced coatings in mitigating these effects.

## Publications/Presentations

M. F. Alzoubi, O. O. Ajayi, O. L. Eryilmaz, O. Ozturk, A. Erdemir, and G. R. Fenske, "Tribological Behavior of Near-Frictionless Carbon Coatings in High- and Low-Sulfur Diesel Fuels," SAE Paper 2000-01-1548, Society of Automotive Engineers, Warrendale, Pennsylvania.

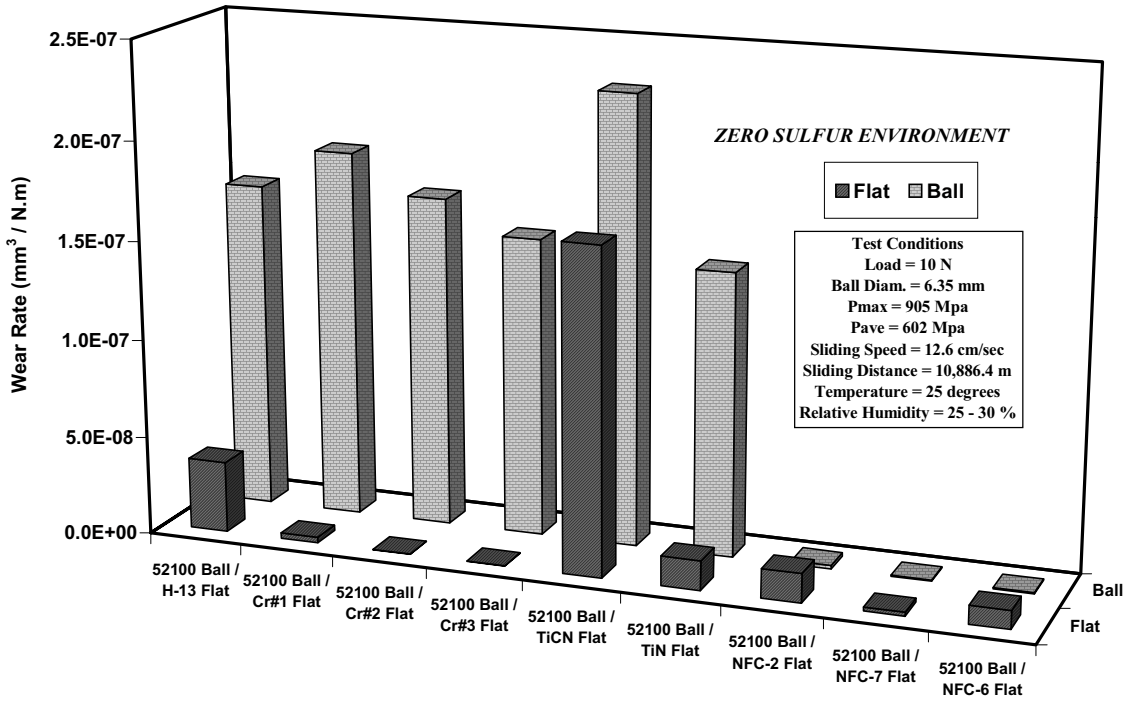


**Figure 4.** Effect of coatings on the durability (wear rates) in synthetic diesel (Fischer Tropsch) fuel.

A. Erdemir, O. Ozturk, M. Alzoubi, J. Woodford, O. Ajayi, and G. R. Fenske, "Near-Frictionless Carbon Coatings for Use in Fuel Injectors and Pump Systems Operating with Low-Sulfur Diesel Fuels," SAE Paper 2000-01-0518, Society of Automotive Engineers, Warrendale, Pennsylvania.

O. O. Ajayi, M. Alzoubi, A. Erdemir, G. R. Fenske, O. L. Eryilmaz, and S. Zimmerman, "Tribological Performance of NFC Coatings under Oil Lubrication," SAE Paper 2000-01-1547, Society of Automotive Engineers, Warrendale, Pennsylvania.

A. Erdemir, O. L. Eryilmaz, and G. R. Fenske, "Synthesis of Diamondlike Carbon Films with Superlow Friction and Wear Properties," presented at the 46th International Symposium of the American Vacuum Society, Oct. 25–29, 1999, Seattle.

# C. Rapid Surface Modifications of Aluminum Engine Bores for Weight Reduction

*C. A. Blue, R. D. Ott, P. J. Blau, M. L. Santella, P. G. Engleman, and D. C. Harper*
*Oak Ridge National Laboratory, P.O. Box 2008, Bldg. 4508*
*Oak Ridge, TN 37831-6083*
*(865) 574-4351; fax: (865) 574-4357; email: blueca@ornl.gov*

*DOE Program Manager: Patrick Davis (202) 586-8061; fax: (202) 586-9811; e-mail: patrick.davis@hq.doe.gov*
*ORNL Technical Advisor: D. P. Stinton (865) 574-4556; fax: (865) 574-6918; email: stintondp@ornl.gov*

---

*Contractor: Oak Ridge National Laboratory, Oak Ridge, Tennessee*
*Prime Contract No.: DE-AC05-00OR22725*

---

## Objectives

- Develop a new durability-enhancing coating for aluminum automotive applications, such as engine block cylinder bores, compressor housings, fuel pumps, and sealing surfaces, using innovative rapid, high-density infrared surface modification processes.
- Characterize the coatings through metallurgical analysis and tribology and ultimately in real-world environments.

## OAAT R&D Plan: Section 3.2: Task 5; Barrier C

## Approach

- Treat the cylinder internal bores and other surfaces with coatings to enhance wear resistance and lower friction with the intention of eliminating the need for heavy cast iron cylinder liners for engines, or to allow for the use of machinable aluminum alloys such as 319 and put 390 in high-wear areas.
- Investigate two separate plasma-assisted coating application techniques, one using a 300,000-W radiant lamp source to directly fuse a pre-sprayed material onto a surface, and the second using a weld-overlay technique to fuse material into the surface.
- Use metallurgical analysis, hardness testing, and energy dispersive X-ray analysis to optimize the coatings metallurgically.
- Perform pin-on-disk wear testing, following ASTM standards, to quantify the wear resistance of the 390 aluminum alloy overlays and coating fused by the high-density radiant source. Compare these results with those from bulk 390 aluminum alloy and gray cast iron to quantify the quality of the coatings.

## Accomplishments

- Successfully fused tungsten carbide and chromium carbide with both copper and nickel-based binders directly onto aluminum.
- Quantified the quality of this coating using metallography and hardness testing.
- Developed a plasma-assisted deposition process, which is capable of depositing 390 aluminum onto 319 aluminum.

- Confirmed through metallurgical analysis, hardness testing, energy-dispersive X-ray analysis, and wear testing that the 390-aluminum overlay has properties comparable to those of bulk 390.

### Future Direction

- Develop and optimize the deposition of wear coatings for automotive applications utilizing the plasma arc lamp.
- Perform additional dry and lubricated wear testing of 390 aluminum overlay and cermet coatings.
- Identify automotive parts for treatment and apply coatings for field-testing.
- Develop funds-in work with DaimlerChrysler and Ford Motor Company to ensure the availability of parts and field-testing.

---

## Introduction

Cast aluminum alloys are being used to reduce the weight of internal combustion engine blocks conventionally made of heavy cast iron. To maintain adequate wear and frictional characteristics, cast-iron cylinder liners are often installed within aluminum blocks. Eliminating the need for these heavy liners requires developing a cost-effective surface treatment for the aluminum alloy surfaces where they mate with the sliding piston rings. Eliminating these liners is expected to reduce engine weight and reduce the costs associated with inserting the cast-iron liners.

Two separate approaches are currently being investigated to obtain a wear-resistant coating on 319 aluminum—which also apply to A359—and both have had substantial success. The first approach fuses WC/Ni, WC/Cu, $Cr_2C_3$/Ni, and $Cr_2C_3$/Cu coatings directly onto aluminum using the high-intensity infrared lamp. In this process, a powder precursor is sprayed at room temperature on aluminum and fused with a 300,000-W plasma arc lamp. The second approach, an overlay process, utilizes simple welding-type equipment. The overlay process melts a high-silicon-content precursor directly into the 319-based material to form a 3- to 5-mm-thick layer with 390 aluminum properties. This process also has been accomplished with TiC and $TiB_2$/390 mixtures.

## Fused Cermet Coatings

The quality of the cermet coatings fused directly onto the aluminum has been quantified by metallography and hardness testing. Figure 1 shows the metallurgical bond between WC/319 aluminum and $Cr_2C_3$/319 aluminum; a nickel-based metal is used

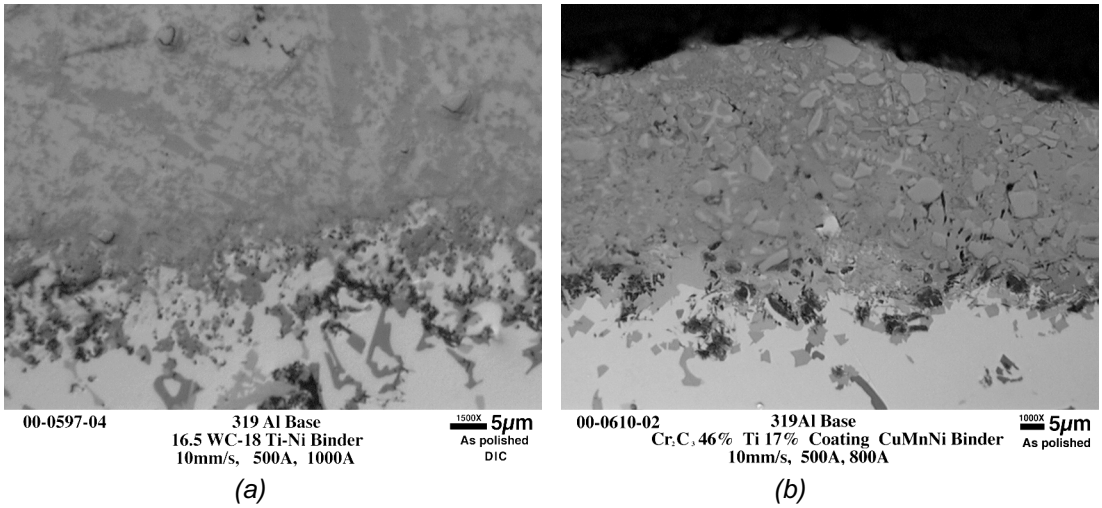


**Figure 1.** (*a*) WC/Ni and (*b*) $Cr_2C_3$/Cu coated onto 319 aluminum.

as the metal binder between the tungsten carbide and copper for the $Cr_2C_3$. These metallurgical bonds produce very adherent coatings. Hardness testing reveals that the average hardness of the $Cr_2C_3$ coating was 600 HV, while the base material had a hardness of 100 HV. In the case of the tungsten carbide, the coating had an average hardness of 900 HV. It should be noted that, with this process, there is no interfacial mixing between the coating and the base material, which is key to maximizing coating properties.

Preliminary calculations reveal a power cost of less than $\$.01/cm^2$ for fusing these materials. The cost of deposition should be minimal, as it is a room-temperature spray process, but the cost has not been quantified. The other associated cost would be that of the coating material, which will depend on the type and thickness. It should be less expensive than competing plasma spray processes because of the limited material needed. Wear and friction testing of these coatings is incomplete at this time.

## Overlay Coatings

The second approach produces a high-silicon-content surface layer on aluminum alloys that dramatically improves the abrasion and wear resistance. This process is relatively simple and straightforward and relies on standard techniques for aluminum manufacturing (i.e., no exotic processing equipment is required). This process is presently being patented.

Using this process, the thickness of the surface layers can be controlled over a wide range. Figure 2 shows the appearance, after machining, of a piece of cast 319 alloy that has been surface-treated with aluminum-silicon alloy on opposing faces. The surface layers are clearly visible. The porosity level in the overlay is lower than that in the casting, and the surface layers are metallurgically bonded to the 319 cast alloy. Microscopic examination of the aluminum-silicon surface layers indicated that they consisted of a fine eutectic microstructure, containing relatively large silicon particles, that is identical to 390 aluminum (Figure 3).

The interface between the 390 coating and 319 base material is metallurgically bonded and consists

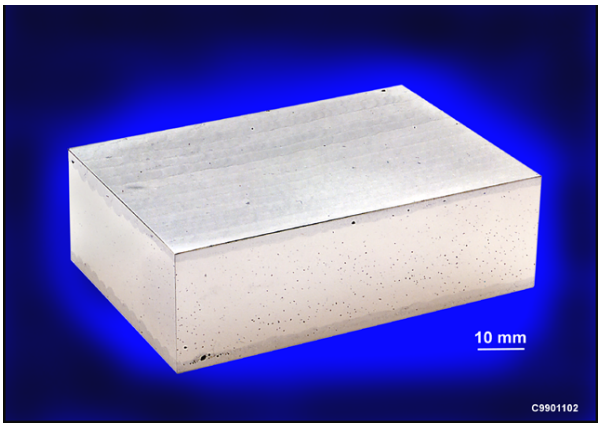


**Figure 2.** Photograph of aluminum alloy 319 casting after surfacing top and bottom with aluminum-silicon and machining.

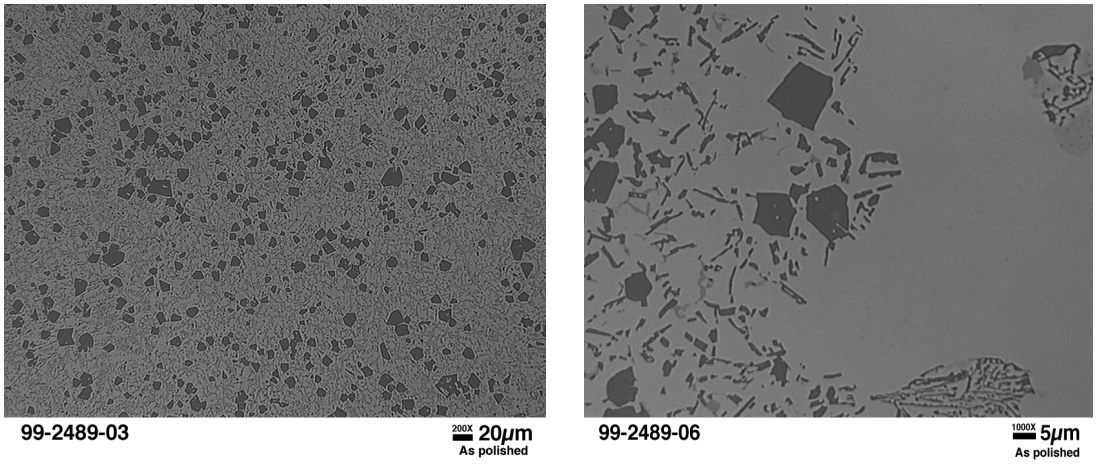


(*a*) (*b*)

**Figure 3.** Microstructure of 319 aluminum coated with high-silicon precursor: (*a*) silicon particle dispersion in the coating and (*b*) coating, 390, and base material, 319, interface.

of a gradual transition from large block and eutectic silicon to primarily eutectic silicon in an aluminum matrix. The overall appearance of the microstructure was characteristic of hypereutectic aluminum-silicon alloys, suggesting that their abrasion and wear properties will be comparable to those of cast alloys such as alloy 390. No heat treatment was performed on the overlay after deposition. Continued work in this area has allowed for the incorporation of both TiC and $TiB_2$. The quality of these overlays is still being analyzed. The cost of this process has not been quantified, but it should be comparable to the cost of simple metal inert gas weld overlays.

## Wear Testing

Test specimens consisting of 390 aluminum alloy overlays on 319 aluminum alloy have been processed and found to mimic bulk 390 aluminum alloys. Pin-on-disk wear tests were performed, following ASTM standards, to quantify the wear resistance of the 390 aluminum alloy overlay with that of bulk 390 aluminum alloy. Wear tests were also performed on bulk 319 aluminum alloy as a baseline. Lubricated and non-lubricated pin-on-disk wear tests were conducted using 440C stainless steel and 52100 steel balls as the pin material. Also evaluated were the frictional forces during the wear tests, scratch hardness, and microhardness. To achieve equivalent surface finishes, all specimens were surface-finished using 600-grit SiC paper.

The pin-on-disk wear tests were conducted with normal loads of 5 and 10 N at a constant velocity of 160 mm/s. Initially, the non-lubricated tests were run for 5 min, but tests of 10 min were performed in order to achieve a steady-state frictional force. There was considerable material transfer from the bulk 319 aluminum alloy samples to the ball specimens, but only a minor amount of material transfer from the bulk 390 and overlay 390 aluminum alloy samples. The smaller amount of material transfer from the bulk 390 and overlay 390 aluminum alloy samples can be attributed to the higher silicon content of these alloys, which aids chip formation.

The wear rate is the ratio of the volume of material displaced to the normal load and number of cycles. The wear rates for the bulk 319 aluminum alloys were 0.0004 $mm^3$/(N-cyc) (0.0001 standard deviation) for the 10-min-long experiments and 0.0008 $mm^3$/(N-cyc) (0.0004 standard deviation) for the 5-min-long experiments. The large standard deviations are attributed to the material transfer to the ball specimen. Wear rates for the 5- and 10-min tests are shown graphically in Figures 4 and 5.

The wear rates for the bulk 390 aluminum alloys were 0.000015 $mm^3$/(N-cyc) (0.000007 standard deviation) for the 5-min-long experiments and 0.00002 $mm^3$/(N-cyc) (0.000003 standard deviation) for the 10-min-long experiments. The wear rates for the 390 aluminum alloy overlays were 0.00002 $mm^3$/(N-cyc) (0.000007 standard deviation) for the 5-min-long experiments and 0.000025 $mm^3$/(N-cyc) (0.000009 standard deviation) for the10-min-long experiments. The wear rates for all the 390 bulk aluminum alloys and 390 aluminum alloy overlays are statistically equivalent and are two orders of magnitude less than for bulk 319 aluminum alloy, as would be expected.

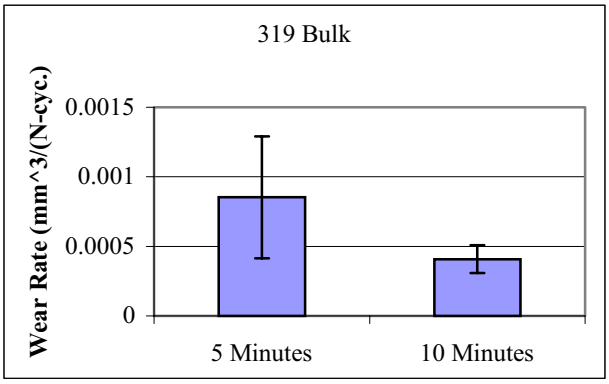


**Figure 4.** Wear rates for the 5- and 10-min. wear tests on the bulk 319 aluminum alloy.

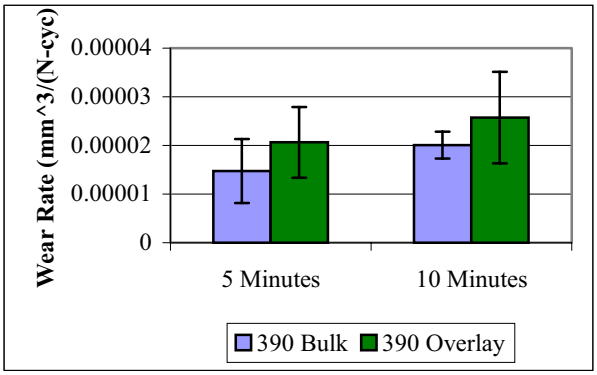


**Figure 5.** Wear rates for the 5- and 10-min. wear tests for the bulk 390 aluminum alloy and the 390-aluminum overlay.

A steady-state frictional force was established with the experiments that ran for 10 min. All three alloys had similar coefficients of friction (COF), on the order of 0.40. There was considerably more variation in the COF for the bulk 319 aluminum alloy (0.15), again because of the material transfer, than for the bulk 390 aluminum alloy (0.02) and the 390 aluminum alloy overlay (0.03).

The lubricated tests were run for significantly longer durations, up to 45 min, but no measurable wear could be detected. The COF dropped to approximately 0.2 for all alloys with no measurable variation. For the wear originating from lubricated tests to be measured, the specimens needed to have a finer surface finish.

Vickers microhardness for each alloy was measured using 300-g normal load. The bulk 319 aluminum alloy's microhardness was 1.1 GPa (0.2 GPa standard deviation), while the microhardness for the bulk 390 aluminum alloy and 390 aluminum alloy overlay was 1.3 MPa (0.6 and 0.3 GPa standard deviation, respectively). There is no statistical difference in the microhardness of these alloys. The scratch hardness ($H_s$) is a more relevant term for reciprocating and sliding contact than the quasistatic indentation hardness, because the same type of abrasive wear is occurring. The bulk 319 aluminum alloy (0.9 GPa) has a statistically lower $H_s$ than the bulk 390 aluminum alloy (1.05 GPa) and the 390 aluminum alloy overlay (1.1 GPa). There is no statistical difference between the bulk 390 and the 390-aluminum alloy overlay.

The samples will undergo heat treatment after the lubricated wear tests have been performed in order to determine the influence that heat treatment had on the wear resistance of the alloys. Based on the tests already conducted, the 390-aluminum alloy overlay shows potential as a replacement for bulk 390 aluminum alloy in high-wear-resistance applications.

## Summary

Two different aluminum-coating processes have been developed. Coatings produced by fusing fine WC and $Cr_2C_3$ particulates in copper and nickel-based binders directly onto aluminum using a high-density radiant heating process have performed well. Metallography and hardness testing have quantified the quality of this coating. A plasma-assisted deposition process has been developed which is capable of depositing 390 aluminum overlays on 319 aluminum. Metallurgical analysis, hardness testing, energy dispersive X-ray analysis, and wear testing have confirmed that the 390 overlay has properties comparable to those of bulk 390. The high-density radiant process needs further process development, while the plasma-assisted process is near commercial part trials and only needs process development for the particular application.

## Publications

C. A. Blue, V. K. Sikka, E. K. Ohriner, P. G. Engleman, and D. C. Harper, "High-Density-Infrared Transient-Liquid Coating," *JOME*, January 2000.

C. A. Blue, V. K. Sikka, E. K. Ohriner, P. G. Engleman, and D. C. Harper, "High-Density-Infrared Transient-Liquid Coating Process and Application," *Coatings* (official publication of the Thermal Spraying and Surface Engineering Association), July 2000.

# D. Material Support for Nonthermal Plasma Diesel Engine Exhaust Emission Control

*Stephen D. Nunn*
*Oak Ridge National Laboratory, P.O. Box 2008, M/S 6087*
*Oak Ridge, TN 37831*
*(865) 576-1668; fax: (865) 574-8271; email: nunnsd@ornl.gov*

*DOE Program Manager: Patrick Davis (202) 586-8061; fax: (202) 586-9811; email: patrick.davis@hq.doe.gov*
*ORNL Technical Advisor: David Stinton (865) 574-455; fax: (865) 574-6918; email: stintondp@ornl.gov*

*Contractor: Oak Ridge National Laboratory, Oak Ridge, Tennessee*
*Prime Contract No.: DE-AC05-00OR22725*

## Objectives

- Provide ceramic material support to Pacific Northwest National Laboratory (PNNL) for development and fabrication of new proprietary ceramic component designs for use in nonthermal plasma (NTP) reactors for the treatment of diesel exhaust gases.
- Fabricate and ship components to PNNL for testing and evaluation in prototype NTP reactors.

## OAAT R&D Plan: Section 3.2: Task 1B; Barriers A, B

## Approach

- Evaluate commercially viable forming methods to fabricate complex-shaped ceramic components that meet PNNL design specifications.
- Modify processing as needed to accommodate material and design changes.
- Investigate metallization materials and processes to apply electrodes to the ceramic components.

## Accomplishments

- Fabricated ceramic components using the gelcasting process and delivered parts to PNNL for testing and evaluation.
- Identified a potential high-volume production process for fabricating the ceramic components for the NTP reactor. In collaboration with PNNL, modified the design of the ceramic components to be compatible with the new fabrication process.
- Designed and procured new forming dies. Purchased new raw materials and began trials of the new component fabrication process.

## Future Direction

- Fabricate ceramic components for testing at PNNL in prototype NTP reactors.
- Modify the component processing as necessary to meet material and design specifications.
- Investigate the processing variables to establish a commercially viable process for ceramic component fabrication.

## Introduction

NTP reactors have shown great potential as an effective means of eliminating unwanted exhaust gas emissions from diesel engines. Researchers at PNNL are developing new, proprietary design configurations for NTP reactors that build on past experimental work. To improve effectiveness, these designs include ceramic dielectric components having complex configurations. Oak Ridge National Laboratory (ORNL) has extensive experience in the fabrication of complex ceramic shapes, primarily based on prior work related to developing ceramic components for gas turbine engines. The ORNL expertise is being utilized to support PNNL in its development of the new NTP reactor designs.

## Approach

Collaborative discussions between ORNL and PNNL are used to establish new ceramic component designs for improved NTP reactors. Meeting NTP reactor design objectives is balanced with the limitations of ceramic manufacturability to arrive at a new component configuration. The ceramic processing facilities and expertise at ORNL are then used to establish fabrication capabilities and to produce components for testing at PNNL. This is an iterative process as both parties gain more knowledge about fabricating the components and about their performance in NTP reactor tests. The ultimate goal is to identify a design that performs well and that can be readily produced by a commercially viable process.

## Results

Complex-shaped ceramic components were fabricated by the gelcasting process and sent to PNNL for testing and evaluation. During discussion at a meeting at PNNL, the ORNL principal investigator suggested a more commercially viable ceramic fabrication method based on materials and processes used in the electronic substrate industry. It was agreed that this alternative processing method would be easier to transition to industry for high-volume production. Modifications were made to the component design to accommodate the new process.

New ceramic component forming dies were designed and procured for fabricating the latest proprietary design of ceramic components. Material of one composition was obtained from a commercial source for use in the new process. An effort was begun at ORNL to produce material of a second composition that would be less expensive than the commercially obtained material. Experiments were undertaken to fabricate components from the two different materials. There are several processing steps involved, including forming, laminating, binder removal, and sintering. In the laboratory, these steps are performed individually and manually. In a commercial process, the steps could be automated and conducted in a continuous manner.

The forming process is done in a mold using pressure at an elevated temperature. Tests were conducted to determine the conditions that were necessary to form the parts without degrading the raw materials or causing defects in the samples. The lamination process is also done using pressure at an elevated temperature. The optimum conditions were determined to ensure satisfactory bonding of the laminates without deformation of the features produced in the forming step. Binder burnout removes the organic chemicals that allow the ceramic powders to be formed into complex shapes. A controlled thermal cycle is used to eliminate the binder. The organics must be removed slowly to prevent bloating, rupturing, or delamination. Sintering densifies the ceramic material and is a key factor in determining the ultimate properties of the ceramic, including strength and dielectric properties. The sintering procedure is carefully controlled to prevent cracking and distortion.

Components were produced in processing trials using both the commercial material and the ORNL-developed material. Examples of the parts were sent to PNNL for examination. Additional experiments will be run to fine-tune the processing procedure and to incorporate the application of metal electrodes.

## Conclusions

Gelcasting was used to fabricate ceramic components for the NTP reactor, and components were delivered to PNNL for evaluation and testing. It was decided, however, that the gelcasting process for forming the components was probably not amenable to high-volume commercial production. An alternative fabrication method was proposed by ORNL and agreed to by PNNL. Design changes were made to

the components, and the required processing capabilities were established at ORNL. Samples of the new components were produced in laboratory trials using two different ceramic compositions. Examples of these parts were sent to PNNL for examination. Components will continue to be produced at ORNL and provided to PNNL for testing. As component testing proceeds at PNNL, any necessary material and design changes will be incorporated in the future fabrication of ceramic components at ORNL.

# ACRONYMS AND ABBREVIATIONS

| | |
|---|---|
| ANL | Argonne National Laboratory |
| ASTM | American Society for Testing and Materials |
| BME | base metal |
| BOTD | ball-on-three-discs |
| CIDI | compression ignition, direct injection |
| CO | carbon monoxide |
| CFO | coefficients of friction |
| CRADA | cooperative research and development agreement |
| CVI | chemical vapor infiltration |
| DF | dissipation factor |
| DLC | diamond-like carbon |
| DOE | U.S. Department of Energy |
| EC | electronic ceramic |
| ECD | electronic ceramic device |
| EDX | energy-dispersive X-ray spectroscopy |
| EGR | exhaust gas recirculation |
| EPMA | electron probe microanalysis |
| F | fluorine |
| FT | Fischer-Tropsch |
| GM | General Motors |
| ICS | Industrial Ceramic Solutions |
| LANL | Los Alamos National Laboratory |
| MEA | membrane electrode assembly |
| MLC | multilayer capacitor |
| NFC | near-frictionless carbon |
| Nm | nanometer ($10^{-9}$ meters) |
| NTP | nonthermal plasma |
| OATT | Office of Advanced Transportation Technologies |
| OEM | original equipment manufacturer |
| ORNL | Oak Ridge National Laboratory |
| OTT | Office of Transportation Technologies |
| PACVD | plasma-assisted chemical vapor deposition |
| PEM | polymer electrolyte membrane |
| PECMFC | proton exchange ceramic membrane fuel cell |
| PNGV | Partnership for a New Generation of Vehicles |
| PNNL | Pacific Northwest National Laboratory |
| Pt | platinum |
| S | sulfur |
| SNL | Sandia National Laboratory |
| T | Tesla |
| TEM | transmission electron microscope |
| TIVM | toroidal intersecting vane machine |
| ULF | ultra-low-fire |
| UW | University of Wisconsin |